+

ADDIS ABABA UNIVERSITY

ADDIS ABABA INSTITUTE OF TECHNOLOGY

SCHOOL OF MECHANICAL AND INDUSTRIAL ENGINEERING

Crack Propagation Analysis and Its Life Prediction for Railroad Rails Using FEA

A Thesis Submitted to the Graduate School of Addis Ababa University in Partial Fulfillment of the Requirements for the Degree of Masters of Science

In

Mechanical Engineering

(Railway Engineering)

By

Abdurahman Haji

Advisor

Dr. Daniel Tilahun

April, 2015

ADDIS ABABA UNIVERSITY

ADDIS ABABA INSTITUTE OF TECHNOLOGY

SCHOOL OF MECHANICAL AND INDUSTRIAL ENGINEERING

DECLARATION

I, the undersigned, declare that this thesis paper is my original work and has not been presented for any degree in any university and all the sources of materials used for the thesis have been appropriately acknowledged.

Abdurahman Haji		01/06/2015
Name	Signature	Date

This thesis has been submitted for examination with my approval as University advisor.

Daniel Tilahun (Dr.)		03/06/15
Advisor	Signature	Date

ADDIS ABABA UNIVERSITY

SCHOOL OF GRADUATE STUDIES

ADDIS ABABA INSTITUTE OF TECHNOLOGY

SCHOOL OF MECHANICAL AND INDUSTRIAL ENGINEERING

Crack Propagation Analysis and Its Life Prediction for Railroad Rails Using FEA

By

Abdurahman Haji

April, 2015

Approved by Board of Examining

Birhanu Beshah(PhD)
Head,Railway
Engineering Centre

Birhanu Besha (Dr.)		03/06/15
Railway Center Head	Signature	Date
Daniel Tilahun (Dr.)		03/06/15
Advisor	Signature	Date
Habtamu Tkubet (MSc)		03/06/15
Internal Examiner	Signature	Date
Tsegaye Feleke (MSc)		03/06/15
External Examiner	Signature	Date

Director of Postgraduates Program
Addis Ababa University
Addis Ababa Institute of Technology

Acknowledgement

First of all I would like to thank my advisor Dr.Daniel Tilahun for his grateful support and continuous advice of the work from the beginning up to the final result of this paper. I want to appreciate also his willingness and giving of motivations to work on research areas focusing on the current situations of our country, Ethiopia, pointing its future development and related problems to lay down the possible respective solutions.

I would like to thank Ethiopian Railway Corporation, for giving me a chance to study this degree and who covers the entire school fee and paying me the pocket money the past two years. Their willingness to produce skilled manpower for the future expansion of Ethiopian Railway is highly appreciated.

Thanks also go to all people who stand on my side during the past two years of my study and work of this paper. Especially to Dr. Abdissa Kurkie (MD, MPH), my friend and colleagues of all time who support and encourage me to study further.

Finally, special thanks to my Family and friends for their patience, advice, support and motivation standing always on my side for the successful accomplishment of this paper and for the success of my life at all.

Abstract

Now a day the railway transport infrastructure in Ethiopia is the major issues in relation to the development of the country. To strengthen this infrastructure, related researches must be conducted at the beginning of the construction of the sector. This paper which mainly concerned about the analysis of crack propagation of rail due to vertical wheel load is done to predict the initiated crack growth rate under different load conditions. The objective of this research is to analyze propagation of initiated crack and determine its growth rate under different load conditions and to identify the maximum axle load used, which is basic to justify the way of crack propagation near to the contacting interface.

A design axle load of 25ton (ERC) and 22.5tons and 20tons are assumed for the calculation of Stress Intensity factors. A wheel of S1002 profile and a UIC60 rail profile are modeled using CatiaV5R19 software. The models are assembled and imported to Ansys 15.0 release workbench and then to Ansys APDL to simulate wheel/rail contact. The material properties of rail steel are taken and a side crack model is made to simulate crack propagation of railroad rail taking only the vertical load from wheel. The cracked plate is assumed as it is taken from a cracked rail. Then, initiated cracks of different sizes are taken and tensile stress loads are applied on each crack length. The analysis is done taking into account the theories of Linear Elastic Fracture Mechanics. The analysis is based on numerical and analytical methods. For numerical methods, the analytical stress intensity factor *KI* is calculated using a formula given by (Ewalds and Wanhill, 1989). The analytical method uses Ansys KCALC (Displacement extrapolation method) based on the stress and strain plane conditions. Both results are compared with the numerical results. The tensile loads which take in to account the effects of the dynamic magnification of the vertical wheel load show higher SIF and the life cycle the cracks under these cases are shorter.

Keywords: Crack Propagation, Crack Growth Rate, Linear Elastic Fracture Mechanics, Wheel-Rail Contact Geometry

Contents **page**

List of Tables

List of Figures

Nomenclatures

R_1: is the wheel nominal rolling radius

R_2: is the rail nominal rolling radius

R_1' and R_2: are the nominal transverse radii of curvature of the wheel and rail respectively

$E_{1:}$ is the Young's modulus of the wheel material

$E_{2:}$ is the Young's modulus of rail materials

K1& K_2: are material properties of wheel and rail respectively (the relative change in the Volume of a Body produced by unit compressive or tensile stress

ν_1: is the Poisson's ratio of the wheel material

ν_2: is the Poisson's ratio of the rail material

ψ : The angle between the radius of the wheel and rail

θ: is the angle between the principal axes

m& n : are Hertz coefficients

Po: the maximum Hertzian pressure

K_{dyn}: dynamic Magnification factor

σ: remote stress

da/dN : is the crack growth rate per cycle

ΔK: is the stress-intensity range

C&m: are material constants of rail steel

F: is a crack geometry correction factor

a: is crack length

B: is thickness of the plate

b: is width of plate

UIC: International union of railways

SIF: stress Intensity Factor

ERC: Ethiopian Railway Corporation

LEFM: Linear Elastic Fracture Mechanics

Chapter One

Introduction

1.1 Background of the Research

The history of rail transport dates back to 500 years ago. The first rail transport was powered with man or horse on rail of wood or stone. The first railway in Britain was built in 1604 out of wood, and it was called a wagon way. Modern rail transport systems, which made use of the steam locomotive, first appeared in England in the 1820s. They were the first practical forms of mechanized land transport, and they remained the primary form of mechanized land transport for the next 100 years. By 1900, the railway was mostly completed, and there were more than a hundred train companies in Great Britain. The electrification of the railways began in 1933. This means that the trains began to run on electricity instead of steam. Railways were originally intended to carry mostly goods rather than passengers but in the 1970s the value of carrying passengers overtook goods for the first time [4].

In Ethiopia, the railway lines construction was first started in October 1897 from Djibouti during the period of Emperor Menelek II. The first commercial service began in July 1901, from Djibouti to Dire Dawa. By 1915 the line reached Akaki, 23 kilometers far from the capital, and two years later it reaches Lagahar (Addis Ababa) [4].
Railway Transportation infrastructure in Ethiopia has been neglected for decades, but currently it is a priority of the government of Ethiopia to expand the Railway transportation both for passenger and freight in every direction through the country via different phases.

The interaction of surfaces with a relative motion is extremely common in any type of machine or industrial system. This relative motion inevitably causes material wastage and energy dissipation. These phenomena are due to friction and the higher the friction between the surfaces, the more important the effects of these phenomena will be. A lubrication film can be introduced between the surfaces in order to reduce friction and its consequences. But finally everything that man makes will eventually wear out as a result of relative motion between surfaces. Analyses of machine breakdowns show clearly that the moving components or parts are in most cases to

blame for the failure or stoppage [6]. Examples of these moving parts are for instance gears, bearings, cams, etc.

Railway transportation system, as one of the notable means of traveling systems in the world, has served for human societies and has pursued its improvements as other promoted aspects of life [1]. Currently, there is a high demand of railway transportation systems in the world, including our country Ethiopia, for a light rail transit and a long distance transport of passengers and goods. To satisfy such demands, it needs to have a railway transportation system with standard safety, comfort to customers, and reliable to user's etc. Such demands need the advanced design and analysis of functional components, which have a direct or an indirect impact on the customers and users demand.

Now days, [1] the carrying axle loads and their travelling velocities for world railways have been improved. The increase in carrying axle load and travelling velocities resulted in increasing the amount of strains and stresses on lines and digression of rails. Therefore, studying interactions between railway components become more considerable.

Mechanics of the rail and wheel at rolling contact is one of the elemental and basic areas of the study in Mechanical and Railway Engineering, requiring both very important and large application skill and reliable analysis approaches. Analytical formulations [2] representing the physics of this fact are defined only for special type of simple contact geometries, so for more complicated and complex geometries, the analytical models employing closed forms remain hard to comprehend. Railway Engineers and Researchers are successfully applied one of the numerical computation methods known as Finite Element Analysis (FEA) or simple direct formulations into rail–wheel contact problems to verify their results by comparing them to their actual life information determined over the past years. Determination of the contact areas requires knowledge of some geometric constants used in the formulation in the rolling bodies. Two solid discs and rolling body are put together to generate an elliptic contact surface factors. The wheel-rail contact can be described by the general case of an elliptic contact surface. Evaluating surface and subsurface stresses requires the determination of the displacements field [3]. Wheel and rail contact, crack and the damage to both surfaces continue to concern railway

Engineers. Understanding the loading into the track and the stresses they generate is the first step in identifying the root cause of the problem.

During this last decades, new technologies and altered ways of exploitation of railroads are facilitating the occurrence of fatigue defects, e.g. increasing traffic density, increasing axle loads, increasing traction loads due to modern-locomotive characteristics and to improved adherence techniques (traction control), increasing rails and wheels grade and wear resistance, geometrical characteristics of the track, stiffer train suspension systems. The resulting load and straining configuration require stresses and slip phenomena. Stress and slip combination determines the degradation state.

Contact stresses are significant when contact is not fixed but cyclic in nature such as in locomotive wheel-rail road rail. In order to study the stress analysis, factors of critical stress must be determined [1, 2, and 4]. One of the frequent flaws and defects of rails which lead to their failure and fracture is a vertical crack on the end of the rails. This is principally because of loading that will make a tensile and compressive stress on the end of the rail. Therefore, these stresses with the tensile and compressive stresses will cause compressive and tensile stresses on the end of rail respectively and these tensions and compressions lead to growth of crack at the end of the rail, and eventually cause failure and fracture in it. Thus, the crack, which is based on vertical wheel load, can be studied.

1.1.1 Railway Track

A railway track consists of two parallel rail tracks, formerly made of iron but now of steel, and generally mounted upon cross beams named “sleepers or railroad ties" which are sometimes made of timber, concrete or steel as shown in Fig.1-1.

Figure 1.1: Rail tracks

During the interaction between the wheelset and the rail track there are different conditions created on the contacting surface. These dynamic contact behaviors depend partly on the track geometry. The most common track geometries having great impact on the railway vehicle dynamic behavior are:

- Track gauge: the distance between the right and left rail inner gauge corners
- Track cant (supper elevation): the difference between the level of the two rail on a curve
- Track curvature: it is the inverse of the radius of the curved track
- Rail head: it is the surface of the rail having a direct contact to the railway vehicle wheel.
- Wheel and rail tread profile

By managing these geometrical parameters of the track it is possible to control the dynamic behaviors of the wheel-rail contact, especially on the curved track.

1.1.2 Rail

Rails are longitudinal steel members that are placed on spaced sleepers to guide the rolling stock. Railway lines are made of straight sections and curves. Train driving on the curves essentially differs from that one on straight sections. On the curves railway gauge is widened (when curve radius is less than 350 m), and cant are ascended [7]. The main tasks of the rail are supporting traffic load and guidance of vehicles. For both tasks the correct contact geometry between wheel and rail is essential [8]. Besides this, rails are used to accommodate and transfer the wheel/axle loads into the supporting sleepers. The most commonly used profile of rail is flat-bottom rail and is divided into three parts:

Rail head: the top surface that contacts with the wheel

Rail web: the middle part that supports the rail head, like columns

Rail foot: the bottom part that distributes the load from the web to the underlying superstructure components.

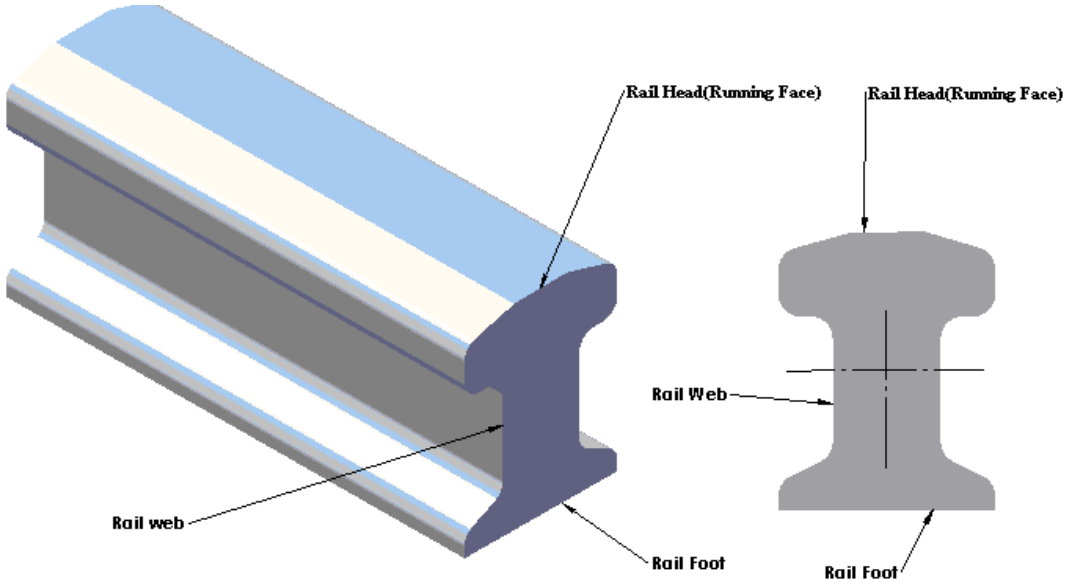

Figure 1.2: Flat bottom rail parts

1.1.3 Wheels

A railway wheel, together with an axle, is one of the fundamental parts that support the safe operation of railway vehicles [9]. Wheels support the entire weight of cars; however, they cannot be designed as a failsafe structure where a backup system by other parts can be applied in case of a serious problem. Therefore, absolutely high reliability is demanded in terms of strength. Accordingly, the most important and fundamental characteristic in designing wheels is strength.

A solid wheel of a railway vehicle consists of three parts, as shown in Fig. 1.3. They include:

Hub: wherein an axle is inserted,

Rim: part that contacts the rail, and

Web: part that unites the two parts (hub and rim).

Tread: the outer circumferential surface of the rim, which contacts the rail,

Flange: the projected part of the rim.

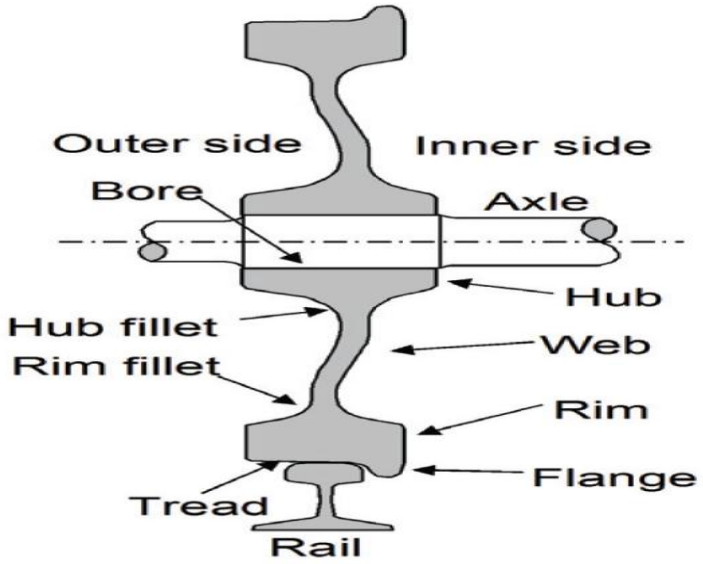

Figure 1.3: Parts of a solid wheel [9]

1.2 Purpose

The purpose of this paper is to analyze the crack propagation of railroad rail under static wheel load with its dynamic magnification and prediction the life of the crack under different axle loads. Initiated Crack of rail due to wheel or axle vertical loading contact that is associated with the cycle of tensile stress will be studied. Finally, the crack propagation of side crack of the rail steel will be studied and discussed. Linear Elastic Fracture Mechanics (LEFM) is used in the models. The results will be analyzed numerically and compared with that of Finite Element Method. Then the results will be discussed and concluded and the future works will be recommended.

1.3 Statements of the Problem

The railroad rail is subjected to important dynamic loads, transmitted for the biggest part at the rail wheel interface, a very small zone. Loads on this spot are vertically and longitudinally transmitted. Repeating loads provoke internal cyclic stress, which will gradually damage the material and will initiate the crack development; it will begin from the damaged zones. Under the influence of this cyclic stress, the material works in an elasto-plastic regime. The behavior of the wheel/rail interface is fundamental for being certain that adequate comfort, stability and safety are guaranteed during the train trip. Depending on the type and position of contacts, the way of

distribution of cyclic axle load and its effects differs accordingly. Due to this, there are different questions to be answered, like:

- ✓ What types of loads (stresses) are induced on the contacting interface?
- ✓ Which type of load causes abrupt fracture on surfaces?
- ✓ How initiated crack is propagated to surfaces?
- ✓ How the life of initiated crack is predicted?

Such and other kinds of questions divert the interest of most researchers to direct their devotions to the area of contact mechanics, especially to wheel/rail contact problems. The higher train speeds and increased axle loads have led to larger wheel/rail contact forces. Fatigue crack growth in wheels and rails may lead to the loss of a part of the wheel or rail. The radial crack extension may happen with the consequence of the release of the press fitting between wheel and axle. The result can be damage of rails and sleepers or vehicle components or even derailment. Therefore, to deal with crack propagation and predicting its life is very essential for railway companies.

1.4 Objective of the Study

1.4.1 General Objective

The general objective of this study is to model 3D Finite Element of wheel and rail and to study the initiated crack propagation of rail steel using different axle loads with dynamic magnifications and varying the speed of the train. The stress distribution around crack tip will be studied by using Finite Element Method. The axle load, the rolling velocities, material properties, strain and stresses are considered and the crack propagation of rail steel and its life prediction will be analyzed using different theories.

1.4.2. Specific Objective

The specific objectives of this research are:

- Modeling 3D Finite Element for wheel/rail rolling contact.
- Modeling an initiated crack for a rail steel
- Fine meshing technique in crack tip region is used to achieve both computation efficiency and accuracy.
- Analyzing the crack propagation of rail (caused by wheel load) and

- predicting life of initiated crack of rail under different wheel load cases
- Analyzing the stress distribution around crack tip of crack initiated rail steel by using elastic-plastic FEA.
- Calculating stress intensity of crack tip and its fracture mode
- Discussing the possible influence on crack propagation

1.5 Limitation of the study

The limitation of this study is that it is only based on the numerical and finite element analysis. Because, at the current situation (up to March 2015) we cannot get a functional railway system in Ethiopia we can't compare it with the real life like investigating field data. Besides this, studying railway systems requires both time-consuming analysis methods and expensive experimental works. But we can compare it with similar research done before for other countries as it can comply with real life.

1.6 Organization of the paper

This thesis consists of five chapters. Chapter 1 starts with an introduction giving a brief background of the research area followed by a review of previous literature and problem description. The purposes of the study, objectives, research questions and the limitations have also been outlined in this chapter.

Chapter 2 will explore the issues of wheel/rail contact geometry and rolling contact fatigue in wheel and rail contact to provide an overview of the study. This chapter also highlights the Linear Elastic Fracture Mechanics and will present the contact mechanics relevant to this thesis with examples. It highlights the similarities and differences of simulator and real world conditions to gain an insight into the analysis of methodology of chapter 3. Chapter 3 details the material, dimensions, methods and conditions used for the thesis. Chapter 4 presents all the analysis results of both numerical and FEA with discussion. Finally, Chapter 5 summarizes the findings of the thesis, presents the conclusions, recommendations and discusses directions of the future works.

Chapter Two

Literature Reviews

2.1 Introduction

Literature review portion of this paper is a part that reviews the previously worked related literatures which are basic guide for the introduction of the current work. Some literatures have a direct relation with this work whereas the others may have indirect relations. The main Principles, Methodologies and Approaches they have used will be selected and applied for the formulation of specific model and analysis. Generally there are many Journals, Conference Papers, Proceedings, Design Works and Books related to the Railway Engineering, Railway Vehicle Dynamics and particularly wheel-rail contacts, interactions etc. Due to time constraint and to manage the paper work, the review of literatures mainly considers more related works to the paper. This strengthens the deep analysis of the previous related works and selection of appropriate conditions, approaches and methodologies for the successful accomplishment of the paper.

2.2. Wheel-Rail Contact Model

In the contact zone between railway wheel and rail the surfaces and bulk material must be strong enough to resist the normal (vertical) forces introduced by heavy loads and the dynamic response induced by track and wheel irregularities. The tangential forces in the contact zone must be low enough to allow moving heavy loads with little resistance, at the same time the tangential loads must be high enough to provide traction, braking, and steering of the trains.

The contact zone (roughly $1cm^2$) between a railway wheel and rail is small compared with their overall dimensions. The shape of contact area depends on the rail and wheel geometry, lateral position and angle of wheel relative to the rail, (i.e. how the wheel meets the rail influence) (as shown by Le The Hung, 1987).

The main interest for the vehicle system dynamic problems was wheel - rail contact model. In this respect, the contact forces along and perpendicular to the rolling direction are of maximum interest. This problem was first solved by Carter [14] by regarding the wheel - rail contact as a

cylinder rolling over a plane (a two dimensional problem). Three decades later, de Pater and Johnson solved the spherical (three-dimensional) case by using the Hertz solution for predicting the shape and size of the contact area and pressure distribution. More approximate solutions for the elliptical contact situation were presented by Haines and Ollerton [15] followed shortly by Vermeulen and Johnson [16].

Apart from the approximated solutions, the general case for modeling the wheel - rail contact must be solved numerically. Kalker [17] was the first to solve the general wheel - rail contact, for which purpose he developed the program CONTACT. The program is widespread and even today it is most frequently used for the wheel - rail contact problem in other countries.
Finite Element Methods are also applied to the wheel - rail contact problem and significant simulations and developments have been recently made by different Researchers [2].

2.3 Rolling Contact Fatigue

Machine element such as rolling bearings, gears, cams, etc. and the wheel-rail contact with sequences contain surfaces that interact with a rolling motion. The repeated interaction can lead to contact fatigue or surface fatigue. Thus, rolling contact fatigue, which is based on repeated high contact stresses with relatively little sliding can be studied.

Characteristic damage observed on machine elements subjected to rolling contact fatigue are fatigue cracks and small craters or spalls [11]. Surface distress is the name widely used to designate micro-scale contact fatigue. The fatigue damage has then a size comparable to the dimensions of asperities on the contacting surfaces. Macro-scale contact fatigue is commonly designated as spalling. According to [11], the fatigue cracks leading to a spall can be initiated at the surface or below the surface. The sub-surface initiated spall has a quite irregular shape, whereas surface initiated fatigue cracks present some typical features such as the entry angle. According to [10] this angle is smaller than 30°. Smaller ranges have been reported by [12], where the entry angle for surface initiated cracks was reported to be in the range of 20 - 24° and [13], where experimentally measured entry angles were in the range of 25 - 30°. The entry angle of sub-surface initiated spalls has been reported to be steeper. According to [10] it is larger than 45° to the contact surface. Another important feature of the observed fatigue cracks is the crack

propagation direction. The crack propagates in the rolling direction. The purpose of this paper is to study the crack propagation analysis of rail by using fracture mechanics theories.

2.4 Fracture Mechanics

Fracture is defined as the local separation of an object or material into two or more pieces under the action of stress. Usually, the fracture of a plate occurs due to the development of certain displacement discontinuity surfaces within the plate [31]. The modern fracture mechanics was born in 1948 when George Irwin [29] formulated the fracture mechanics and devised workable parameters like stress intensity factor (SIF) and energy release rate (ERR). Once the breakthrough took place, many investigators jumped into the wagon and fracture mechanics became a separate and important discipline with several journals and text books. Irwin's development was mainly for brittle or less ductile materials. The analysis was conservative for most engineering materials which are generally ductile. Other parameters like crack tip opening displacement by Wells in 1961 and J-integral by Rice in 1968, were developed to account for large plastic zone at the crack tip.

Cracks frequently initiate and grow at stress concentration zones such as notches, holes, an indentation corners and welded joints in structural components. Because such elements occur frequently in structural components, understanding the severity of cracks is important in the development of static strength, fatigue crack growth and fatigue life prediction methodologies. The stress intensity factor (SIF) is the key parameter in linear elastic fracture mechanics (LEFM) for quantifying the severity of cracks. It reflects the effect of loading; crack size, crack shape and component geometry in life and strength prediction methods [29].

An accurate knowledge of the stress intensity factor is essential for the prevention of brittle fractures arising from cracks; in particular, the use of the LEFM principles in preventing the fracture of engineering components depends largely on the availability of accurate SIFs. As a result, analytical, numerical and experimental methods for SIF determination in cracked bodies have been developed for several decades [Sanford 2003].

Recent development in engineering structures shows that fracture can be caused by small cracks in the body of structures despite the validity of elasticity theory and strength of materials. As a

result, fracture mechanics filed which is concerned with the propagation of cracks in materials has developed to study more about this subject, Ali and et al. [31].

According to the types of load, there are three linearly independent cracking modes are used in fracture mechanics as follow:

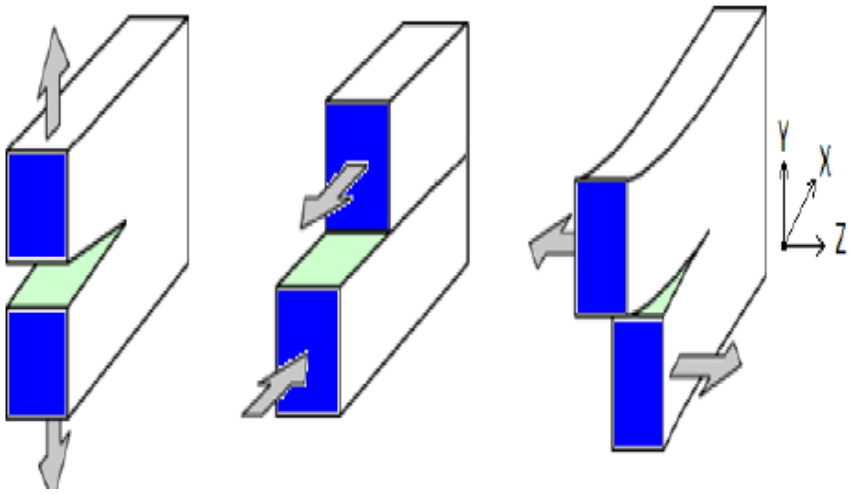

Figure 2.1: Fracture modes: (a) mode I (tensile Mode), (b) Mode II (in plane shear mode) (c) Mode III (out of plane shear Mode) [31]

- ✓ Mode I: a tensile stress normal to the plane of the crack (tensile mode),
- ✓ Mode II: shear stress acting parallel to the plane of the crack and perpendicular to the crack front (in-plane shear mode).
- ✓ Mode III: shear stress acting parallel to the plane of the crack and parallel to the crack front (out- of- plane shear mode). Where Mode I is the most common load type encountered in engineering design.

2.5 Stress Intensity Factor

Stress intensity factor is measure of the stress-field intensity near the tip of an ideal crack in a linear-elastic solid when the crack surfaces are displaced in the opening mode. The problem of determining the stress intensity factors of cracks in a plate is of considerable importance in the

design of safe structures because of stress intensity factors the main key value defining the stresses around the crack tip arising from that crack.

As it is discussed in [31], Azevedo studied the stress intensity factors KI and KII for an inclined central crack on a plate subjected to uniform tensile loading were calculated for different crack orientations (angles) using FEM analysis, which was carried out in ABAQUS software. The stress intensity factors were obtained using the J integral method and the modified Virtual Crack Closure Technique (VCCT).

A. Gopichand, and Y. Srinivas [35] used two different techniques for the calculation of Stress Intensity Factor, SIF KI of brass plate with edge crack. The two techniques they carried out for their study were the Displacement Extrapolation Technique, and J- Integral Technique.

The Displacement Extrapolation Technique is based on point matching techniques (or extrapolation methods) with nodal displacements. They are widely used extrapolation techniques due to its simple applicability to various crack configurations. The second method, the J-Integral Technique is based on energy-based methods like J-Integral, energy release and the stiffness derivative methods are also used for the determination of SIF. From this study, it has been observed that the Stress Intensity Factor, SIF value increases with increase in crack length and the component failed when the SIF reaches its critical value i.e. fracture toughness.

Upamanyu Banerjee [36] studied simulation of stress intensity factor as function of rolling contact fatigue cracks of railway tracks and the vehicle load with the help of COMSOL Multi-physics software. In view of the predominance of failure due to abrupt growth of rolling contact fatigue, cracks in railway tracks, attempts are made to simulate stress intensity factor under plane strain situation with the aid of COMSOL Multi-physics software. In his investigation, Upamanyu Banerje used the J-Integral method (which is a two-dimensional line integral, along a counterclockwise contour, Γ, surrounding the crack tip). This method is employed to find the stress intensity factor of Rail Steel under Situation of Growing Fatigue Crack. The simulation provides us with a direct relationship between crack length and stress intensity factor.

The main purpose of this paper is to study the crack of railroad rail behavior by considering a rectangular finite plate taken from cracked rail track with a side crack under the effect of

dynamically magnified wheel load numerically and analytically by KCALC (displacement extrapolation method) command in ANSYS software.

The FEA of this study considers the strain and stress plain conditions. Parameters like a ratio of crack length to width plate, applied stress for different load cases will be considered and the stress intensity factors KI and Von-Mises stress to the crack tip will be calculated. The relationship between the stress intensity factor with crack length and applied loads will be studied.

Chapter Three

Analysis, Method and Conditions of Crack Propagation of Railroad Rail

3.1 Materials of Wheel and Rail

Railroad rails are grouped according to their standards, strength, grade, quality and length. The rail steel qualities can be distinguished in to two categories.

- Normal steel quality, with an ultimate tensile strength of 700-900MPa.
- Hard steel quality, used mainly on curves, and crossings etc. with an ultimate tensile strength of 900-1200MPa.

Depending on their requirements, the chemical compositions of rail steels have great varieties of Carbon, Manganese, Chromium and Silicon contents. Since the rails have to withstand the impact load, friction and stress of freights, they should have sufficient strength, hardness, toughness and good welding performance. However a large increase in rail mechanical strength may result in brittle failure and as a result a further increase is not desirable.

Table 3.1: Mechanical Property of selected materials

1	**Rail track material (R260)**						
	Mechanical properties						
	UIC Standard (Kg)	Axle load (KN)	Young's Modulus (GPa)	Poisson's ratio	Ultimate tensile strength [MPa]	Tensile Strength [MPa]	Yield strength [MPa]
	60	25	207	0.3	700-900	880	410
2	**Wheel material**						
	Mechanical properties						
	UIC Standard (Kg)	Axle load (KN)	Young's Modulus (GPa)	Poisson's ratio	Ultimate tensile strength [MPa]	Tensile Strength [MPa]	Yield strength [MPa]
	64	25	207	0.3	700-900	880	410

Source ERC, UIC and reference [34]

3.2 Wheel-Rail Contact

The general conditions considered during the wheel rail contact simulation are the assumption of the Hertz contact theory. The common Hertz assumptions are:

- Isotropic and homogenous material
- no friction (Hertz wrote that the surfaces of both bodies had to be completely smooth)
- both bodies were considered as half-spaces
- The contact is elastic

When two bodies (wheel and rail) are in contact, stresses and strains appear. A large force from the first body (wheel) is transferred to the second body (rail) through a small contact region of about $1cm^2$.

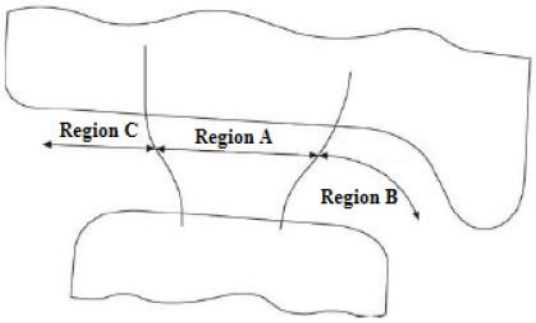

Figure 3.2: Wheel- Rail Contact Zones

Wheel rail contact regions can be classified as shown in the above figure:

a) **Region A** - wheel tread -rail head contact: this contact zone is most common contact region with lower contact stress.

b) **Region B** – wheel flange- rail gauge corner: this contact zone is much smaller contact area and more severe; higher contact stresses and wear rates occurs.

c) **Region C** - wheel and rail outer sides contact: this contact zone is least likely contact region with high contact stress, and undesirable wear lead to incorrect steering of wheelset

3.2.1 Wheel-Rail Contact Stresses

The forces arising between wheel and rail contact generate contact stresses in a local volume of the two bodies. The most well-known calculation model for this local stresses is the Hertzian one. Hertzian model describes the local stresses with good accuracy for the most common wheel-rail contact problems. This model also provides a good understanding of general contact phenomena. Although Hertzian theory is valid only for elastic contacts it can be useful far beyond that. Limited plasticity will not affect the contact stresses very much.

3.2.2 Hertizian Contact

When a wheel and a rail are brought into contact under the action of the static wheel load, the contact area and the pressure distribution are usually determined using the Hertz theory [6]. In Hertz contact theory, no plastic deformation in the contact patch is assumed, and the radii of the curvature of wheel and rail profiles in the contact patch are assumed to be constant. According to Hertz theory, the normal pressure is distributed as an ellipsoid over the elliptic contact area. The distribution of the contact pressure in this elliptical area represents a semi-ellipsoid, which can be expressed as:

$$P(x,y) = p_o\sqrt{1 - \frac{x^2}{a^2} - \frac{y^2}{b^2}}, \quad \text{----------3.1}$$

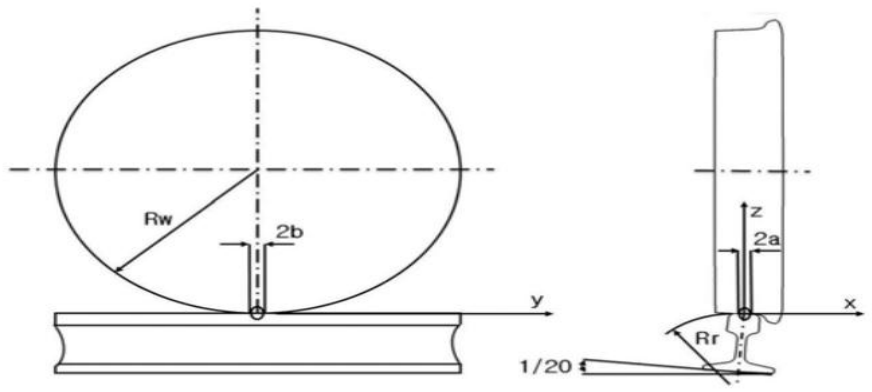

Figure 3.2: wheel- rail contact area [20]

Based on the Hertz contact theory, the contact point is very small relative to the overall dimension of railway wheel and rail surfaces. This very small contact point has elliptical shape. From the above formula **a** and **b** are semi axes of the contact ellipse whereas X and Y are the

required coordinates to specify the point of contacts on the rail surface based on the lateral rail surface parameter.

If x=0 and y=0 that is if the point of contact is on the centerline of the rail head the stress is maximum, which is equal to:

$P_o = \frac{3N}{2\pi ab}$ is the maximum pressure----------3.2

Where, *a* and *b* are the half width of the contact area in the longitudinal *x* and lateral *y* directions, respectively, and *N* is the total normal contact force.

Important assumptions that are made here are linear elastic material, small contact area compared to the radii at the contact of the bodies and to other dimensions (semi-infinite bodies are assumed), and smooth surfaces at both macro and micro scale.

The contact ellipse semi-axes a and b are determined as follows:

$a = m \sqrt[3]{\frac{3\pi}{4}\frac{(K_1+K_2)N}{(A+B)}}$ ----------3.3

$b = n \sqrt[3]{\frac{3\pi(K_1+K_2)N}{4(A+B)}}$ ----------3.4

Where the modulus K_1 and K_2 are material properties of wheel and rail (the relative change in the volume of a body produced by unit compressive or tensile stress acting uniformly over its surface) and are given by;

$K_1=\frac{1-{\nu_1}^2}{\pi E_1}$, ----------3.5

$K_2=\frac{1-{\nu_2}^2}{\pi E_2}$, ----------3.6

$A+B=\frac{1}{2}\left(\frac{1}{R_1}+\frac{1}{R_1'}+\frac{1}{R_2}+\frac{1}{R_2'}\right)$,----------3.7

$A-B = \frac{1}{2}\sqrt{\left(\frac{1}{R_1}-\frac{1}{R_1'}\right)^2+\left(\frac{1}{R_2}-\frac{1}{R_2'}\right)^2+2\left(\frac{1}{R_1}-\frac{1}{R_1'}\right)\left(\frac{1}{R_2}-\frac{1}{R_2'}\right)(\cos(2\psi))}$----------3.8

$$\cos(\theta) = \frac{B-A}{A+B}$$----------3.9

Where: R_1 is the wheel nominal rolling radius, R_2 is the rail nominal rolling radius, R_1' *and* R_2' are the nominal transverse radii of curvature of the wheel and rail respectively. E_1 is the Young's moduli of the wheel material; E_2 is the Young's moduli of rail materials, ν_1 is the Poisson's ratios of the wheel material, and ν_2 is the Poisson's ratios of the rail material. A and B are geometrical properties of the two bodies (wheel and Rail)

The angle ψ is between the radius of the wheel and rail and θ is the angle between the principal axes. m and n are Hertz coefficients and they are given as a function of the angle θ. The values of m and n for the angle θ are given in the table 3.2 below.

The direction of the axes of the contact ellipse can be determined based on the radii of curvature and the rolling radii for the two bodies in contact.

If $\frac{1}{R_1} + \frac{1}{R_2} \geq \frac{1}{R_1'} + \frac{1}{R_2'}$, the transverse semi axis of the contact ellipse (y direction) is greater than or equal to the longitudinal semi-axis

If $\frac{1}{R_1} + \frac{1}{R_2} \leq \frac{1}{R_1'} + \frac{1}{R_2'}$, the transverse semi axis of the contact ellipse (y direction) is less than or equal to the longitudinal semi-axis

Table 3.2: m,n values (Hertz Coefficients) for different angle, θ [24]

θ(deg)	**m**	**n**	θ(deg)	**m**	**n**	θ(deg)	**m**	**n**
0.5	61.4	0.1018	10	6.604	0.3112	60	1.486	0.717
1	36.89	0.1314	20	3.813	0.4125	65	1.378	0.759
1.5	27.48	0.1522	30	2.731	0.493	70	1.284	0.802
2	22.26	0.1691	35	2.397	0.530	75	1.202	0.846
3	16.5	0.1964	40	2.136	0.567	80	1.128	0.893
4	13.31	0.2188	45	1.926	0.604	85	1.061	0.944
6	9.79	0.2552	50	1.754	0.641	90	1.0	1.0
8	7.86	0.285	55	1.611	0.678			

Source: Railroad Vehicles: A computational Approach (2008)

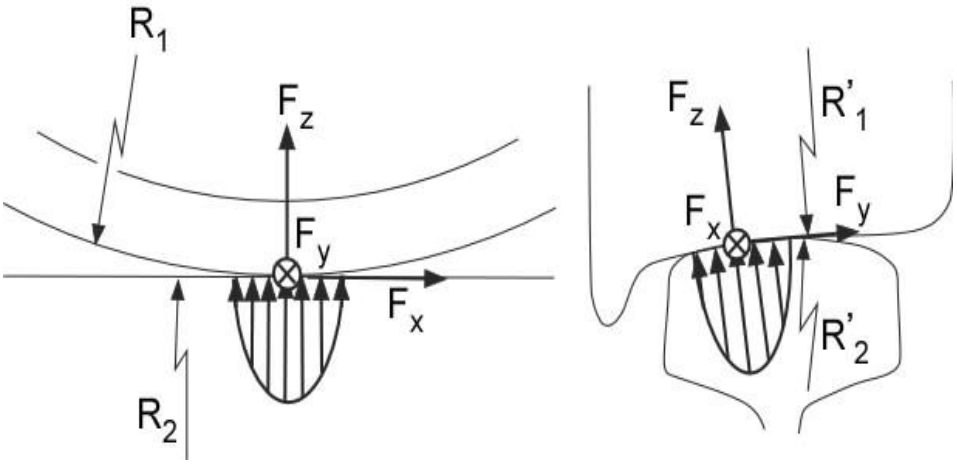

Figure 3.3: Wheel in contact with the rail. [19]

Body 1 (wheel) is assumed to have principal radii R_1 and R_1' and Body 2 (rail) have principal radii R_2 and R_2' at the contact. Forces F_x, F_y and F_z acting on wheel. Contact pressure distribution with semi-axes a, and b corresponding to force F_z is indicated. The radii are counted positive for a convex curvature and negative for a concave curvature. The two bodies (wheel and rail) are here assumed to have the same material parameters: elastic modulus E and Poisson´s ratio *v*. This means that locally identical stress fields will be induced in the wheel and the rail. The coordinate system is assumed to have its origin at the center of the contact patch which will be elliptic with semi-axes a, and b.

3.3 Rail Loading

In order to construct an accurate numerical model of rail fatigue damage a brief understanding of rail loading is needed. Rails are subjected to primary and secondary loading components**.** The loading by the wheel is applied to the rail as bending stresses, axial stresses, and Hertzian pressure, from rolling contact. The structure of a conventional railway track contains elements such as the rails, the sleepers including rail pads and fastening elements (e.g. clips, the ballast) bed and the subgrade.

Esveld [6] showed that highest stresses occur at the running surface of the rail where the wheel-rail contact stresses typically can reach 1500MPa for an axle load of 25KN. The stresses between

rail and sleeper are much smaller; in the order of 2.5MPa and between the ballast and the subgrade is only 50kPa. The ballast causes damping of dynamic forces during train passages.

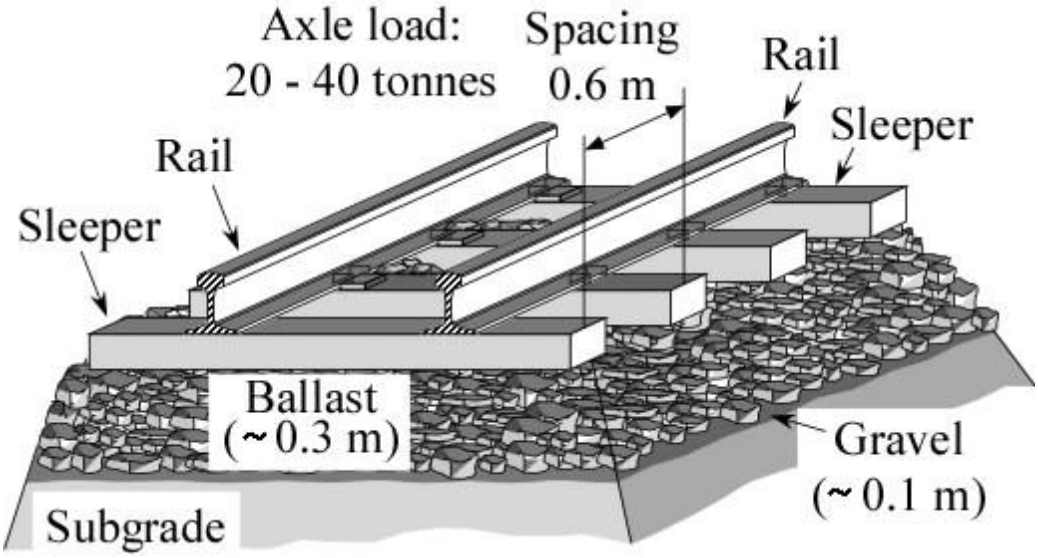

Figure 3.4: Basic elements of a railway track (dimensions according to) [5]

The propagation of a fatigue crack in a rail is driven by the contact stresses as well as bending and shear stresses arising from the load during wheel passage. These stresses are superimposed by further loading components such as residual stresses from manufacturing and thermal stresses which depend on the ambient temperature. The complex longitudinal stress state in a rail is illustrated in Figure 3.5. Additionally, the rail is subjected to longitudinal and lateral forces as shown in Figure 3.6.

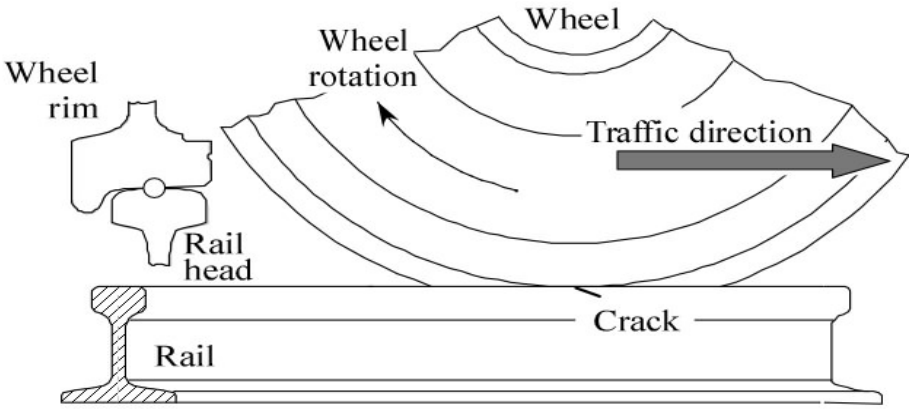

Figure 3.5: A wheel rolling on a continuously welded rail

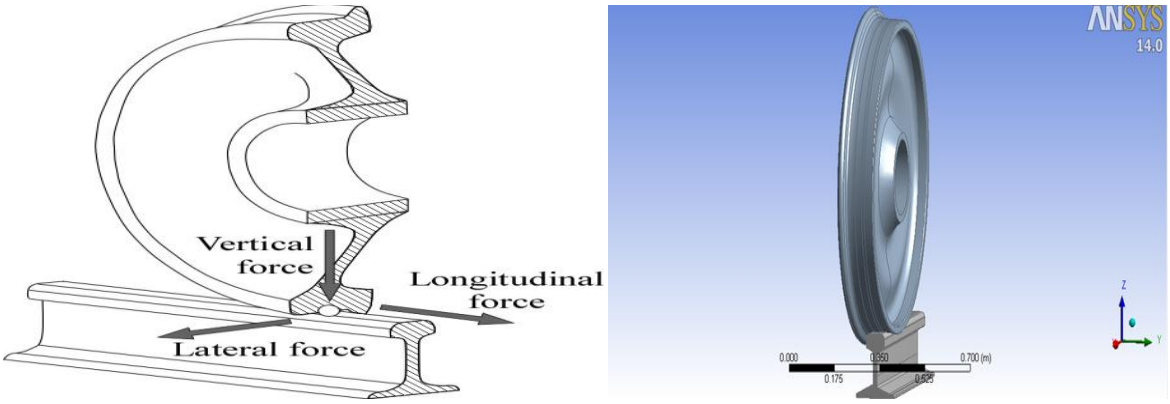

Figure 3.6: Vertical, longitudinal and lateral forces introduced by a railway wheel on a rail.

3. 3.1 Rail Stress Due to Wheel Loading

Fatigue in rail and wheel is concerned with Rolling Contact Fatigue which is produced during rolling movement under the effect of alternative contact stresses [27]. Contact forces between the wheel and rail produce stresses which guide material behavior to the elastic or elastic-plastic surface.

3.3.1.1 Bending Stress

The bending stresses for railroad rail arise from the static axle load which is usually between 8 and 22.5tonnes and its dynamic magnification by a moving train. The overall magnitude also depends on the up and down motion of the sleepers, i.e., on the quality of the grounding of the track**.** Usually, quite different types of vehicles with different axle loads are operated on one track. A contribution to the bending stresses comes also from the weight of the rails itself. Defects in the running surface of the rails such as joints, dips and twists and irregularities in the wheel such as flats and out-of-roundness may play a role as well.

Rail bending comprises a vertical and a lateral component. Based on the beam-on-elastic foundation theory for plane bending applied to rails by Zimmermann (according to [19]) the bending moments M_y and M_z for continuous portions of rails can be determined by:

$$M_y(x) = -\frac{F_V}{4\lambda_V}(\cos\lambda_V x - \sin\lambda_V x) * \exp(-\lambda_V x) \quad \text{----------3.10}$$

And

$$M_z(x) = -\frac{F_L}{4\lambda_L}(\cos\lambda_L x - \sin\lambda_L x) * \exp(-\lambda_L x)$$----------3.11

With x being the longitudinal position on the rail, F_V is vertical wheel load, and F_L lateral wheel load and λ_V and λ_L are parameters which depend on the rail geometry and the vertical and lateral foundation stiffness k_V and k_L. These are different for high-speed tracks, tracks for mixed traffic etc. Assuming $k_L = 0.85\ k_V$ as assumed in [23], λ_V and λ_L are obtained as:

$$\lambda_V = \sqrt[4]{\frac{K_V}{4EI_{yy}}}$$----------3.12

$$\lambda_L = \sqrt[4]{\frac{8.85K_V}{4EI_{ZZ}}}$$----------3.13

Where E is the modulus of elasticity of the rail steel and I_{yy} and I_{zz} are the second area moments of inertia with respect to the horizontal and vertical axis respectively, through the rail centroid. Values for I_{yy} and I_{zz} for some common rail sections are given in Table below.

Table 3.3: Second area moments of inertia for some rail profile [19]

Rail type (EN 13674)	60 E 1	56 E 1	54 E 3		
Previous designation	UIC 60	BS 113 lb BR Variant	DIN S54	JIS 60	136 RE
I_{yy}	3038cm^4	2321cm^4	2074cm^4	3083 cm^4	3950cm^4
I_{zz}	512cm^4	422cm^4	355cm^4		604cm^4

The formulae above are strictly valid only when the external loading and the support forces pass through the shear centre axis of the rail.

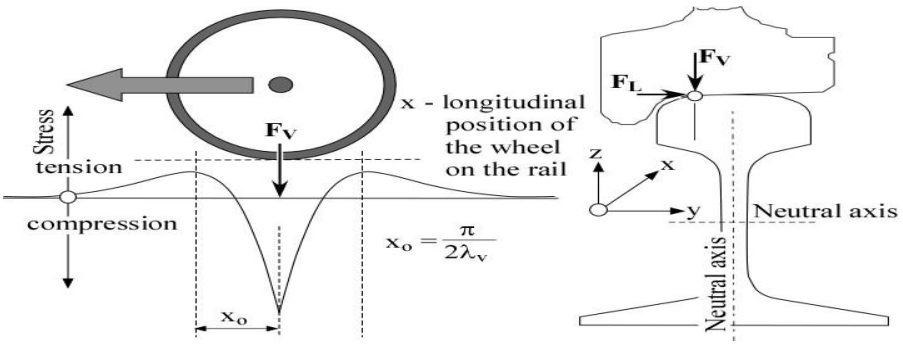

Figure 3.7: Rail head bending stress as a function of the wheel position (left); Lateral and eccentric vertical loading, F_L and F_V, of a rail (right). [19]

According to Eq. (3.10) the maximum tensile stress at the rail head surface occurs at a distance

$x_o = \frac{\pi}{2\lambda_V}$ ----------3.14

Although the bending stresses induced by the lateral load contribute to fatigue damage, bending stresses induced by the vertical load dominate rail failure.

3.3.1.2 Shear stresses

Wheel load also generates shear stresses in the rail section. Shear stresses play a major role in rails with cracks where they cause mixed mode loading conditions as shown in Figure 3.8.

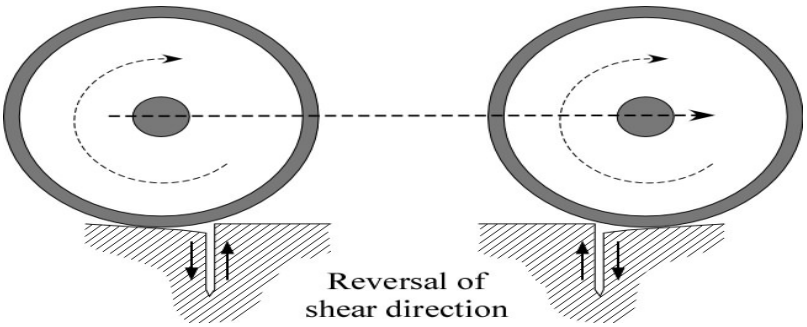

Figure 3.8: Shear loading of a vertical crack during wheel passage. Mode II loading mode is shown. At the ends of a semi-elliptical surface crack also mode III loading will occur.

3.3.1.3 Dynamic effects

Dynamic effects are due to car and bogie motions**.** Dynamic response of the track including its ballast bed and subgrade which makes the wheel loads vary at frequencies up to 10 Hz [19]. Stresses in the wheel and rail contact area at dynamic load modes usually occur in the elastic-plastic areas and loading this area usually leads to a breakage which is a result of low cyclic fatigue. In wheel and rail contact, plastic deformation gradually occurs [27].

For a static axle or wheel load, the dynamic load F_V (dyn) can be modeled as a statistical distribution, the upper bound of which can be used as worst condition for design purposes.

This is realized by multiplying the static load with a magnification factor K_{dyn} as:

F_V (dyn) = K_{dyn} · F_V (stat)----------3.15

The magnification factor depends on the properties and quality of the train and the track**,** and on the train speed. As an example, Deutsche Bahn recommends [19]:

K_{dyn} = 1+3*n*φ ----------3.16

With n= 0.15 to 0.25 for different types of tracks and φ is coefficient due to speed

$$\varphi=\begin{cases} 1 \; for \; v \leq 60km/hr \\ 1+\frac{0.5(v-60)}{190} \; for \; 60 \leq v \leq \frac{300km}{hr} passenger \; train \\ 1+\frac{0.5(v-60)}{80} for \; 60 \leq v \leq \frac{140km}{hr} freight \; train \end{cases}$$ ----------3.17

The irregularities in the rails (e.g. at sites damaged by spalling, at rail joints or, corrugation) and in the wheels (e.g. out-of roundness, flat spots) can significantly increase the dynamic effect, particularly at high speed.

3.3.1.4 Thermal Stresses

Thermal stresses in the rail develop due to the difference between the neutral temperature of the rail and the service temperature. If the service temperature is higher than the neutral temperature compressive stresses are built up and there is the danger that these may be released by buckling in the rail, with risk of train derailment, an effect on the rail which sometimes is called “sun kinks”. For the service temperature that is lower than the neutral temperature, tensile thermal stresses arise which act as an additional static loading component together with the wheel loads and the residual stresses.

For continuously welded straight rail tracks the thermal stress σ_T can be determined as:

$\sigma_T = \alpha E(T_N - T)$----------3.18

where, α is the coefficient of thermal expansion (in the order of 12×10^{-6}/ ^{o}C at 20°C for rail steels), E the modulus of elasticity (Young's modulus), T_N the neutral rail temperature and T the service temperature.

The neutral rail temperature is the temperature at which the longitudinal force in the rail is zero. This refers to the temperature at which the track has been installed, i.e. the rail is then anchored at the track and the delivered rail lengths are joined by welding.

3.4 Crack Initiation and Growth

Cracks start at rolling contact surfaces as a result of the accumulation of shear deformation from repeated rolling – sliding contact loading. In this paper, initiation may be considered to have occurred when stage I is complete. In railway tracks, this corresponds to crack sizes of about 0.5mm. Ringsberg (2001) explained these three phases with the help of an illustration.

The life of a fatigue crack is normally divided in to three phases covering crack initiation and growth (Miller, 1997) as shown in the figure below (fig.3.9).

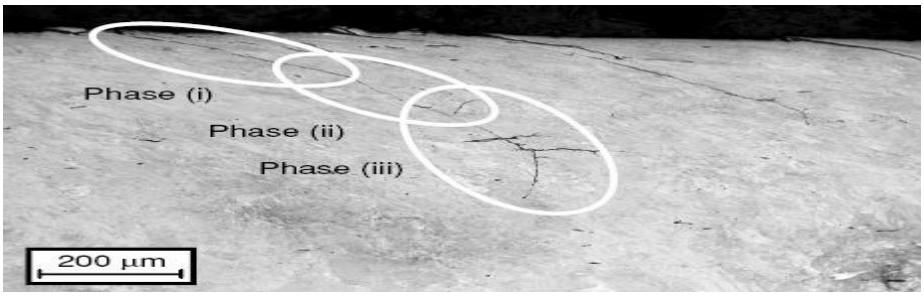

Figure 3.9: Three phases of RCF initiated crack propagation [Ringsberg, 2001]

The three mechanism model of RCF initiated crack growth proposed by Fletcher and Beynon (2000) is a prediction model for crack growth propagation. In this study, the tensile stress intensity factors are compared for different modes and tensile crack growth. Thereafter a decision is made as to whether or not crack growth will take place under particular loading conditions.

3.4.1 Crack propagation

Fracture mechanics often plays a role in life prediction of components that are subject to time dependent crack growth mechanisms such as fatigue or stress corrosion cracking. The rate of

cracking can be correlated with fracture mechanics parameters such as the stress-intensity factor, and the critical crack size for failure can be computed if the fracture toughness is known. In fracture mechanics, the fatigue crack growth rate in metals can usually be described by the following empirical relationship:

$$\frac{da}{dN} = C(\Delta K)^m \text{----------} 3.19$$

Where da/dN is the crack growth per cycle, ΔK is the stress-intensity range, and C and m are material constants. In the above empirical equation C is the slope of the curve in the linear region and m is the value found by extending the straight line to the stress intensity factor where it is 1 MPa (m) $^{1/2}$. The constant C in the equation includes effects of material, loading frequencies, mean load and environment. The constant m in the equation is an empirical constant which is in the range of 2 and 7. For ductile materials exponent m is between 2 and 4.

In accordance with the principles of elastic plastic fracture mechanics, there is a critical magnitude of stress intensity factor ahead of the crack tip, (K_{Ic} for mode I loading) beyond which unstable crack growth sets in and causes premature material failure. Incidentally K_{Ic} is dependent on both the RCF crack size and the range of operating cyclic stress.

3.4.2 Linear Elastic Fracture Mechanics (LEFM)

Linear elastic fracture mechanics is a practical analytical tool for studying structural fracture, where the plastic deformation surrounding a crack tip is small. Fracture mechanics deals with the conditions under which cracks form and grow. As a consequence, fracture mechanics can be used in structural design to determine acceptable stress levels, defect sizes, and material properties for certain working conditions [29]. Linear elastic fracture mechanics is based on an analytical procedure that relates the stress field in the vicinity of the crack tip to the nominal stress in the structure, to the size, shape, and orientation of the crack, and to the material properties of the structure [29]. Elasticity is defined by a fully recoverable response, a component loaded and unloaded without any permanent change to its shape. Plasticity and fracture both involve permanent shape changes under load. Plasticity is shape change without cracking, whereas fracture involves the creation or propagation of a crack that separates a portion of the component from the remainder. The occurrence of flaws in a structural component is an unavoidable circumstance of material processing, fabrication, or service. Flaws may appear as

cracks, voids, metallurgical inclusions, weld defects, design discontinuities or some combination of these. Cracks are especially likely to be found in any service hardware after some usage has occurred.

The method used to analyze crack propagation is LEFM. This approach uses the flaw size and shape, component geometry, loading conditions and the material property fracture toughness to determine the rate of growth.

3.4.3 Mode of fracture

Consider a cracked plate to distinguish several manners in which a force can be applied on the plate which might enable the crack to propagate. Irwin [29] proposed a classification corresponding to the three situations represented in Figure 3.10.

Mode 1: opening mode: the body or structure is loaded by tensile forces such that the crack surfaces are pulled apart in the y direction. The deformed surfaces are symmetric with respect to the planes perpendicular to the y-axis and the z-axis.

Mode II: sliding mode: the body or structure is loaded by shear forces parallel to the crack surfaces which slide over each other in the x-direction. The deformed surfaces are symmetric with respect to the plane perpendicular to the z-axis and skew symmetric with respect to the plane perpendicular to the y-axis.

Mode III: tearing mode: the body or structure is loaded by shear forces parallel to the crack front and the crack surfaces slide over each other in the z-direction. The deformed surfaces are skew-symmetric with respect to the plane perpendicular to the z-axis and the y-axis.

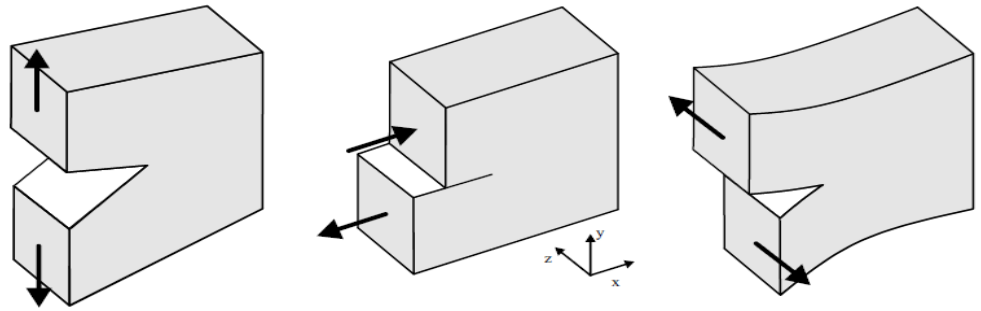

Figure 3.10: fracture Modes: a) mode I-opening, b) mode II-sliding, c) mode III-tearing [28]

3.4.4 Stress Intensity Factor

The stress intensity factor "*K*" is used in fracture mechanics to predict the stress state (stress intensity) near the tip of a crack caused by a remote load or residual stresses [29]. It is a theoretical construct usually applied to a homogeneous, linear elastic material and is useful for providing a failure criterion for brittle materials, and is a critical technique in the discipline of damage tolerance. The concept can also be applied to materials that exhibit small-scale yielding at the crack tip.

3.5 Numerical Examples

3.5 .1 Numerical Example for Hertzian Contacts

Considering a standard Railway Vehicle car with axle load 25ton and wheel diameter D = 920mm, slowly rolling in the x-direction on a straight rail with railhead radius 300 mm(source ERC and UIC). The wheel vertical load (contact load) applied on rail for this case is:

Fz = mg = (25000 kg /2) × 9.81 m/s2 = **122.625KN** (no dynamic magnification factor is considered).

For the calculation of the Hertzian contact pressure the radii are R_1= 0.460 m, R_1' = ∞, R_2= ∞ and R_2' = 0.300 m. The material parameters are taken as E_1 =E_2= 207GPa and υ_1=υ_2 = 0.30. The angle ψ between the radius of the wheel and rail is ψ =π/2

Substituting these radii values in equations 3.7 and 3.8 gives:

A+B=$\frac{1}{2}\left(\frac{1}{R_1}+\frac{1}{R_1'}+\frac{1}{R_2}+\frac{1}{R_2'}\right)$ = **2.7536/m**

A-B = $\frac{1}{2}\sqrt{\left(\frac{1}{R_1}-\frac{1}{R_1'}\right)^2+\left(\frac{1}{R_2}-\frac{1}{R_2'}\right)^2+2\left(\frac{1}{R_1}-\frac{1}{R_1'}\right)\left(\frac{1}{R_2}-\frac{1}{R_2'}\right)(\cos(2\psi))}$ =**0.5842/m**

Then, the angle θ can be calculated as:

$\cos(\theta)=\frac{B-A}{A+B}$ =0.5842/2.7536=**0.21215**

$\boldsymbol{\theta}$**= 77.75°** from equation 3.9.

Then, by interpolation, the values of m and n can be determined from the table 3.2 and their values are:

m =1.1613, and n = 0.872

Case-1(axle load 25 tons), the semi-axes are:

$$a = m \sqrt[3]{\frac{3\pi}{4}\frac{(K_1+K_2)N}{(A+B)}}$$

$k_1 = K_2 = \frac{1-{\nu_1}^2}{\pi E_1} =$ **$1.3993*10^{-12}$**

a = 0.00772m = 7.72mm using equation 3.2 and

$$b = n \sqrt[3]{\frac{3\pi(K_1+K_2)N}{4(A+B)}}$$

b = 0.00576m = 5.76mm (using equations 3.4)

Thus, the calculation yields the maximum Hertzian pressure: $\mathbf{P_o = \frac{3N}{2\pi ab}}$

=1320.1MPa using equation 3.2

Including the dynamic effect for extreme case:

Case-2 (axle load 25 tons with dynamic magnification) for a passenger train travelling at a speed of **70km/hr**, the magnification factor, K_{dyn} becomes **1.62** and a track coefficient of 0.2). Therefore wheel load or static load becomes **198.16KN**. (Using equations 3.15-3.17)

Accordingly, the semi axes **a= 9.03mm and b= 6.77mm and the maximum Hertzian pressure is Po= 1534.06Mpa**

Depending on the size and orientation of the contact ellipse the positions of the contact point may be shifted in different directions based on the magnitude of x or y. However, based on the above general Hertz contact formula and assumptions, the stress due to wheel/rail contact decreases and becomes zero if it goes far away from the centerline of the rail head. Similarly, the wheel/rail contact stress is inversely proportional to the major and minor axis of the contact ellipse.

Table 3.4: Calculation of Hertzian pressure

Case	Fz[KN]	Train Speed [km/hr]	R1 [mm]	R1' [mm]	R2 [mm]	R2' [mm]	a [mm]	b [mm]	Po [Mpa]
1	122.625	60	460	∞	∞	300	7.7	5.76	1320.1
2	198.16	70	460	∞	∞	300	9.06	6.8	1534.06
3	110.4	60	460	∞	∞	200	7.89	4.53	1474
4	110.4	70	460	-400	∞	300	5.85	11.05	816
5	98.1	80	460	∞	∞	300	11.37	8.54	482.4
6	160	80	460	∞	∞	1000	11.98	7.17	889.4

Case 2 (K_{dyn}=1.62) and case 6 (k_{dyn}=1.632) includes dynamic effects

For analysis of the crack propagation, the following axle loads are chosen. The track in this case is assumed as a mixed track that is it used for different axle loads with the maximum as a design axle load. The axle loads in case 2, 4 and 6 are dynamically magnified according to section 3.3.1.3. The considered train speed and their magnification factors (that are calculated by using equations 3.15-3.17) are shown in table below. The considered track coefficient factor, n is 0.2.

Table 3.5: Wheel loads for assumed axle load cases

Case	**Axle load[tons]**	**Speed of train[km/hr]**	**Wheel load, F_z[KN]**	**Dynamic magnification factor used**
1	25	60	122.625	
2	25	70	198.16	1.616(for n=0.2)
3	22.5	60	110.36	
4	22.5	70	178.35	1.616(for n=0.2)
5	20	80	98.1	
6	20	80	160.06	1.6316(for n=0.2)

3.5.2 Initiated Crack Model

In a material it is very difficult to avoid a crack formation. The stress and the deformation can also depend on how the cracks are loaded. In this study a crack which will be open in Y-direction, surfaces are separated from each other under mode-I will be studied.

3.5.2.1 Single Side crack model of Rail

To simulate a side cracked model of a railway rail, the head dimensions of a UIC 60(72mm width and 51mm height) rail is taken. It is assumed that the rectangular plate geometry shown in figure 3.11 which is used for the analysis is taken from the portion of rail steel head. A plate with dimension (40mm *x 50*mm *x 20*mm) with an initial crack (a = 10mm) is considered for 2-dimensional finite element analysis as shown below. The material properties of the steel used in this study were taken as Young's modulus, E = 207GPa, Poisson's ratio, υ = 0.3.

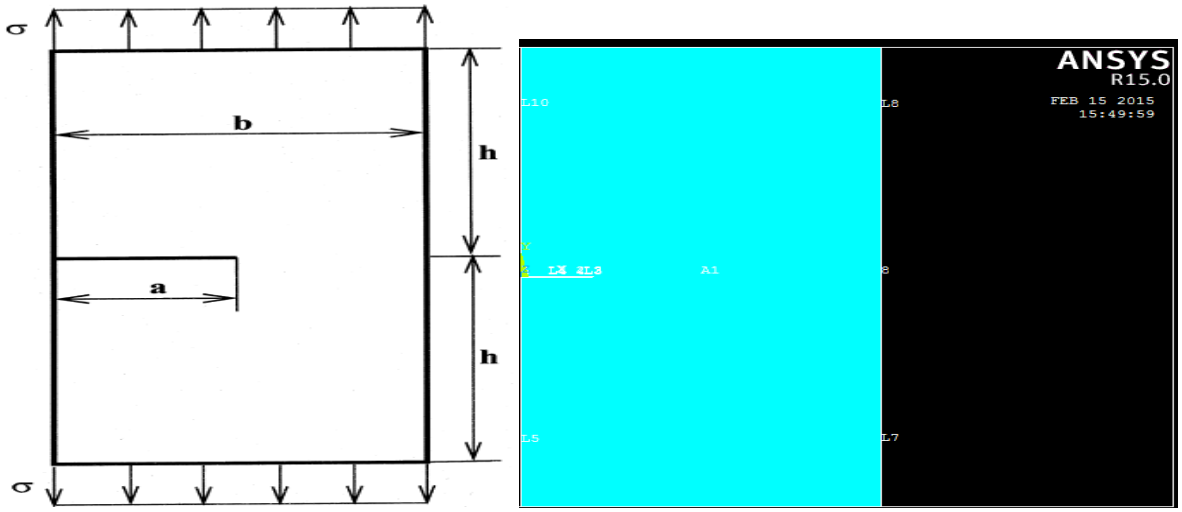

(a) (b)

Figure 3.11: (a) Finite plate with side crack. (b) FE model of a plate with a crack of 10mm.

The cracked plate is submitted under a uniform tensile load at both ends as shown in figure (a) above. The FE standard code ANSYS 15.0 release has been employed for modeling the problem. For mesh generation of the cracked plate, the element type 'PLANE183' of ANSYS code is used, as shown in Figure 3.12 (a). It is a higher order two-dimensional, 8-node element having two degrees of freedom at each node (translations in the nodal x and y directions), quadratic

displacement behavior and the capability of forming a triangular-shaped element, which is required at the crack tip areas. Due to the singular nature of the stress field in the vicinity of the crack, the singular elements shown in Fig. 3.12(b) are considered at each crack tip area, which are modeled with a finer mesh.

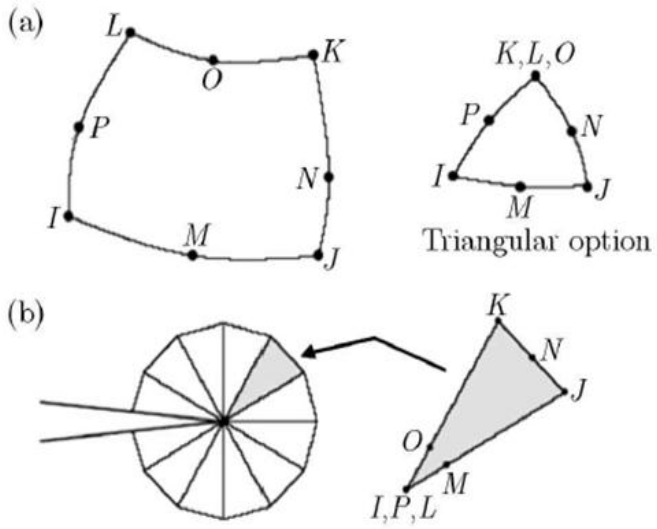

Figure 3.12: (a) PLANE 183 eight-node finite element and (b) singular option [30]

A typical FE model of the cracked plate is shown in Fig. 3.13. The special quarter point singular elements proposed by Barsoum are used for the modeling of the singular field near the crack tip. This mesh will serve to calculate the stress intensity factors *KI* and *KII* using the displacement extrapolation method implemented in ANSYS software.

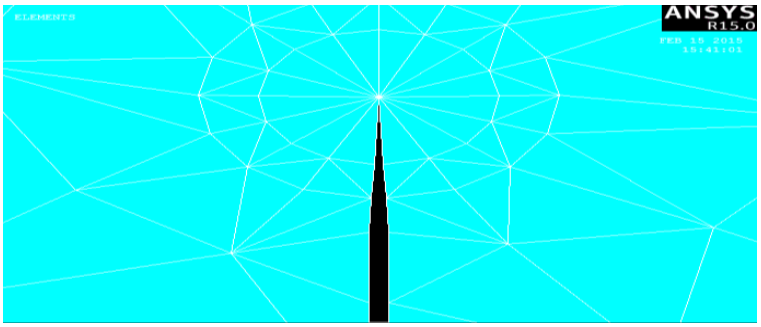

Figure 3.13: FE Model fine meshes around crack tip

In fracture mechanics, the stress intensity factor KI is frequently used to predict the stress state close to the crack tip. The stress may be caused by a remote load. It can be theoretically used to

provide a criterion for failure of homogeneous elastic materials. The magnitude of this factor depends on many factors, such as the geometry of the structure, the size of the crack and the location of the crack and type of load acting on the structure. In this paper, a plate of rail steel with side crack is chosen and a tensile stress is applied on it.

The analytical stress intensity factor *KI* for this problem is given by (Ewalds and Wanhill, 1989) as:

$K_I = F\sigma\sqrt{\pi a}$----------3.20

Where F is a crack geometry correction factor and given by [30];

$F = 1.12 - 0.231\frac{a}{b} + 10.55\left(\frac{a}{b}\right)^2 - 21.72\left(\frac{a}{b}\right)^3 + 30.39\left(\frac{a}{b}\right)^4$ with $\frac{a}{b} \ll 0.6$----------3.21

3.5.2.2 Finite Element Simulation of crack

Fracture analysis is a combination of stress analysis and fracture mechanics parameter calculation. The stress analysis is a standard linear elastic or nonlinear elastic plastic analysis. Because high stress gradients exist in the region around the crack tip, the finite element modeling of a component containing a crack requires special attention in that region[13]. Figure 3.14 shows crack tip zone.

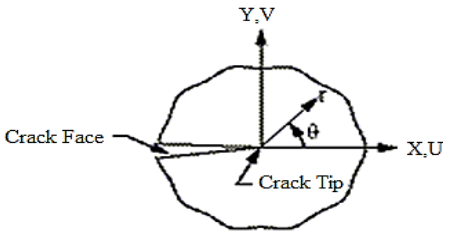

Figure 3.14: Crack coordinate system for 2D model [30]

To calculate stress intensity factor first local crack-tip or crack-front coordinate system is defined. The X - axis must be parallel to the crack face and the Y-axis perpendicular to the crack face as shown in Fig. 3.14. This coordinate system must be the active model coordinate system (CSYS) and results coordinate system (RSYS) when calculation of SIF is done by executing KCALC command. The co-ordinate system is then set as active co-ordinate system by selecting the

specified co-ordinate system and giving the reference number. The global co-ordinate system is changed to local co-ordinate system and the defined local reference number is specified.

Then the propagation path along the crack face is defined. This path along the crack face can be defined in two ways, one is half crack model which is used when the model is symmetric, and the second is full cracked model which is used when the model is asymmetric.

For modeling half crack, three points are chosen with the first one at the crack tip point or node and the other two along crack face as shown in figure 3.15 (a). For the full crack model five points are required with the first one at the crack tip point or node, two points along right face of the crack face and the rest two along the left face of the crack as shown in figure 3.15 (b).

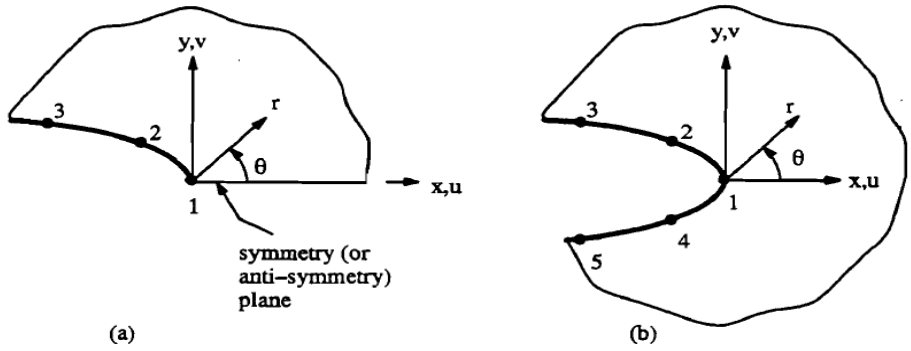

Figure 3.15: typical path definitions for a) half crack model and b) full crack model

3.6 Finite Element Modeling of Wheel / Rail Contact

In order to build a realistic model of wheel/rail contact problem a 3D elastic-plastic finite element model is needed. This model should be able to accurately calculate the 3D stress response in the contact region as well as includes both material and geometric nonlinearity. It may be used to simulate large and complex wheel motions, such as rotation, sliding, hunting movement and even dynamic impact response. Through Fine meshing techniques in contact region, the proposed model is made very efficient in computing and hardware requirements.

3.6.1 Modeling of wheel and Rail

A rail profile of UIC 60 and a wheel profile of S1002 are modeled using Catia V5R19 software as a separate part. The 3D geometric model of the wheel is generated by revolving the 3D curves that describe the profile of the wheel tread. The rail model is created by extruding railhead

profile curves a distance of 600 mm, which is the distance between the sleepers. The two model parts are then assembled in catia workbench using constraints contact surface to surface assembly. The assembly is then imported to the ANSYS workbench, updated and edited in ANSYS Mechanical APDL and saved as a new file. The file is then reopened using the mechanical APDL and the element type, material property, contact type and boundary conditions are applied.

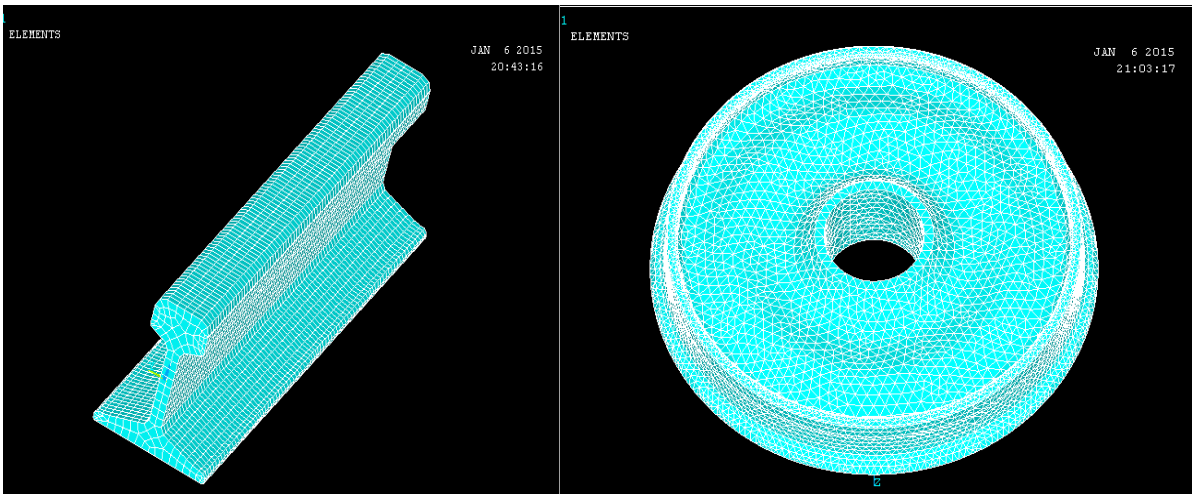

Figure 3.16: meshed rail (left) and meshed wheel (right) FE models

The two view of wheel-rail assembly for the new wheels and rails are shown in Figure below.

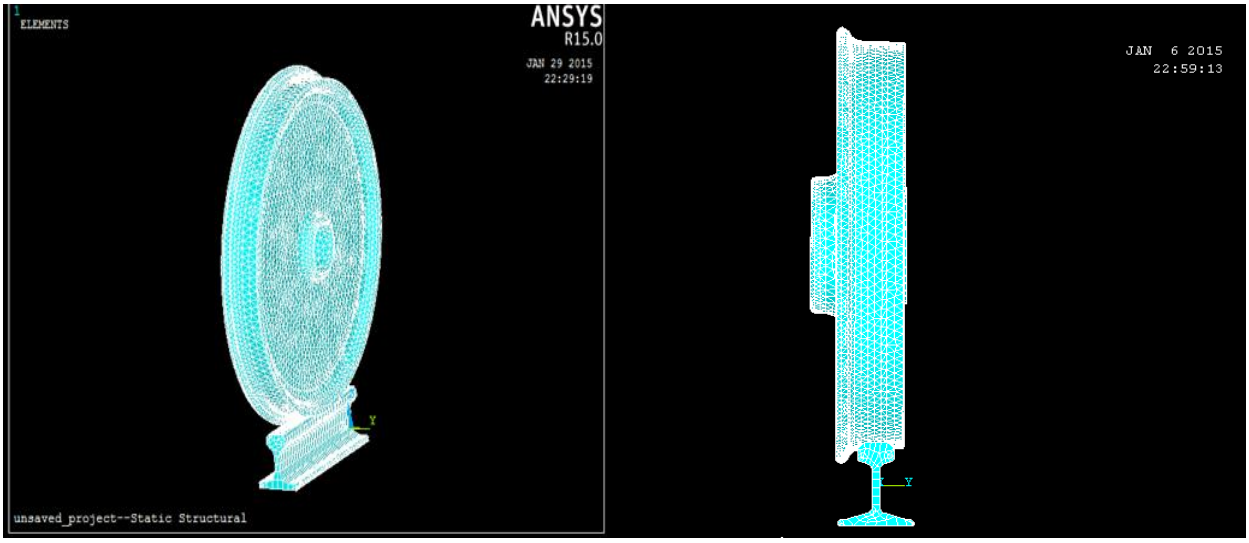

Figure 3.17: Meshed Wheel-Rail Assembly

Chapter Four

Analysis, Results and Discussion

4. 1 Numerical Analysis and Results

For the considered axle loads and wheel vertical loads calculated in table 3.5 the following analysis is made for stress intensity factor of mode-I, KI

Considering a rectangular plate (40mm width x 50mm height and 20mm thickness) with an initial crack (a = 10mm) as shown in figure 3.12 (a), for 2-dimensional finite element analysis. The material properties of the steel used in this study were taken as Young's modulus, E = 207GPa, Poisson's ratio, υ = 0.3

Stress intensity factor is given by: KI=$F\sigma\sqrt{\pi a}$

Where F is a crack geometry correction factor and given by [30];

F= 1.12- $0.231\frac{a}{b} + 10.55\left(\frac{a}{b}\right)^2 - 21.72\left(\frac{a}{b}\right)^3 + 30.39\left(\frac{a}{b}\right)^4$ with $\frac{a}{b} \ll 0.6$ and $2h/b > 1.0$

1. For a wheel load of **122.625KN and crack length of a=10mm and width b=40mm,**

F=1.12- $0.231\frac{10}{40} + 10.55\left(\frac{10}{40}\right)^2 - 21.72\left(\frac{10}{40}\right)^3 + 30.39\left(\frac{10}{40}\right)^4$

=**1.501**

The remote stress on the plate is given as:

$\boldsymbol{\sigma = \frac{F_Z}{bB}}$ **, where Fz= is vertical wheel load, b= is width and B= is thickness of the plate**

$\boldsymbol{\sigma = \frac{122625N}{0.04*0.02}}$**= 153.28MPa**

KI= 1.501*153.28MPa*$\sqrt{\pi * 0.01m}$

=40.78MPa$\sqrt{m}$

Similarly the following stress intensity factor values are tabulated for other cases for a crack length of a=10mm, 12mm, 14mm and 16mm

Table 4.1: Numerical stress intensity values for different crack lengths

case	**Wheel Vertical load(KN)**	**Remote Stress Applied,[MPa]**	**KI(stress intensity factor –mode-I) MPa$\sqrt{m}$**			
			Crack length			
			a=10mm, a/b=0.25, F=1.501	**a=12mm, a/b=0.3, F=1.6599**	**a=14mm, a/b=0.35, F=1.8564**	**a=16mm, a/b=0.4, F=2.1035**
1	122.625	153.28	40.78	49.4	59.67	72.29
2	**198.16**	**247.7**	**65.89**	**79.83**	**96.43**	**116.82**
3	110.4	138	36.71	44.48	53.72	65.08
4	**178.35**	**222.94**	**59.3**	**71.85**	**86.79**	**105.14**
5	98.1	122.625	32.62	39.52	47.74	57.83
6	**160.06**	**200.08**	**53.22**	**64.48**	**77.89**	**94.36**

4.2 Finite Element Results

Half of the geometry is modeled for Finite Element Analysis is used and symmetry boundary condition is applied on the symmetry plane:

ANSYS Main menu: **Solution → Define Loads → Apply → Structural → Displacement → Symmetry B.C. → on lines**

The crack surface is not restricted in its movement in any direction that is no boundary condition should be applied to that line. Of course, if a negative force is applied and the crack surfaces moves towards each other, a contact definition needs to be defined. But here we assume that the crack surfaces moves away from each other.

Apply the load on the top line of the model as pressure for each six cases of table 3.5. The pressure is defined positive in the negative normal direction; therefore a minus sign should be included when defining the pressure. The command is:

ANSYS Main menu: Solution → Define Loads → Apply → Structural → Pressure → On Lines,

Boundary Condition

Half model of the chosen plate is shown below. The boundary condition of the plate is: the plate is constrained at middle end node in the x-direction with 0 displacements. Then symmetry condition is applied on bottom line. The remote stress is applied on the top line so that the solution obtained is for a full model.

Figure 4.1: FE model of a plate

The next figure shows the meshed model of the plate. 2599 elements are created. The stress concentration key point is created at the crack tip point or node. Then the following load cases are applied for each crack and the solutions are shown.

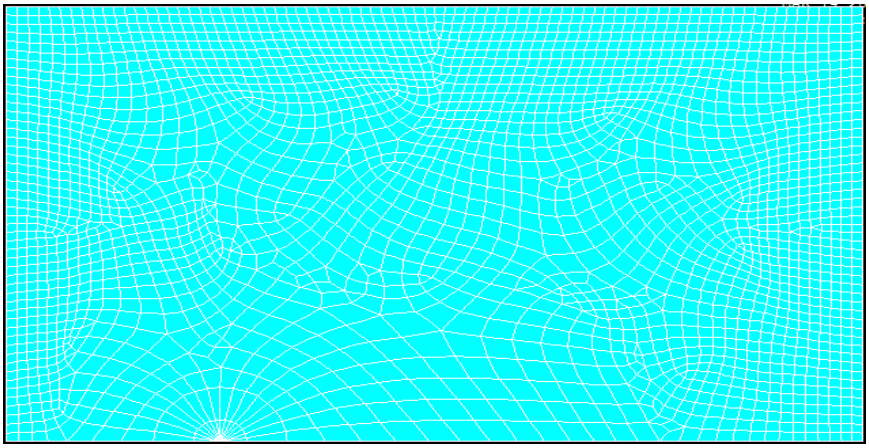

Figure 4.2: Meshed Model

For crack length, a=10mm

Case -1 when a pressure of **153.28MPa** is applied on the plate (crack length, a=10mm, width, b=40mm, 2h=50mm and thickness=20mm). Wheel vertical load is **122.625KN** and speed of train is V=60km/hr. no dynamic magnification factor.

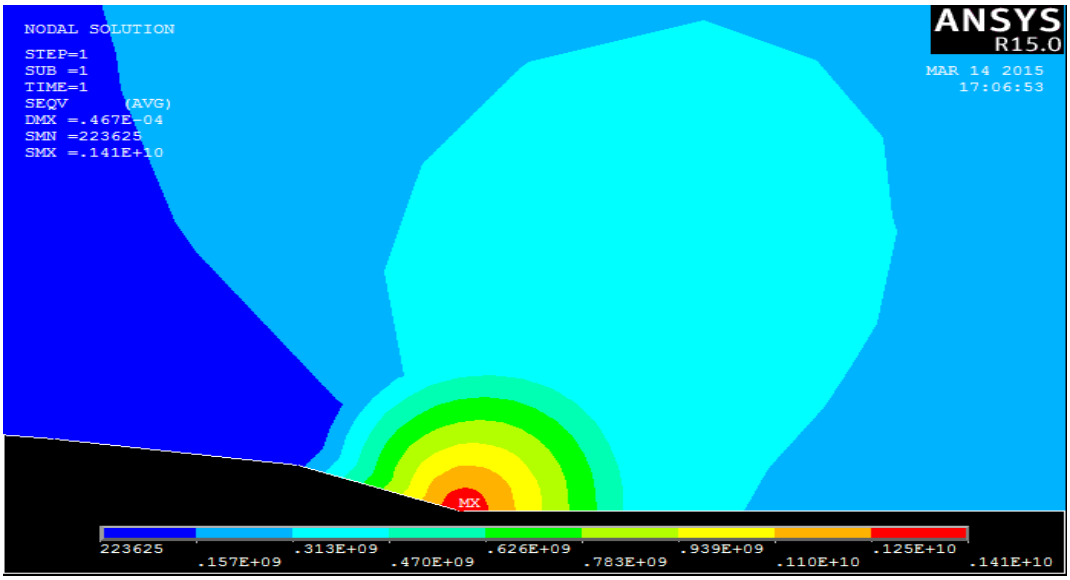

Figure 4.3: Nodal Von Mises Stress Solution for a=10mm and, σ=153.28MPa

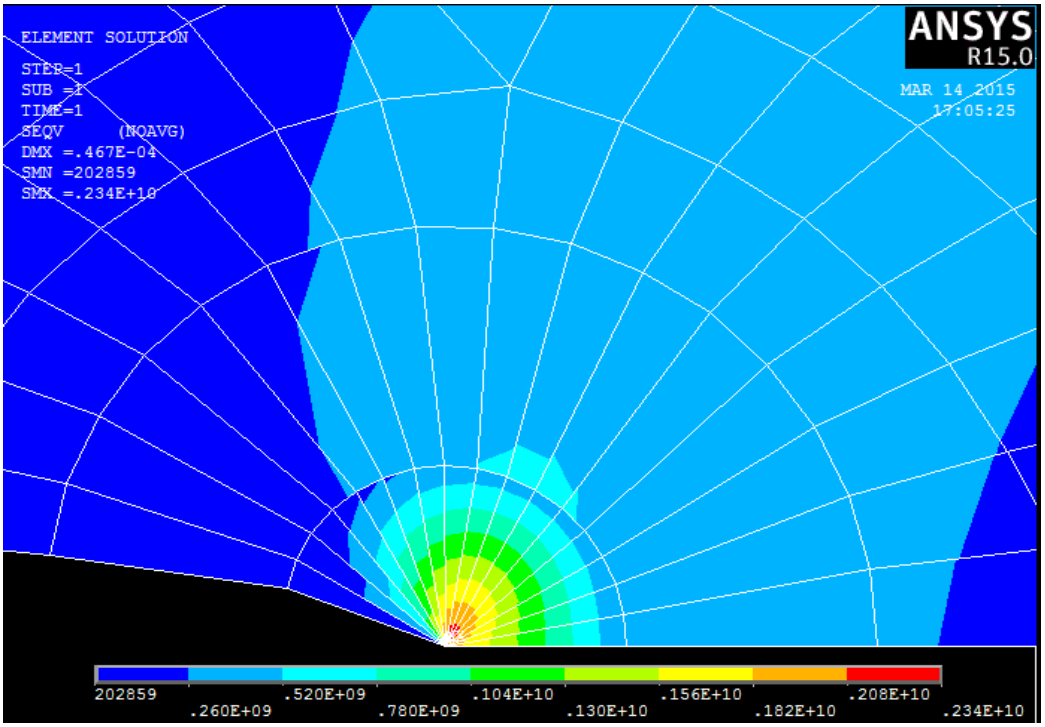

Figure 4.4: Element Von-Mises Stress solution for a=10mm and, σ=153.28MPa

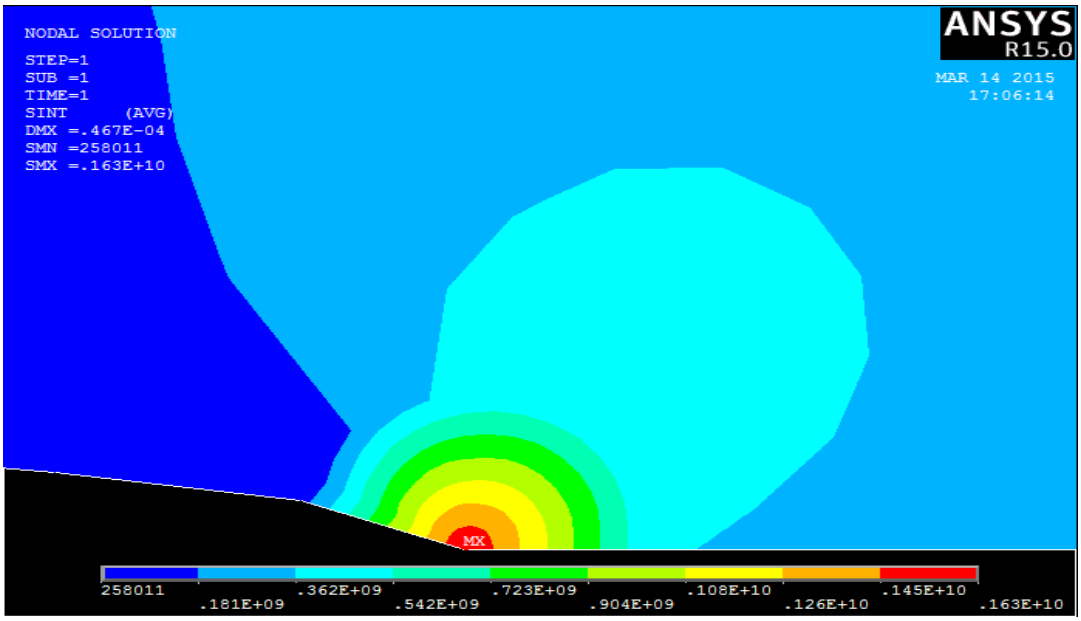

Figure 4.5: Nodal Stress intensity for a=10mm and, σ=153.28MPa

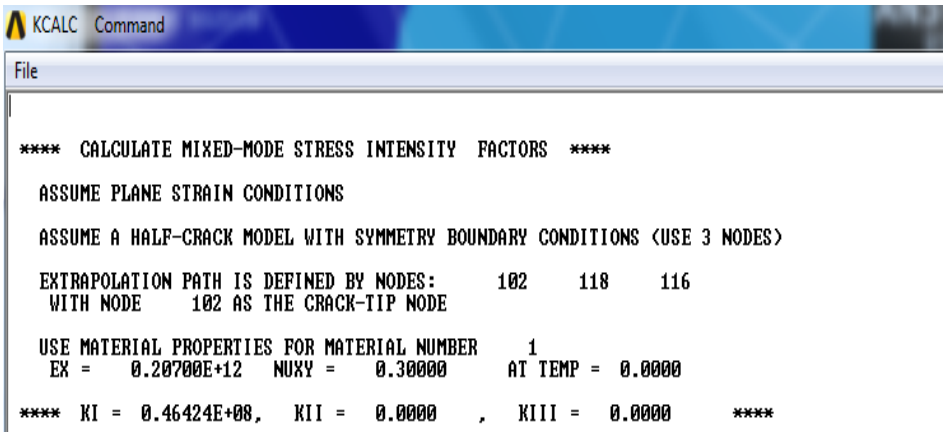

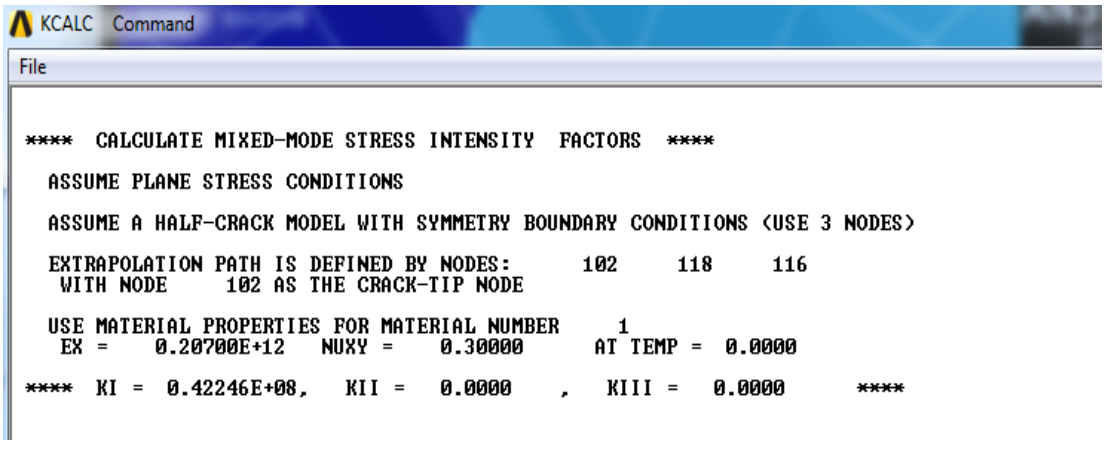

Figure 4.6: Stress Intensity Factor for a=10mm and, σ=153.28MPa

Case-2 when a pressure of **247.7 MPa** is applied on the plate (crack length a=10mm, width, b=40mm, 2h=50mm and thickness=20mm). Wheel vertical load is **198.16KN** and speed of train is **V=70km/hr**. dynamically magnified load. (k_{dyn}=1.616)

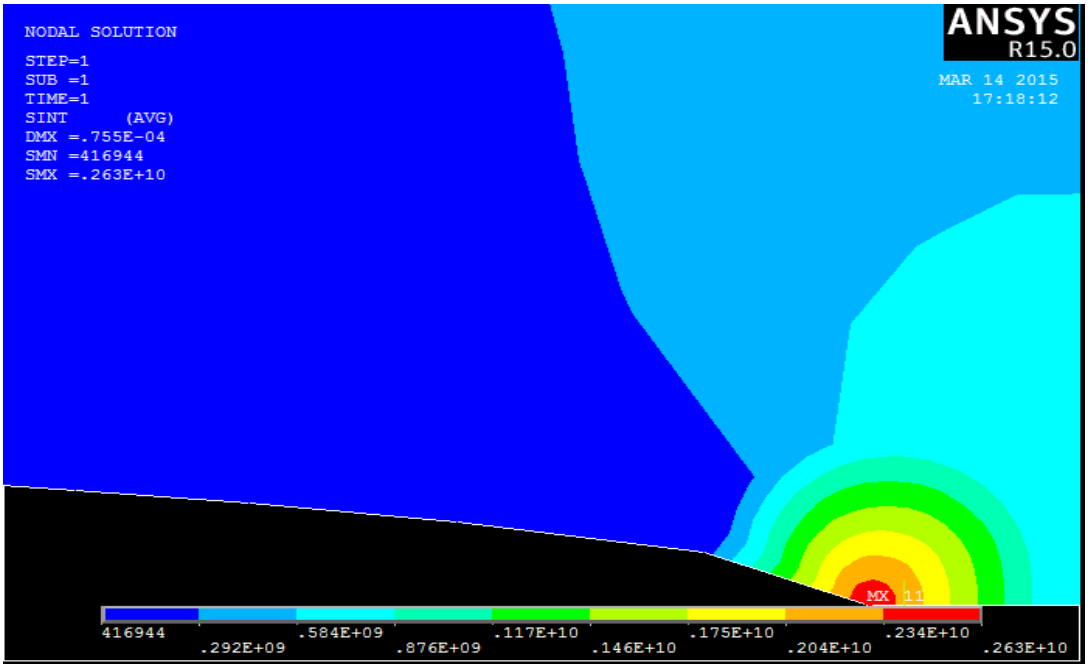

Figure 4.7: Nodal Stress Intensity for a=10mm and, σ=247.7MPa

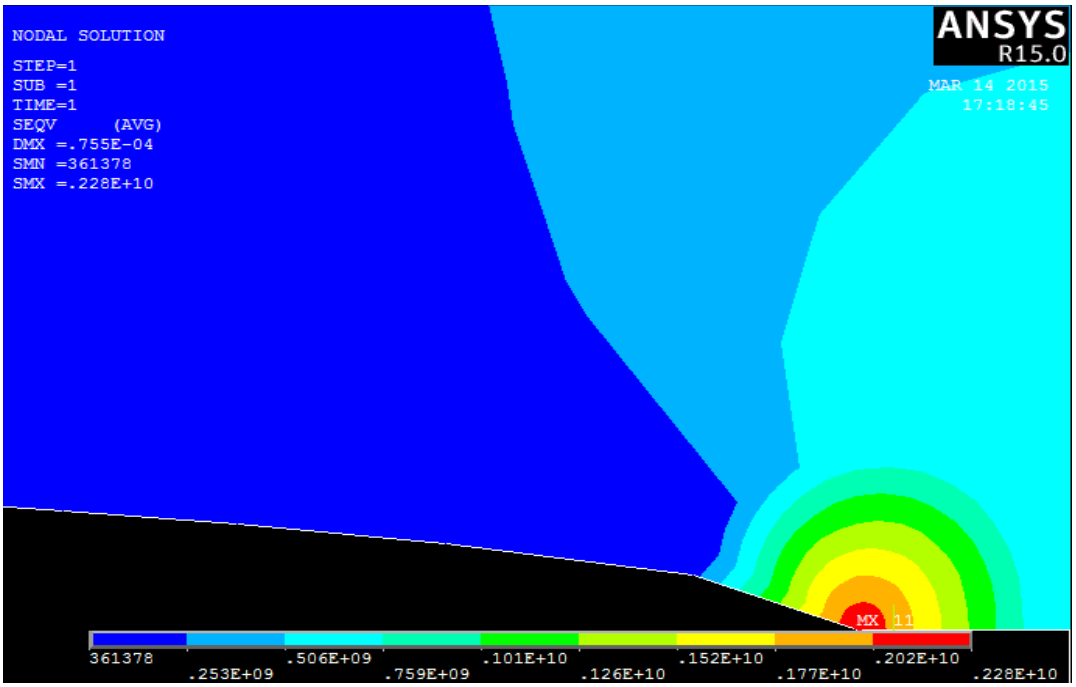

Figure 4.8 : Nodal Von-Mises Stress solution for a=10mm and, σ=247.7MPa

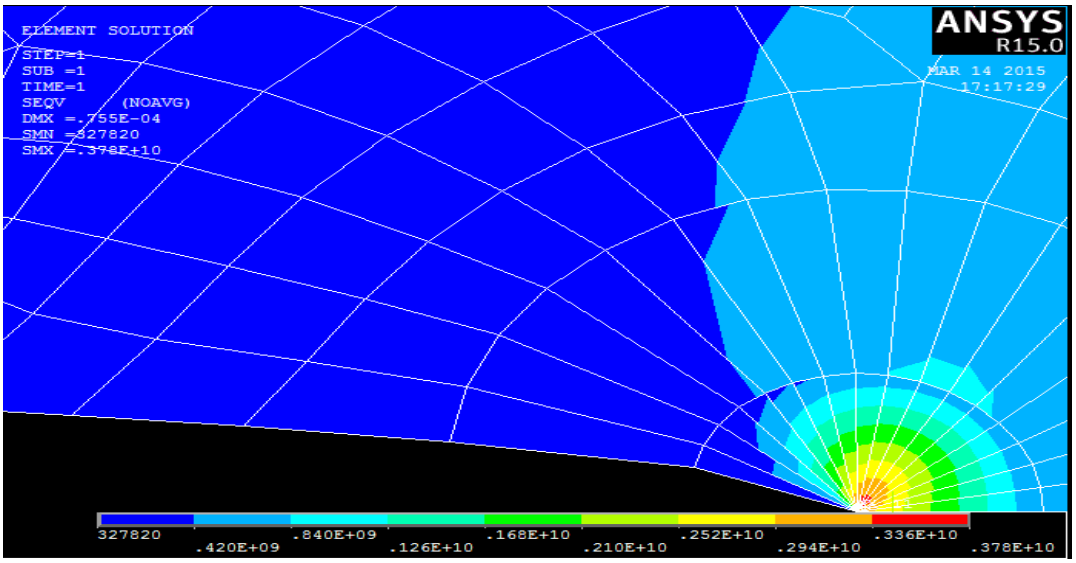

Figure 4.9: Element Von-Mises Stress solution for a=10mm and, σ=247.7MPa

```
****  CALCULATE MIXED-MODE STRESS INTENSITY  FACTORS  ****

  ASSUME PLANE STRAIN CONDITIONS

  ASSUME A HALF-CRACK MODEL WITH SYMMETRY BOUNDARY CONDITIONS (USE 3 NODES)

  EXTRAPOLATION PATH IS DEFINED BY NODES:      102     118     116
   WITH NODE     102 AS THE CRACK-TIP NODE

  USE MATERIAL PROPERTIES FOR MATERIAL NUMBER     1
   EX =    0.20700E+12   NUXY =    0.30000      AT TEMP =  0.0000

****  KI =  0.75021E+08,   KII =   0.0000    ,   KIII =   0.0000      ****
```

File

```
****  CALCULATE MIXED-MODE STRESS INTENSITY  FACTORS  ****

  ASSUME PLANE STRESS CONDITIONS

  ASSUME A HALF-CRACK MODEL WITH SYMMETRY BOUNDARY CONDITIONS (USE 3 NODES)

  EXTRAPOLATION PATH IS DEFINED BY NODES:      102     118     116
   WITH NODE     102 AS THE CRACK-TIP NODE

  USE MATERIAL PROPERTIES FOR MATERIAL NUMBER     1
   EX =    0.20700E+12   NUXY =    0.30000      AT TEMP =  0.0000

****  KI =  0.68269E+08,   KII =   0.0000    ,   KIII =   0.0000      ****
```

Figure 4.10: Stress intensity factor for a=10mm and, σ=247.7MPa

Case 3 when a pressure of **138MPa** is applied on the plate (crack length a=10mm, width, b=40mm, 2h=50mm and thickness=20mm). Wheel vertical load is **110.36KN** and speed of train is **V=60km/hr**. no dynamic magnifying factor is used.

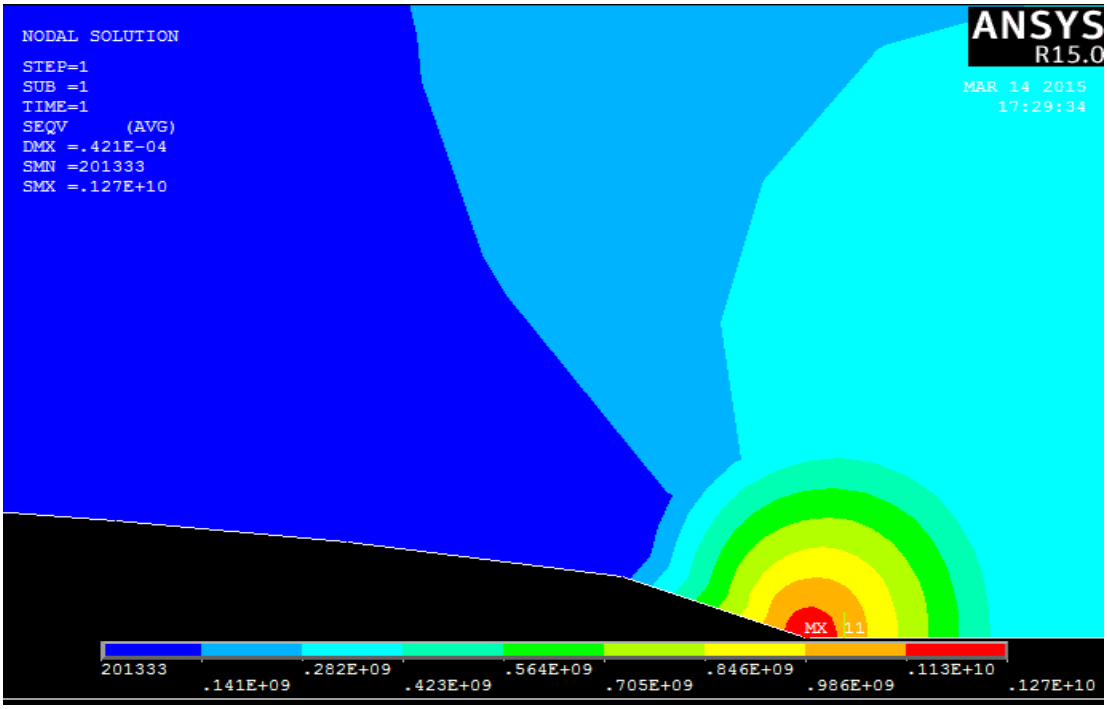

Figure 4.11: Nodal Von-Mises Stress solutions for a=10mm and, σ=138MPa

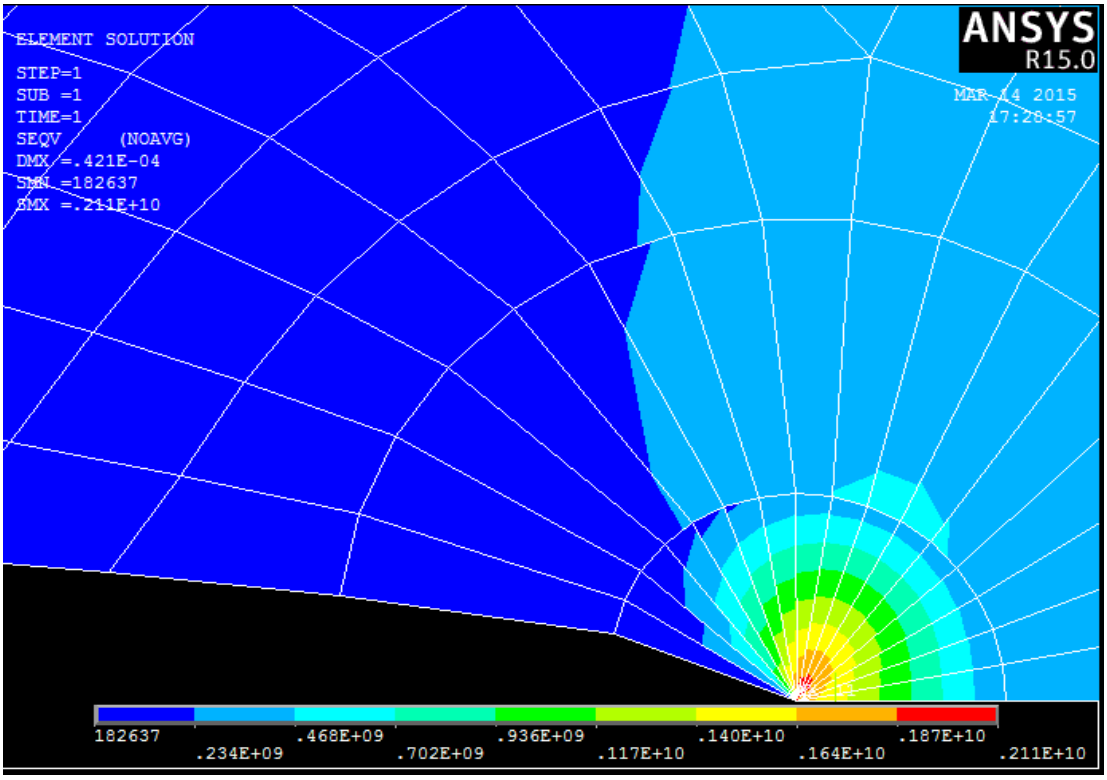

Figure 4.12: Element Von-Mises Solution for a=10mm and, σ=138MPa

```
****  CALCULATE MIXED-MODE STRESS INTENSITY  FACTORS  ****

  ASSUME PLANE STRAIN CONDITIONS

  ASSUME A HALF-CRACK MODEL WITH SYMMETRY BOUNDARY CONDITIONS (USE 3 NODES)

  EXTRAPOLATION PATH IS DEFINED BY NODES:      102     118     116
   WITH NODE     102 AS THE CRACK-TIP NODE

  USE MATERIAL PROPERTIES FOR MATERIAL NUMBER     1
   EX =    0.20700E+12   NUXY =    0.30000      AT TEMP =  0.0000

****  KI =  0.41796E+08,   KII =   0.0000    ,   KIII =   0.0000      ****
```

```
****  CALCULATE MIXED-MODE STRESS INTENSITY  FACTORS  ****

  ASSUME PLANE STRESS CONDITIONS

  ASSUME A HALF-CRACK MODEL WITH SYMMETRY BOUNDARY CONDITIONS (USE 3 NODES)

  EXTRAPOLATION PATH IS DEFINED BY NODES:      102     118     116
   WITH NODE     102 AS THE CRACK-TIP NODE

  USE MATERIAL PROPERTIES FOR MATERIAL NUMBER     1
   EX =    0.20700E+12   NUXY =    0.30000      AT TEMP =  0.0000

****  KI =  0.38034E+08,   KII =   0.0000    ,   KIII =   0.0000      ****
```

Figure 4.13: Stress intensity factor for a=10mm and, σ=**138**MPa

Case 4 when a pressure of **222.94MPa** is applied on the plate (crack length a=10mm, width, b=40mm, 2h=50mm and thickness=20mm). Wheel vertical load is **178.35KN** and speed of train is **V=70km/hr**. dynamically magnified load. (Kdyn=1.616)

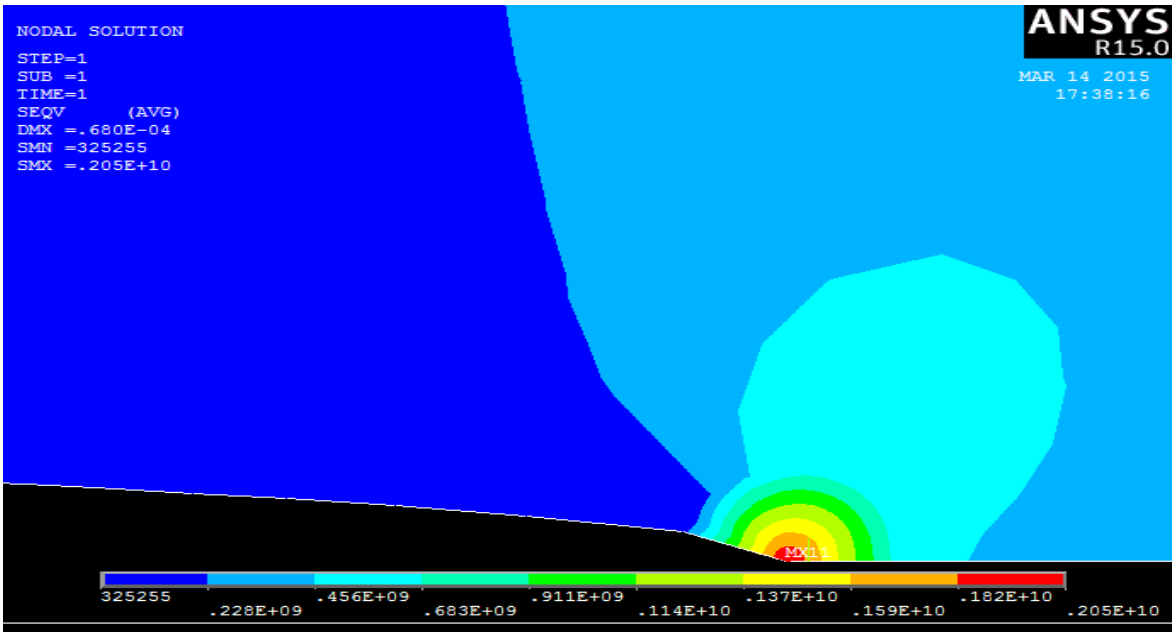

Figure 4.14: Nodal Von-Mises Stress Solution for a=10mm and, σ=222.94MPa

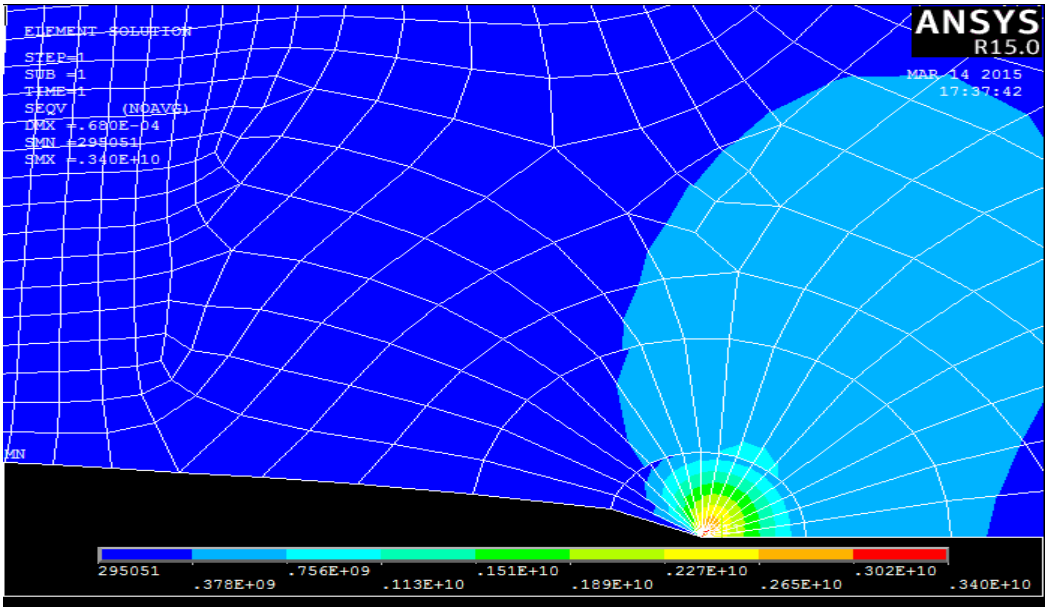

Figure 4.15 : Element Von-Mises Stress Solution for a=10mm and, σ=222.94MPa

File

```
****  CALCULATE MIXED-MODE STRESS INTENSITY  FACTORS  ****

  ASSUME PLANE STRAIN CONDITIONS

  ASSUME A HALF-CRACK MODEL WITH SYMMETRY BOUNDARY CONDITIONS (USE 3 NODES)

  EXTRAPOLATION PATH IS DEFINED BY NODES:      102     118     116
   WITH NODE     102 AS THE CRACK-TIP NODE

  USE MATERIAL PROPERTIES FOR MATERIAL NUMBER     1
   EX =    0.20700E+12   NUXY =    0.30000      AT TEMP =  0.0000

****  KI =  0.67522E+08,   KII =   0.0000    ,   KIII =   0.0000      ****
```

File

```
****  CALCULATE MIXED-MODE STRESS INTENSITY  FACTORS  ****

  ASSUME PLANE STRESS CONDITIONS

  ASSUME A HALF-CRACK MODEL WITH SYMMETRY BOUNDARY CONDITIONS (USE 3 NODES)

  EXTRAPOLATION PATH IS DEFINED BY NODES:      102     118     116
   WITH NODE     102 AS THE CRACK-TIP NODE

  USE MATERIAL PROPERTIES FOR MATERIAL NUMBER     1
   EX =    0.20700E+12   NUXY =    0.30000      AT TEMP =  0.0000

****  KI =  0.61445E+08,   KII =   0.0000    ,   KIII =   0.0000      ****
```

Figure 4.16: Stress intensity factor for a=10mm and, σ=222.94MPa

Case 5 when a pressure of **122.625MPa** is applied on the plate (crack length a=10mm, width, b=40mm, 2h=50mm and thickness=20mm). Wheel vertical load is **98.1KN** and speed of train is **V=80km/hr**. No dynamically magnification factor is used.

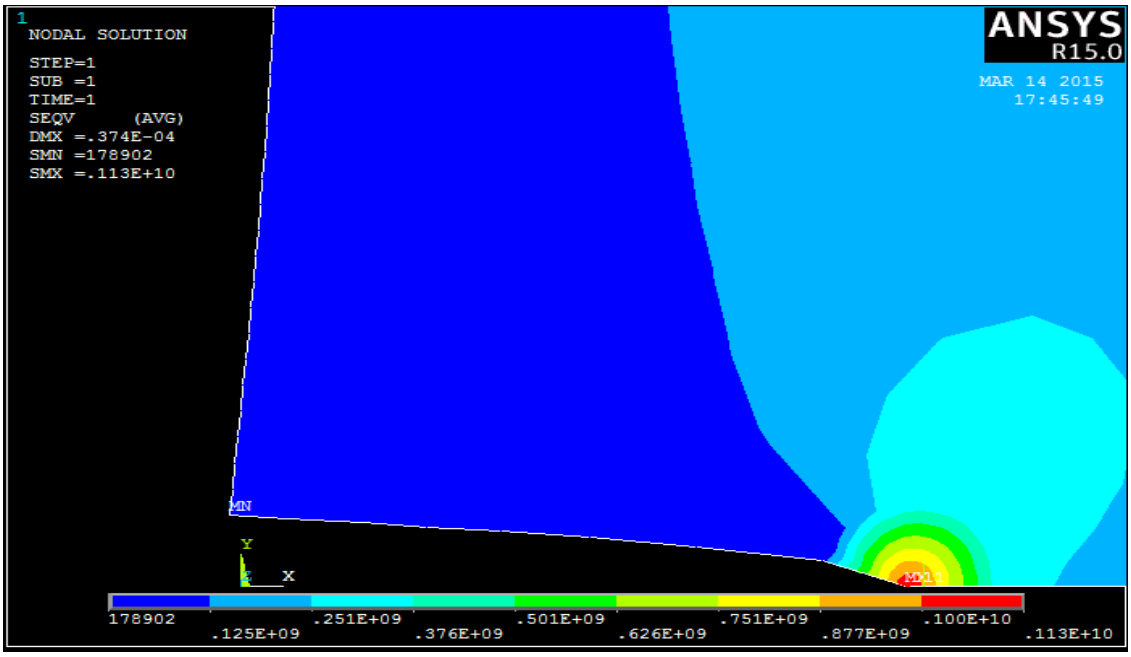

Figure 4.17 : Nodal Von-Mises Stress Solution for a=10mm and, σ=122.625MPa

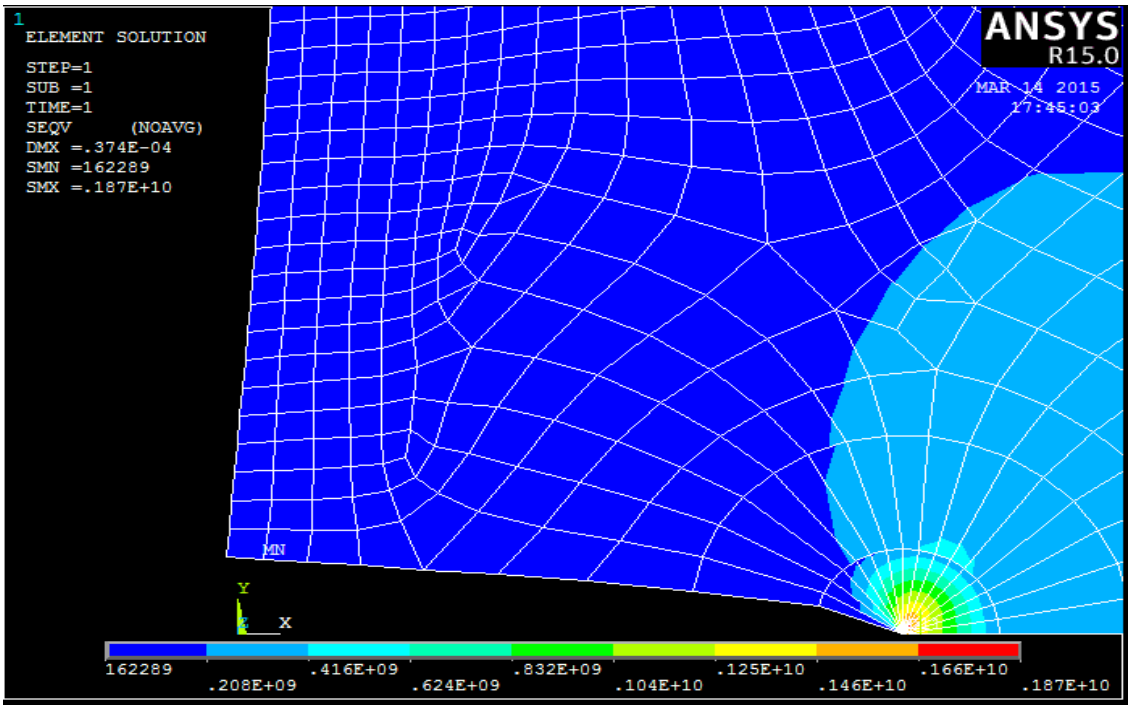

Figure 4.18 : Element Von-Mises Stresses solution for a=10mm and, σ=122.625MPa

File

```
****  CALCULATE MIXED-MODE STRESS INTENSITY  FACTORS  ****
  ASSUME PLANE STRAIN CONDITIONS
  ASSUME A HALF-CRACK MODEL WITH SYMMETRY BOUNDARY CONDITIONS (USE 3 NODES)
  EXTRAPOLATION PATH IS DEFINED BY NODES:      102     118     116
   WITH NODE     102 AS THE CRACK-TIP NODE
  USE MATERIAL PROPERTIES FOR MATERIAL NUMBER     1
   EX =    0.20700E+12   NUXY =    0.30000      AT TEMP =  0.0000
****  KI =  0.37140E+08,   KII =   0.0000    ,   KIII =   0.0000      ****
```

File

```
****  CALCULATE MIXED-MODE STRESS INTENSITY  FACTORS  ****
  ASSUME PLANE STRESS CONDITIONS
  ASSUME A HALF-CRACK MODEL WITH SYMMETRY BOUNDARY CONDITIONS (USE 3 NODES)
  EXTRAPOLATION PATH IS DEFINED BY NODES:      102     118     116
   WITH NODE     102 AS THE CRACK-TIP NODE
  USE MATERIAL PROPERTIES FOR MATERIAL NUMBER     1
   EX =    0.20700E+12   NUXY =    0.30000      AT TEMP =  0.0000
****  KI =  0.33797E+08,   KII =   0.0000    ,   KIII =   0.0000      ****
```

Figure 4.19: Stress intensity factor for a=10mm and, σ=122.625MPa

Case 6 when a pressure of **200.08MPa** is applied on the plate (crack length a=10mm, width, b=40mm, 2h=50mm and thickness=20mm). Wheel vertical load is **160.06KN** and speed of train is **V=80km/hr**. dynamically magnified load. (Kdyn=1.6316)

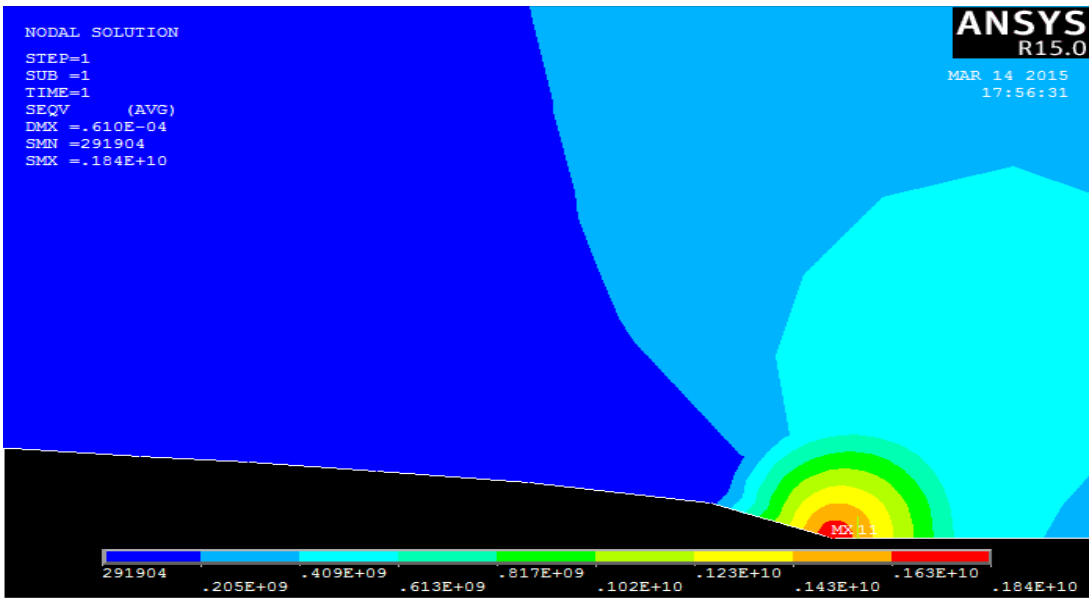

Figure 4.20 : Nodal Von-Mises Stresses Solution for a=10mm and, σ=200.08MPa

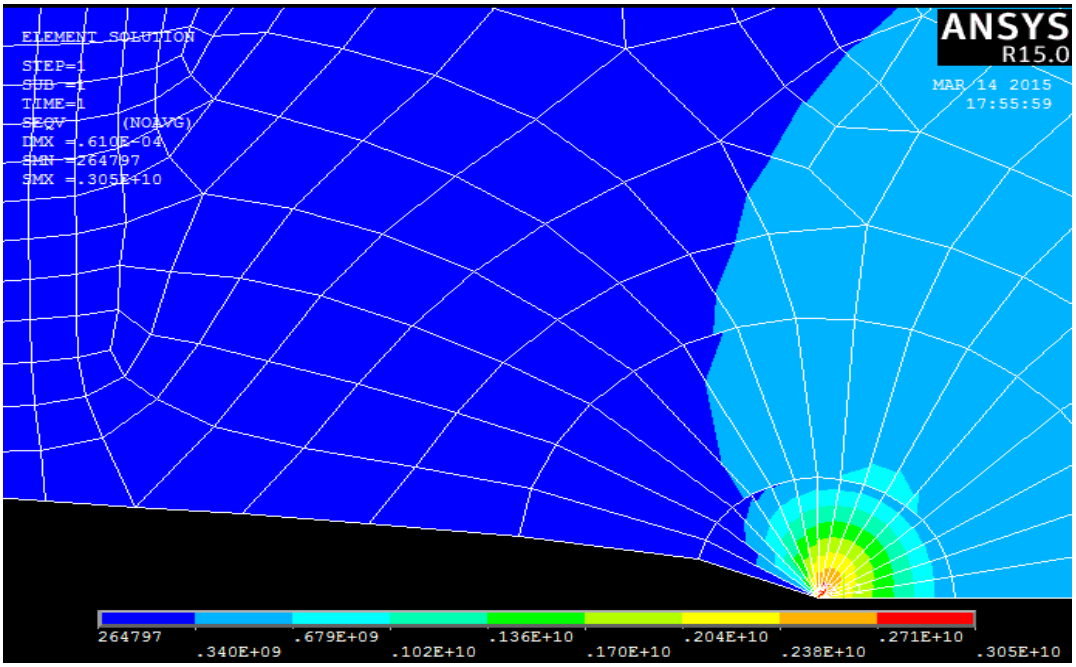

Figure 4.21: Element Von-Mises Stresses Solution for a=10mm and, σ=200.08MPa

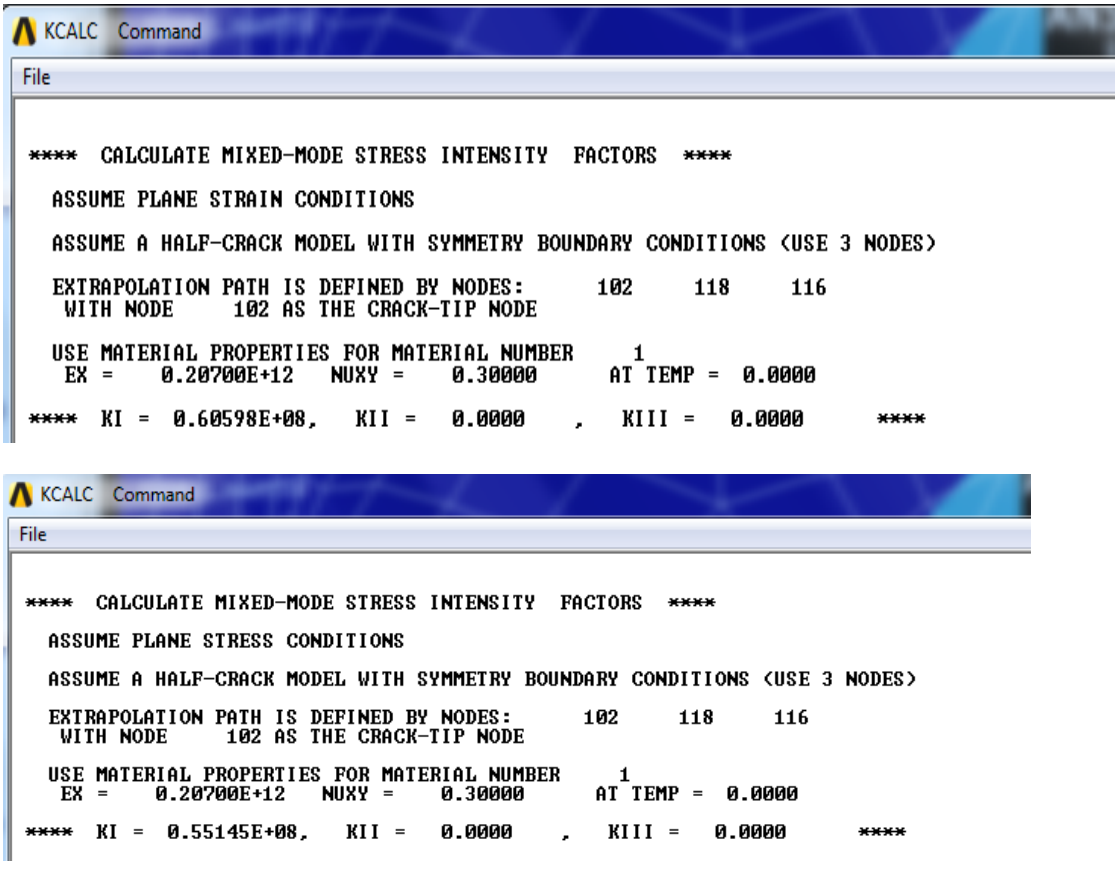

Figure 4.22: Stress intensity factor for a=10mm and, σ=200.08MPa

For a crack length of 12mm

Case -1 when a pressure of 153.28MPa is applied on the plate (crack length a=12mm, width, b=40mm, 2h=50mm and thickness=20mm). Wheel vertical load is 122.625KN and speed of train is V=60km/hr. no dynamically magnification factor

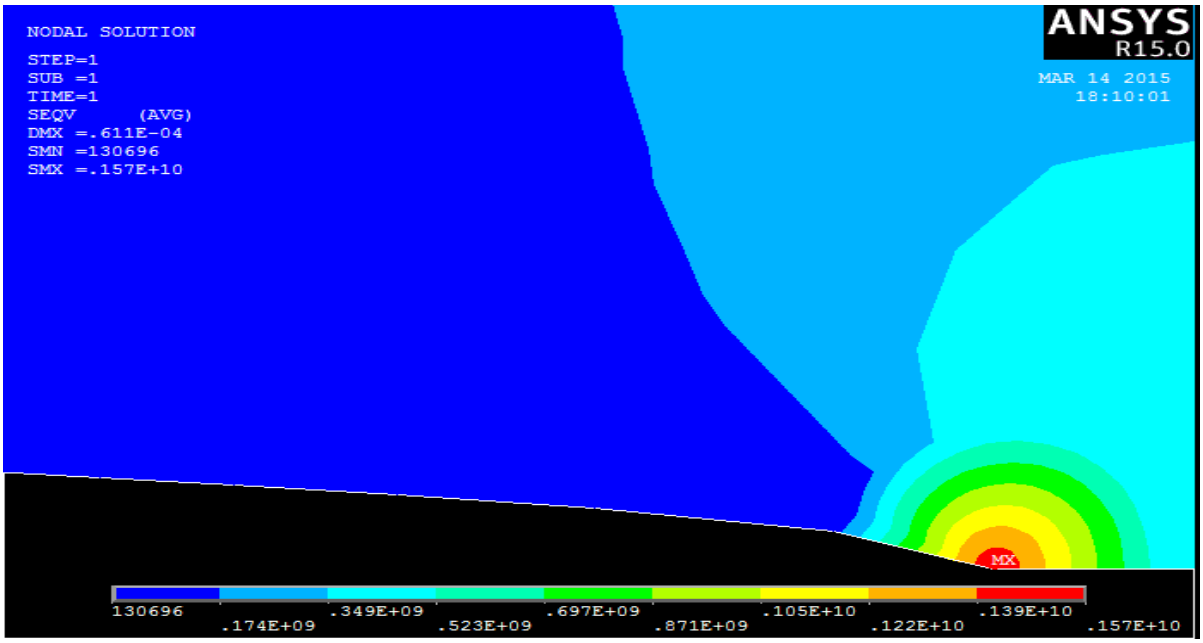

Figure 4.23: Nodal Von-Mises stress solution for a=12mm and, σ=153.28MPa

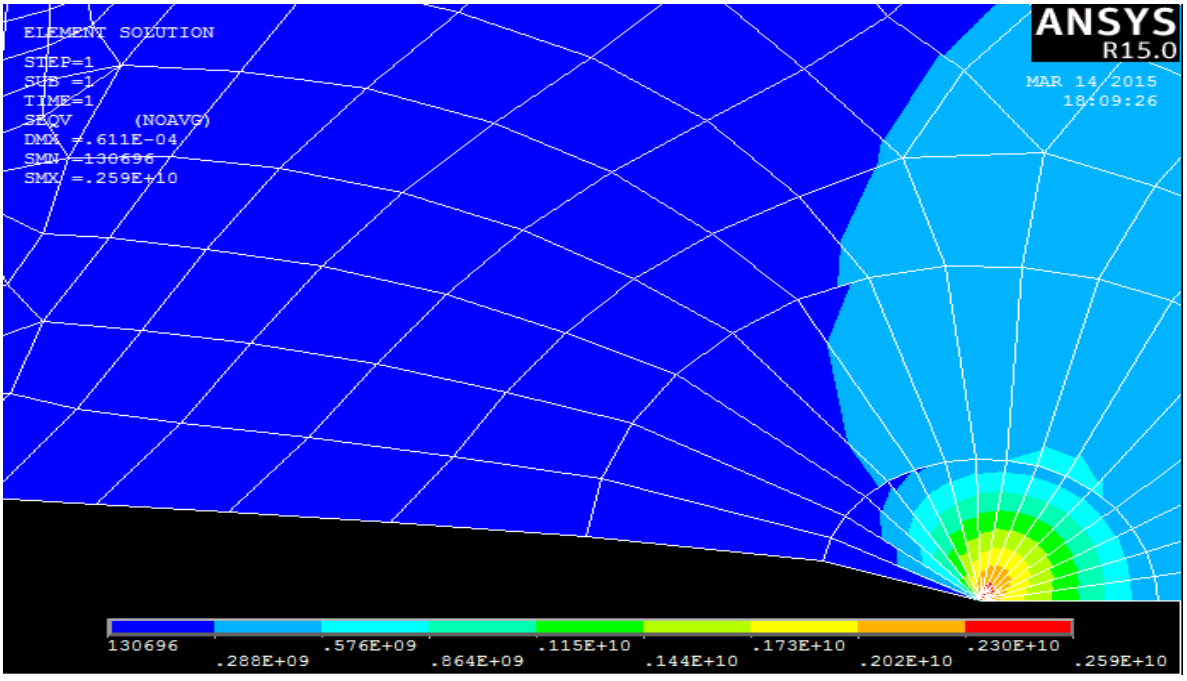

Figure 4.24: Element Von-Mises Stress solution for a=12mm and, σ=153.28MPa

File

```
****  CALCULATE MIXED-MODE STRESS INTENSITY  FACTORS  ****

  ASSUME PLANE STRAIN CONDITIONS

  ASSUME A HALF-CRACK MODEL WITH SYMMETRY BOUNDARY CONDITIONS (USE 3 NODES)

  EXTRAPOLATION PATH IS DEFINED BY NODES:      102     120     118
   WITH NODE     102 AS THE CRACK-TIP NODE

  USE MATERIAL PROPERTIES FOR MATERIAL NUMBER     1
   EX =    0.20700E+12   NUXY =    0.30000      AT TEMP =  0.0000

****  KI =  0.56531E+08,   KII =   0.0000    ,   KIII =   0.0000      ****
```

File

```
****  CALCULATE MIXED-MODE STRESS INTENSITY  FACTORS  ****

  ASSUME PLANE STRESS CONDITIONS

  ASSUME A HALF-CRACK MODEL WITH SYMMETRY BOUNDARY CONDITIONS (USE 3 NODES)

  EXTRAPOLATION PATH IS DEFINED BY NODES:      102     120     118
   WITH NODE     102 AS THE CRACK-TIP NODE

  USE MATERIAL PROPERTIES FOR MATERIAL NUMBER     1
   EX =    0.20700E+12   NUXY =    0.30000      AT TEMP =  0.0000

****  KI =  0.51443E+08,   KII =   0.0000    ,   KIII =   0.0000      ****
```

Figure 4.25: Stress Intensity Factor for a=12mm and, σ=153.28MPa

Case-2 when a pressure of 247.7MPa is applied on the plate (crack length a=12mm, width, b=40mm, 2h=50mm and thickness=20mm). Wheel vertical load is 198.16KN and speed of train is V=70km/hr. dynamically magnification factor is 1.616

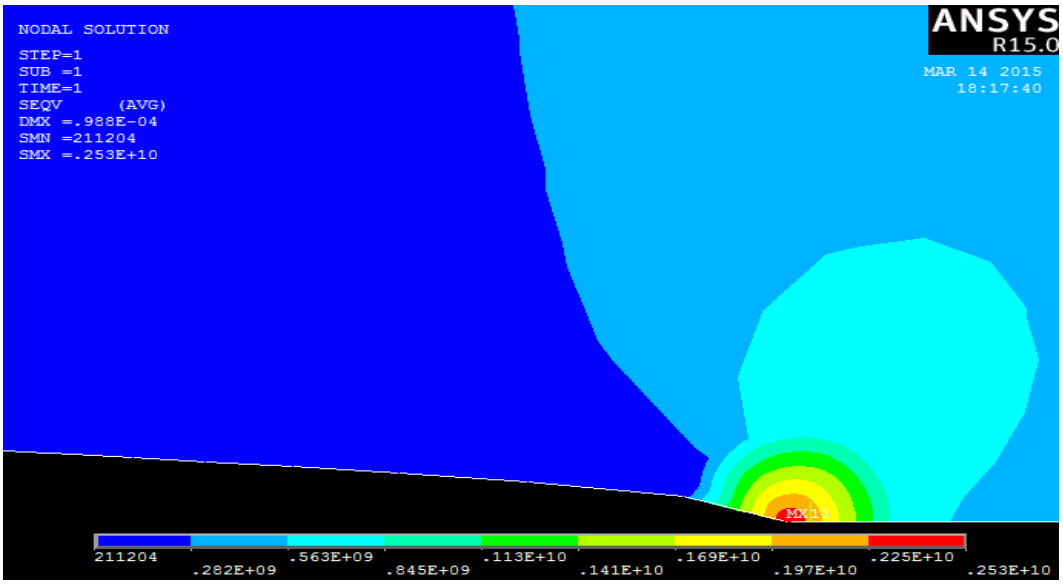

Figure 4.26: Nodal Von-Mises stress solution for a=12mm and, σ=247.7MPa

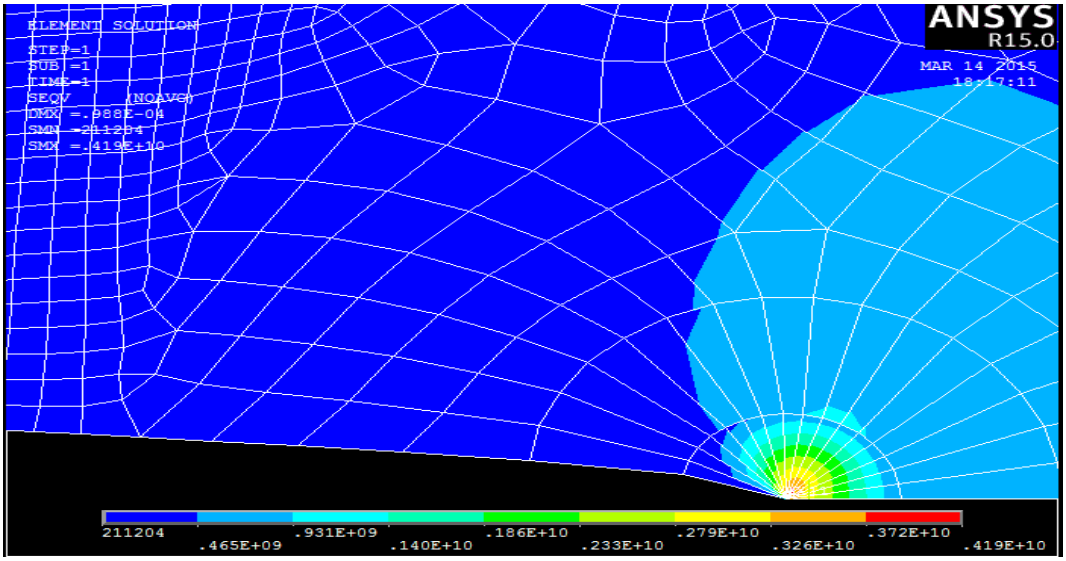

Figure 4.27: Element Von-Mises stress solution for a=12mm and, σ=247.7MPa

File

```
****  CALCULATE MIXED-MODE STRESS INTENSITY  FACTORS  ****

  ASSUME PLANE STRAIN CONDITIONS

  ASSUME A HALF-CRACK MODEL WITH SYMMETRY BOUNDARY CONDITIONS (USE 3 NODES)

  EXTRAPOLATION PATH IS DEFINED BY NODES:      102     120     118
   WITH NODE     102 AS THE CRACK-TIP NODE

  USE MATERIAL PROPERTIES FOR MATERIAL NUMBER     1
   EX =    0.20700E+12   NUXY =    0.30000      AT TEMP =  0.0000

****  KI =  0.91353E+08,   KII =   0.0000    ,   KIII =   0.0000      ****
```

File

```
****  CALCULATE MIXED-MODE STRESS INTENSITY  FACTORS  ****

  ASSUME PLANE STRESS CONDITIONS

  ASSUME A HALF-CRACK MODEL WITH SYMMETRY BOUNDARY CONDITIONS (USE 3 NODES)

  EXTRAPOLATION PATH IS DEFINED BY NODES:      102     120     118
   WITH NODE     102 AS THE CRACK-TIP NODE

  USE MATERIAL PROPERTIES FOR MATERIAL NUMBER     1
   EX =    0.20700E+12   NUXY =    0.30000      AT TEMP =  0.0000

****  KI =  0.83132E+08,   KII =   0.0000    ,   KIII =   0.0000      ****
```

Figure 4.28: Stress Intensity Factor **for a=12**mm and, σ=**247.7**MPa

Case-3 when a pressure of 138MPa is applied on the plate (crack length a=12mm, width, b=40mm, 2h=50mm and thickness=20mm). Wheel vertical load is 110.36KN and speed of train is V=60km/hr. no dynamically magnification factor

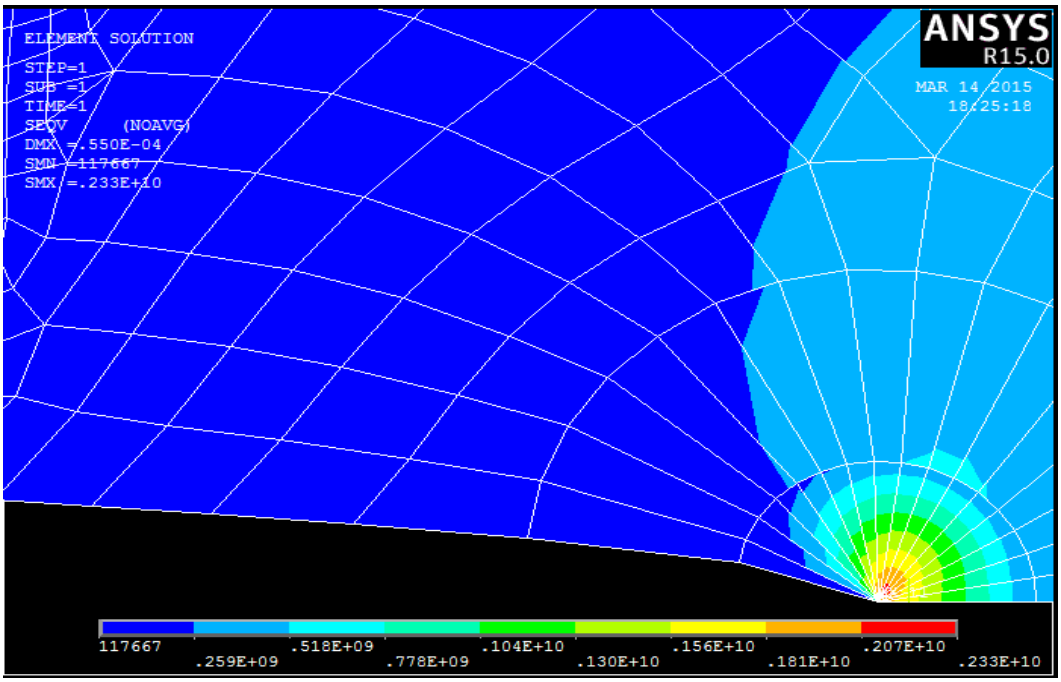

Figure 4.29: Element Von-Mises stress solution for a=12mm and, σ=138MPa

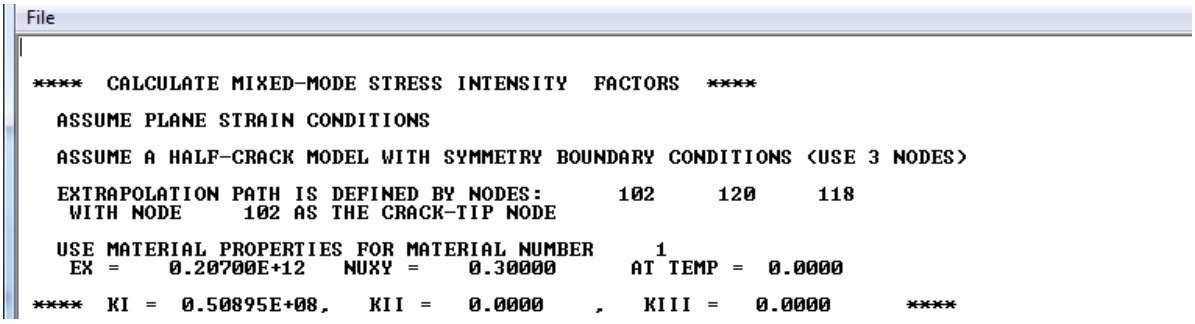

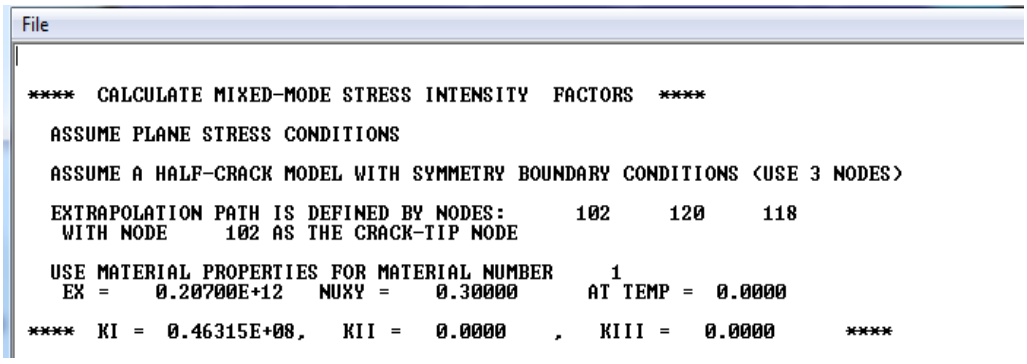

Figure 4.30: Stress Intensity Factor for a=12mm and, σ=138MPa

Case-4 when a pressure of 222.94MPa is applied on the plate (crack length a=12mm, width, b=40mm, 2h=50mm and thickness=20mm). Wheel vertical load is 178.35KN and speed of train is V=70km/hr. dynamically magnification factor is 1.616

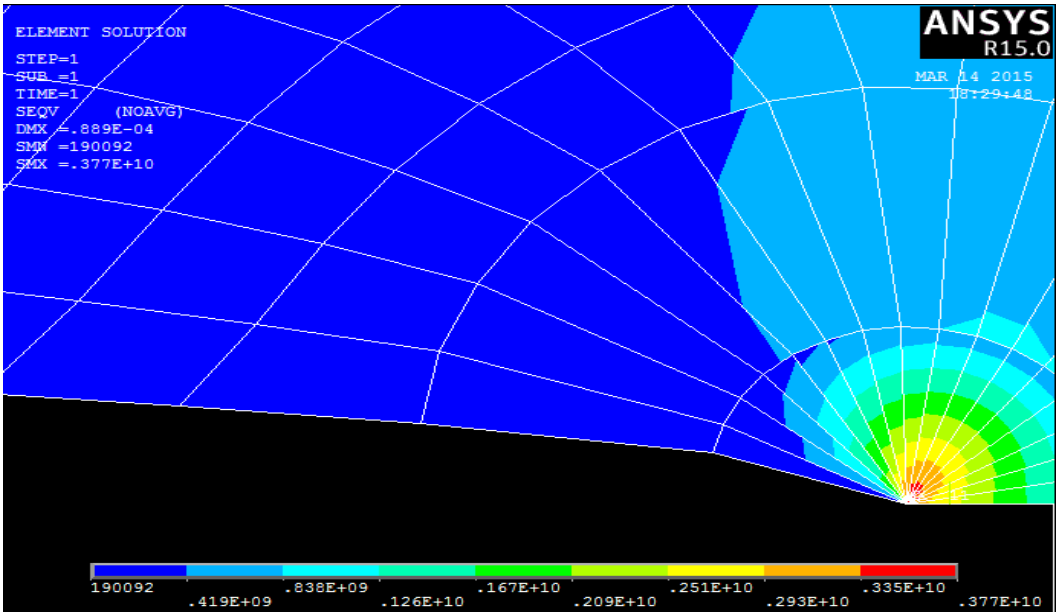

Figure 4.31: Element Von-Mises Stresses solution for a=12mm and, σ=222.94MPa

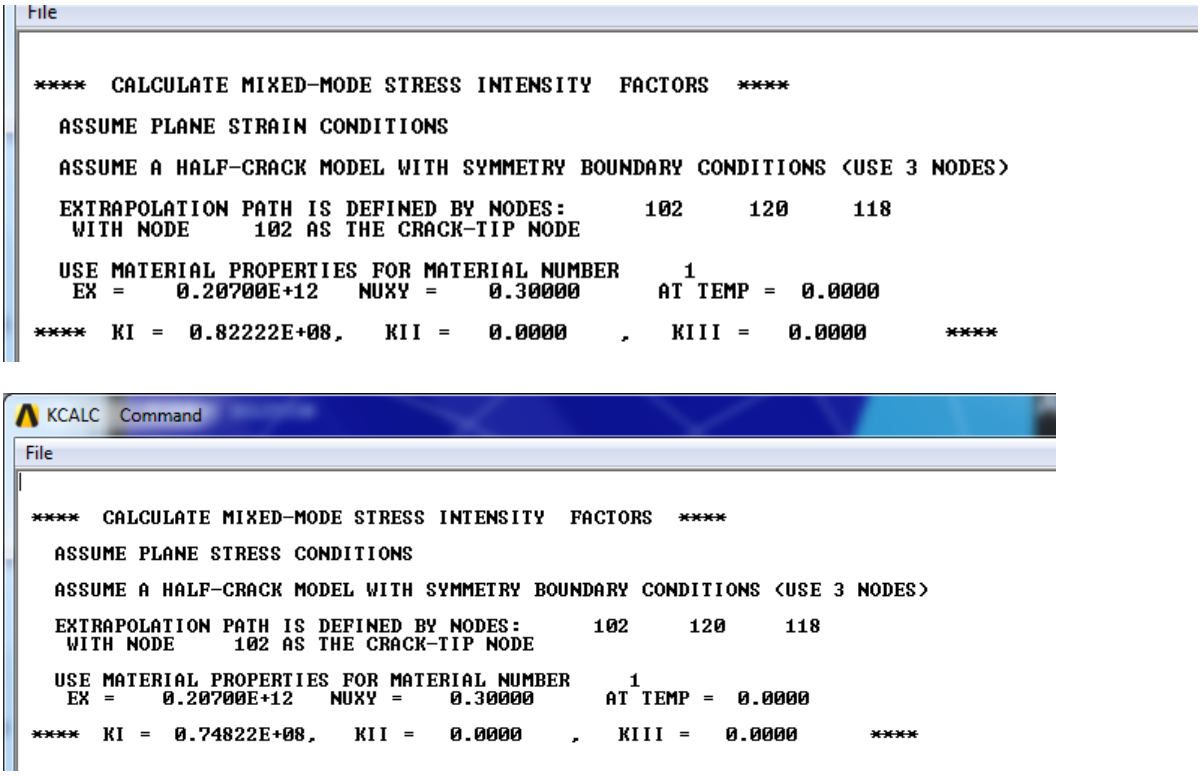

Figure 4.32: Stress Intensity Factor for a=12mm and, σ=222.94MPa

Case-5 when a pressure of **122.625MPa** is applied on the plate (crack length a=12mm, width, b=40mm, 2h=50mm and thickness=20mm). Wheel vertical load is **98.1KN** and speed of train is **V=80km/hr**. no dynamically magnification factor

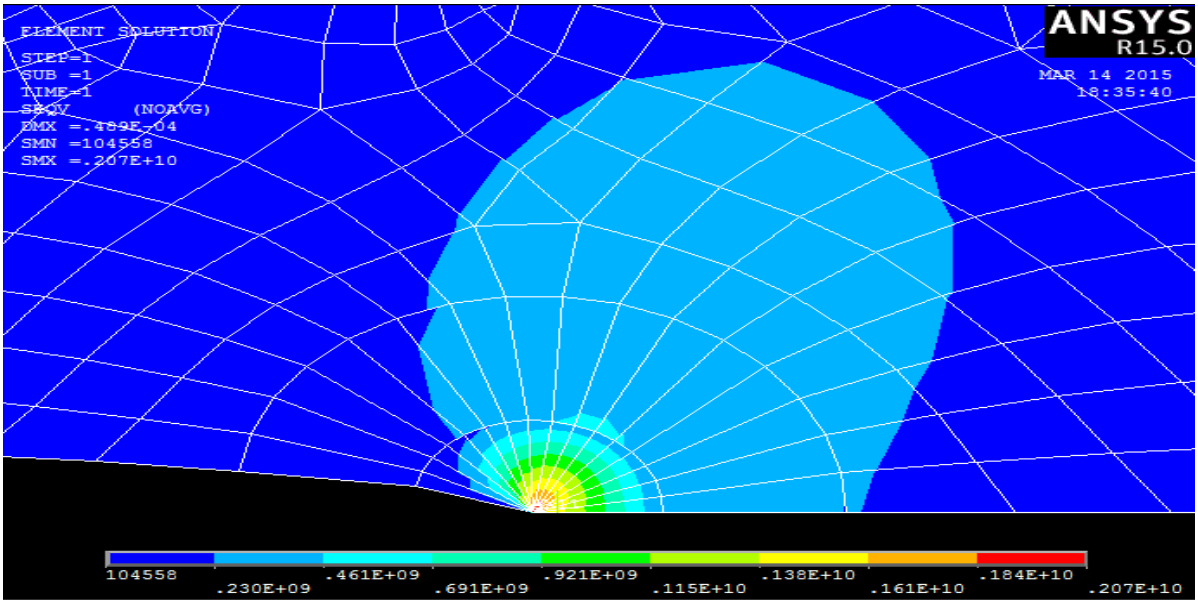

Figure 4.33: Element Von-Mises Stresses solution for a=12mm and, σ=122.625MPa

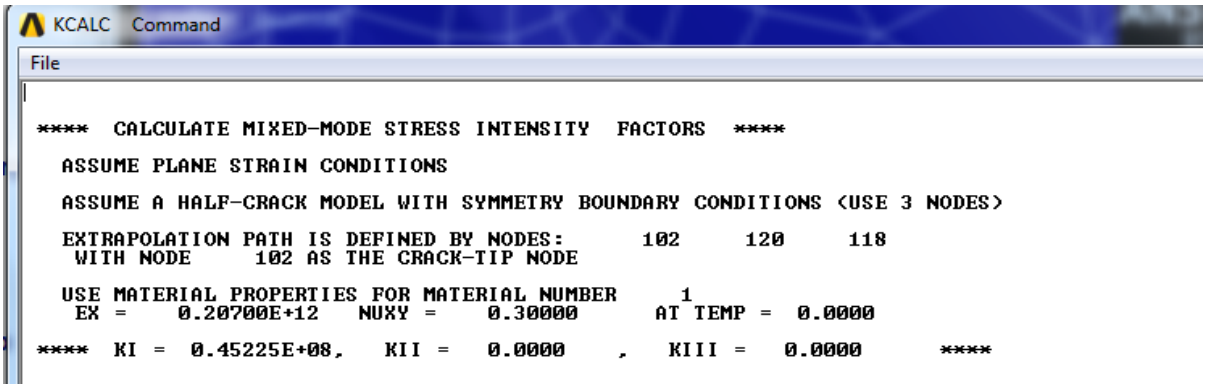

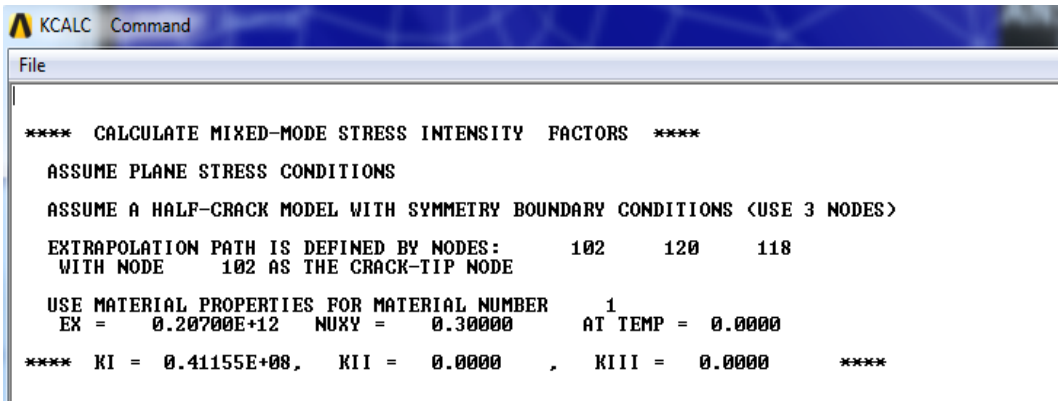

Figure 4.34: Stress Intensity Factor for a=12mm and, σ=122.625MPa

Case-6 when a pressure of 200.08MPa is applied on the plate (crack length a=12mm, width, b=40mm, 2h=50mm and thickness=20mm). Wheel vertical load is 160.06KN and speed of train is V=80km/hr. Dynamically magnification factor is 1.6316

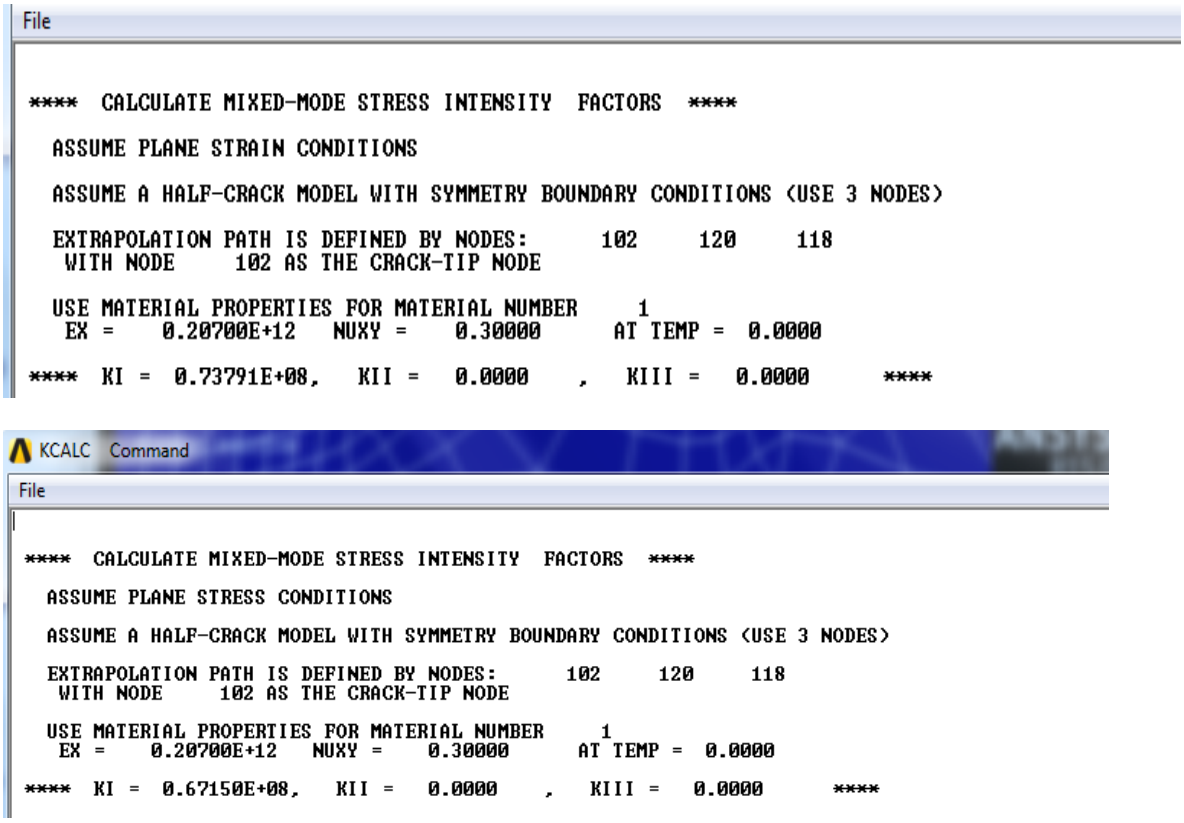

Figure 4.35: stress intensity factor for a=12mm and, σ=200.08MPa

For crack length of 14mm

Case-1 when a pressure of 153.28MPa is applied on the plate (crack length a=14mm, width, b=40mm, 2h=50mm and thickness=20mm). Wheel vertical load is 122.625KN and speed of train is V=60km/hr. no dynamically magnification factor

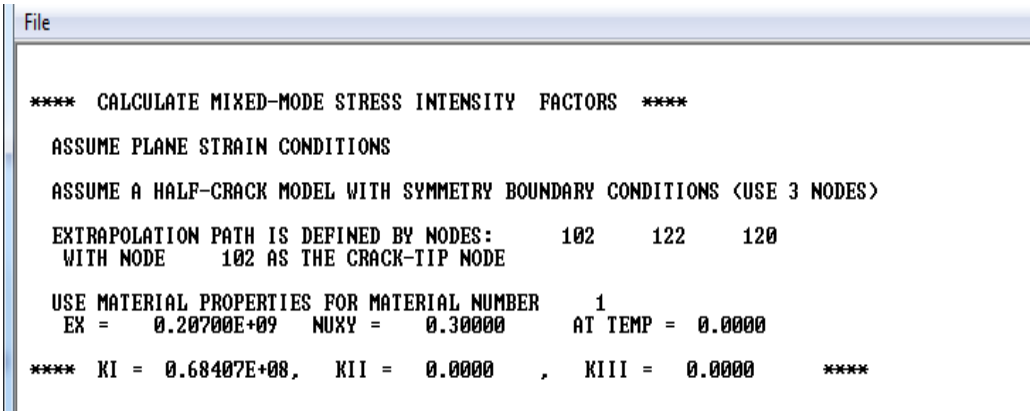

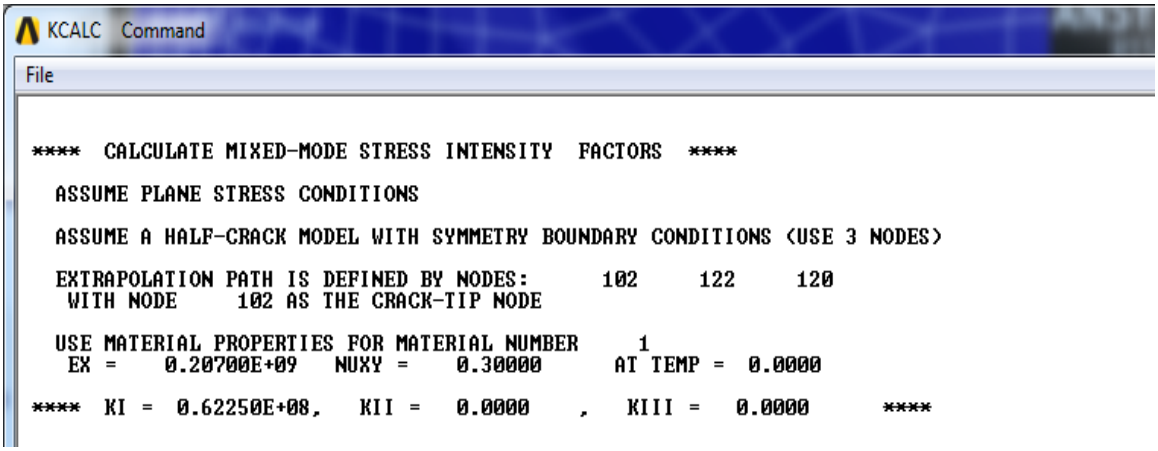

Figure 4.36: stress intensity factor solution for a=14mm and, σ=153.28MPa

Case-2 when a pressure of 247.7MPa is applied on the plate (crack length a=14mm, width, b=40mm, 2h=50mm and thickness=20mm). Wheel vertical load is 198.16KN and speed of train is V=70km/hr. Dynamically magnification factor is 1.616

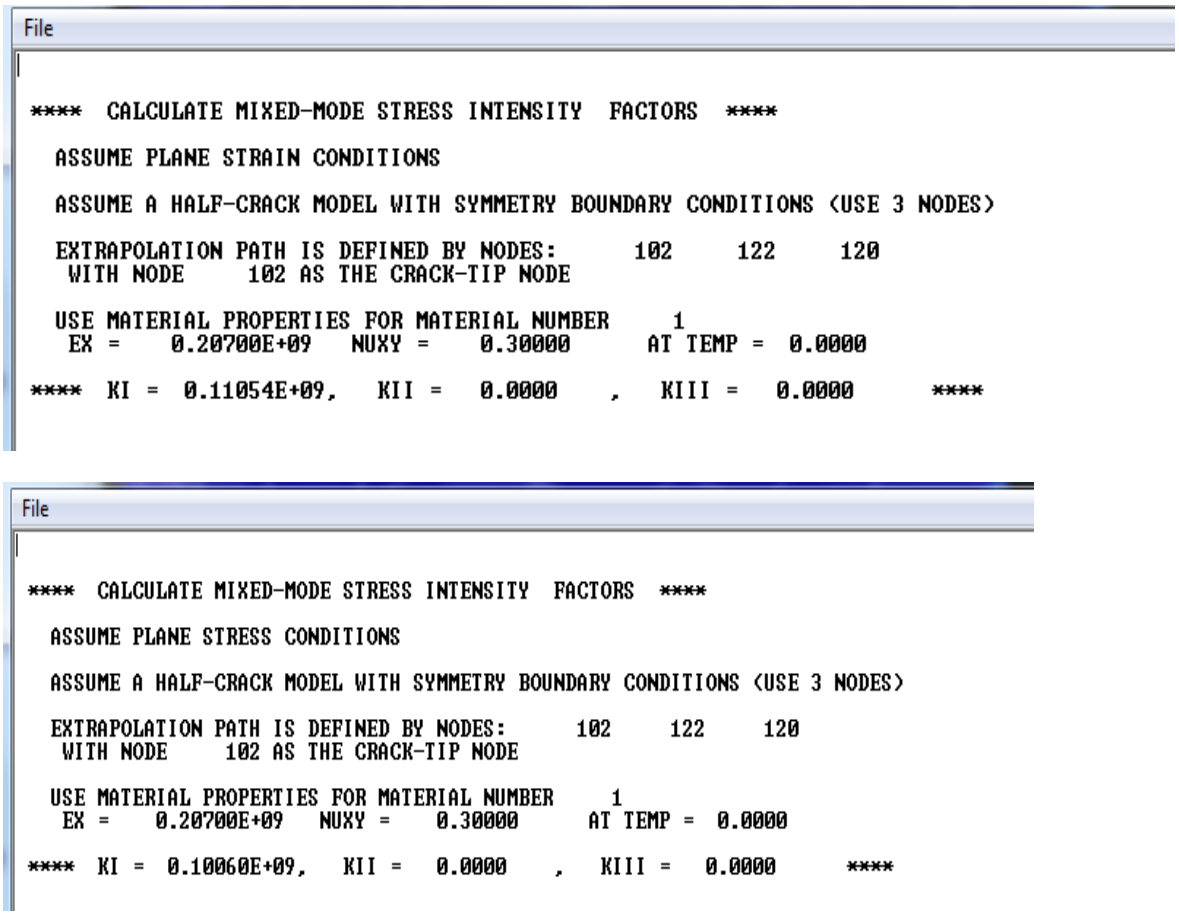

Figure 4.37: Stress Intensity Factor solution for a=14mm and, σ=247.7MPa

Case-3 when a pressure of 138MPa is applied on the plate (crack length a=14mm, width, b=40mm, 2h=50mm and thickness=20mm). Wheel vertical load is 110.36KN and speed of train is V=60km/hr. no dynamically magnification factor

File

```
****  CALCULATE MIXED-MODE STRESS INTENSITY  FACTORS  ****

  ASSUME PLANE STRAIN CONDITIONS

  ASSUME A HALF-CRACK MODEL WITH SYMMETRY BOUNDARY CONDITIONS (USE 3 NODES)

  EXTRAPOLATION PATH IS DEFINED BY NODES:      102     122     120
   WITH NODE     102 AS THE CRACK-TIP NODE

  USE MATERIAL PROPERTIES FOR MATERIAL NUMBER     1
   EX =    0.20700E+09   NUXY =    0.30000      AT TEMP =  0.0000

****  KI =  0.61587E+08,   KII =   0.0000    ,   KIII =   0.0000      ****
```

File

```
****  CALCULATE MIXED-MODE STRESS INTENSITY  FACTORS  ****

  ASSUME PLANE STRESS CONDITIONS

  ASSUME A HALF-CRACK MODEL WITH SYMMETRY BOUNDARY CONDITIONS (USE 3 NODES)

  EXTRAPOLATION PATH IS DEFINED BY NODES:      102     122     120
   WITH NODE     102 AS THE CRACK-TIP NODE

  USE MATERIAL PROPERTIES FOR MATERIAL NUMBER     1
   EX =    0.20700E+09   NUXY =    0.30000      AT TEMP =  0.0000

****  KI =  0.56044E+08,   KII =   0.0000    ,   KIII =   0.0000      ****
```

Figure 4.38: stress intensity factor solution for a=14mm and, σ=138MPa

Case-4 when a pressure of 222.94MPa is applied on the plate (crack length a=14mm, width, b=40mm, 2h=50mm and thickness=20mm). Wheel vertical load is 178.35KN and speed of train is V=70km/hr. dynamically magnification factor is 1.616

File

```
****  CALCULATE MIXED-MODE STRESS INTENSITY  FACTORS  ****

  ASSUME PLANE STRAIN CONDITIONS

  ASSUME A HALF-CRACK MODEL WITH SYMMETRY BOUNDARY CONDITIONS (USE 3 NODES)

  EXTRAPOLATION PATH IS DEFINED BY NODES:      102     122     120
   WITH NODE     102 AS THE CRACK-TIP NODE

  USE MATERIAL PROPERTIES FOR MATERIAL NUMBER     1
   EX =    0.20700E+09   NUXY =    0.30000      AT TEMP =  0.0000

****  KI =  0.99495E+08,   KII =   0.0000    ,   KIII =   0.0000      ****
```

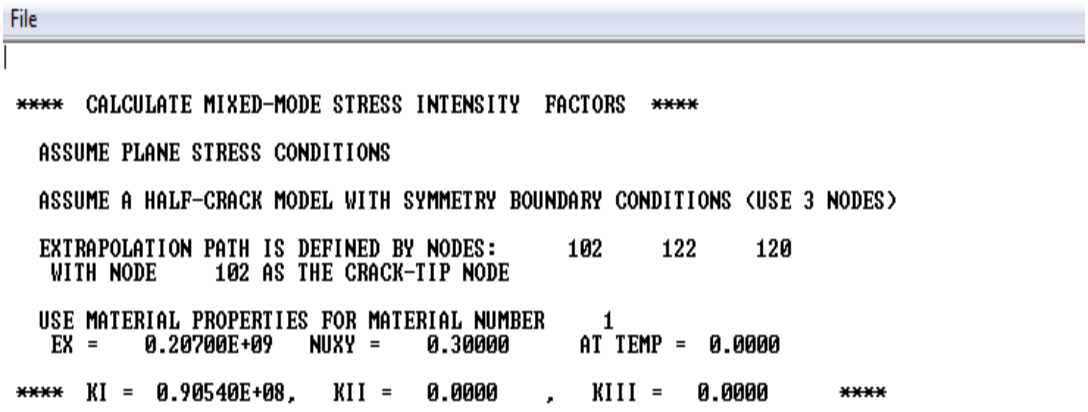

Figure 4.39: stress intensity factor solution for a=14mm and, σ=222.94MPa

Case-5 when a pressure of 122.625MPa is applied on the plate (crack length a=14mm, width, b=40mm, 2h=50mm and thickness=20mm). Wheel vertical load is 98.1KN and speed of train is V=80km/hr. no dynamically magnification factor

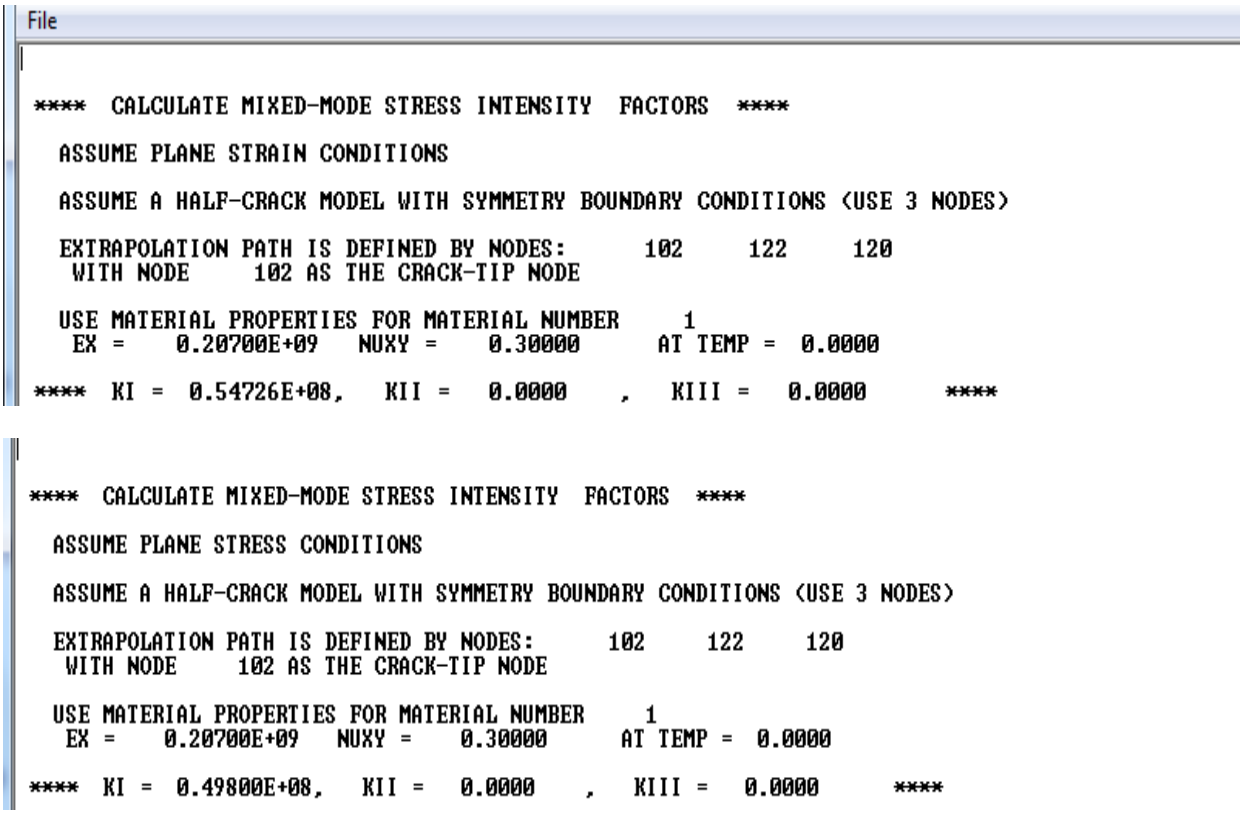

Figure 4.40: stress intensity factor solution for a=14mm and, σ=122.625MPa

Case-6 when a pressure of 200.08MPa is applied on the plate (crack length a=14mm, width, b=40mm, 2h=50mm and thickness=20mm). Wheel vertical load is 160.06KN and speed of train is V=80km/hr. dynamically magnification factor is 1.6316

File

```
****  CALCULATE MIXED-MODE STRESS INTENSITY  FACTORS  ****

  ASSUME PLANE STRAIN CONDITIONS

  ASSUME A HALF-CRACK MODEL WITH SYMMETRY BOUNDARY CONDITIONS (USE 3 NODES)

  EXTRAPOLATION PATH IS DEFINED BY NODES:      102     122     120
   WITH NODE     102 AS THE CRACK-TIP NODE

  USE MATERIAL PROPERTIES FOR MATERIAL NUMBER     1
   EX =    0.20700E+09   NUXY =    0.30000      AT TEMP =  0.0000

****  KI =  0.89293E+08,   KII =   0.0000    ,   KIII =   0.0000      ****
```

```
****  CALCULATE MIXED-MODE STRESS INTENSITY  FACTORS  ****

  ASSUME PLANE STRESS CONDITIONS

  ASSUME A HALF-CRACK MODEL WITH SYMMETRY BOUNDARY CONDITIONS (USE 3 NODES)

  EXTRAPOLATION PATH IS DEFINED BY NODES:      102     122     120
   WITH NODE     102 AS THE CRACK-TIP NODE

  USE MATERIAL PROPERTIES FOR MATERIAL NUMBER     1
   EX =    0.20700E+09   NUXY =    0.30000      AT TEMP =  0.0000

****  KI =  0.81256E+08,   KII =   0.0000    ,   KIII =   0.0000      ****
```

Figure 4.41: stress intensity factor solution for a=14mm and, σ=200.08MPa

For crack length of 16mm

Case-1 when a pressure of 153.28MPa is applied on the plate (crack length a=16mm, width, b=40mm, 2h=50mm and thickness=20mm). Wheel vertical load is 122.625KN and speed of train is V=60km/hr. no dynamically magnification factor

File

```
****  CALCULATE MIXED-MODE STRESS INTENSITY  FACTORS  ****

  ASSUME PLANE STRAIN CONDITIONS

  ASSUME A HALF-CRACK MODEL WITH SYMMETRY BOUNDARY CONDITIONS (USE 3 NODES)

  EXTRAPOLATION PATH IS DEFINED BY NODES:      102     122     120
   WITH NODE     102 AS THE CRACK-TIP NODE

  USE MATERIAL PROPERTIES FOR MATERIAL NUMBER     1
   EX =    0.20700E+12   NUXY =    0.30000      AT TEMP =  0.0000

****  KI =  0.82638E+08,   KII =   0.0000    ,   KIII =   0.0000      ****
```

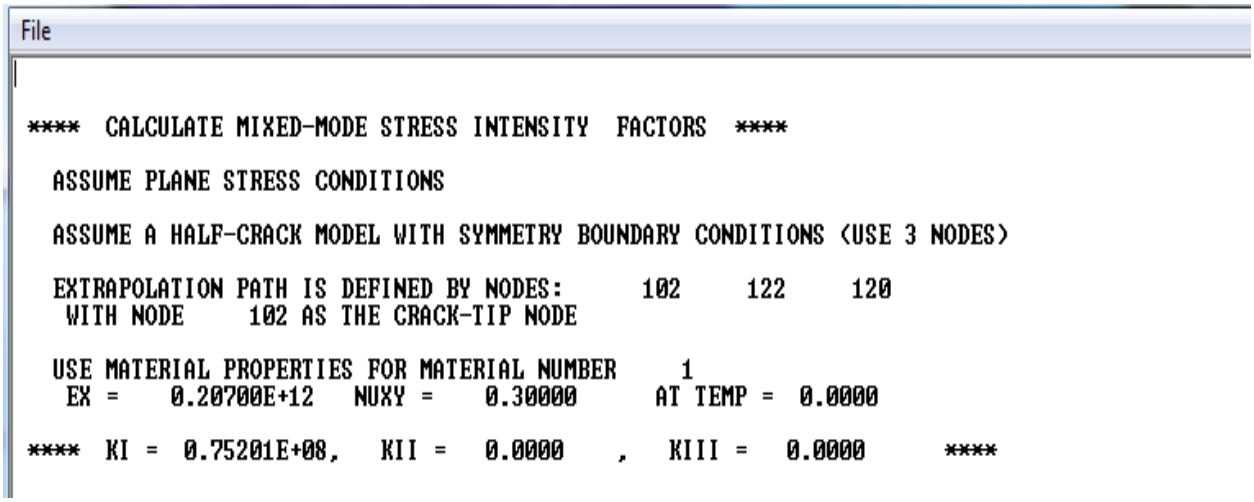

Figure 4.42: stress intensity factor **solution** for a=1**6**mm and, σ=153.28MPa

Case-2 when a pressure of 247.7MPa is applied on the plate (crack length a=16mm, width, b=40mm, 2h=50mm and thickness=20mm). Wheel vertical load is 198.16KN and speed of train is V=70km/hr. dynamically magnification factor is 1.616

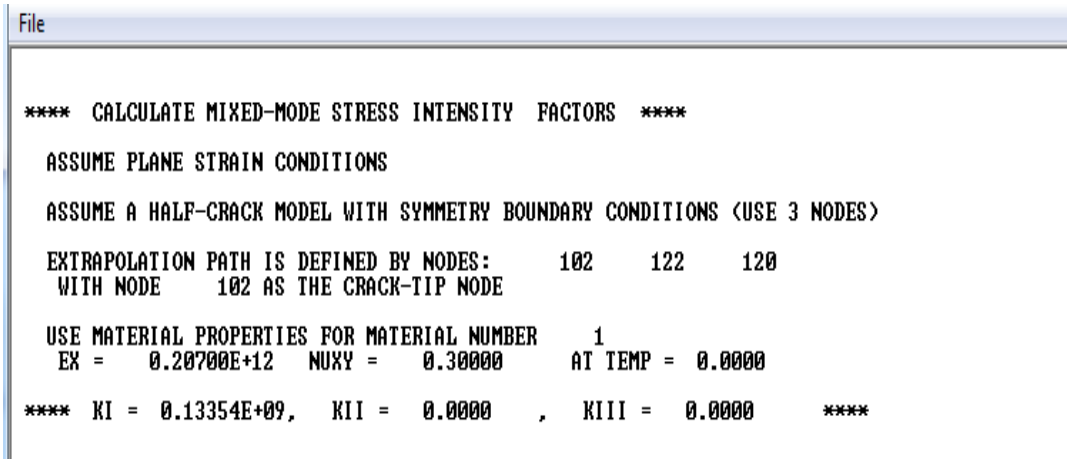

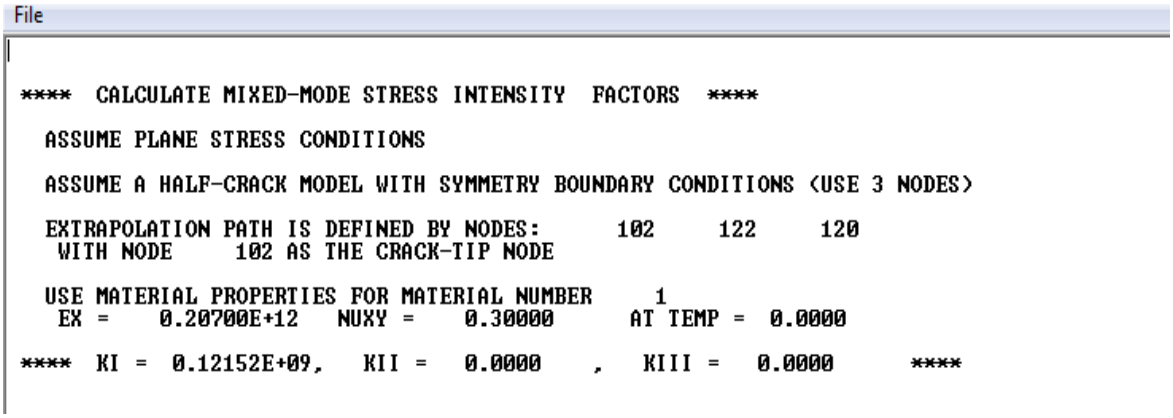

Figure 4.43: Stress Intensity Factor solution for a=16mm and, σ=153.28MPa

Case-3 when a pressure of 138MPa is applied on the plate (crack length a=16mm, width, b=40mm, 2h=50mm and thickness=20mm). Wheel vertical load is 110.36KN and speed of train is V=70km/hr. no dynamically magnification factor

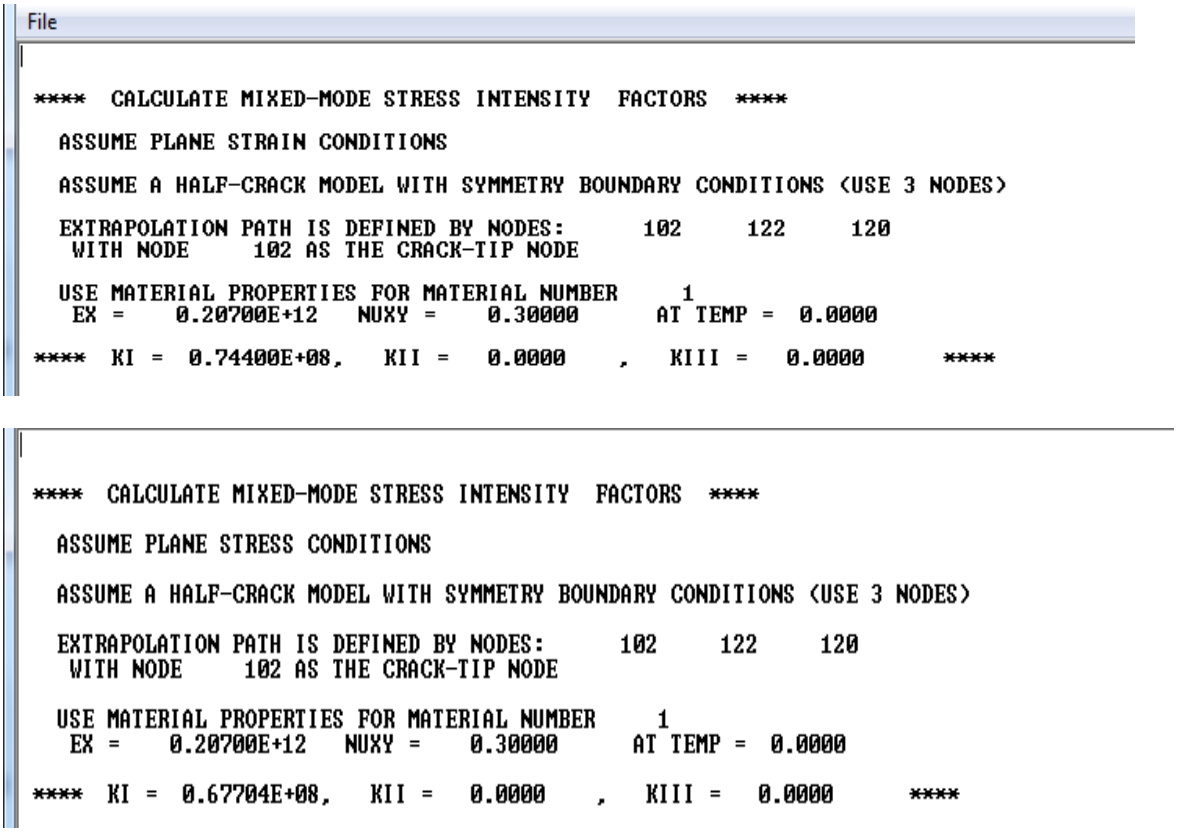

Figure 4.44: stress intensity factor solution for a=1**6**mm and, σ=**138**MPa

Case-4 when a pressure of 222.94MPa is applied on the plate (crack length a=16mm, width, b=40mm, 2h=50mm and thickness=20mm). Wheel vertical load is 178.35KN and speed of train is V=70km/hr. dynamically magnification factor is 1.616

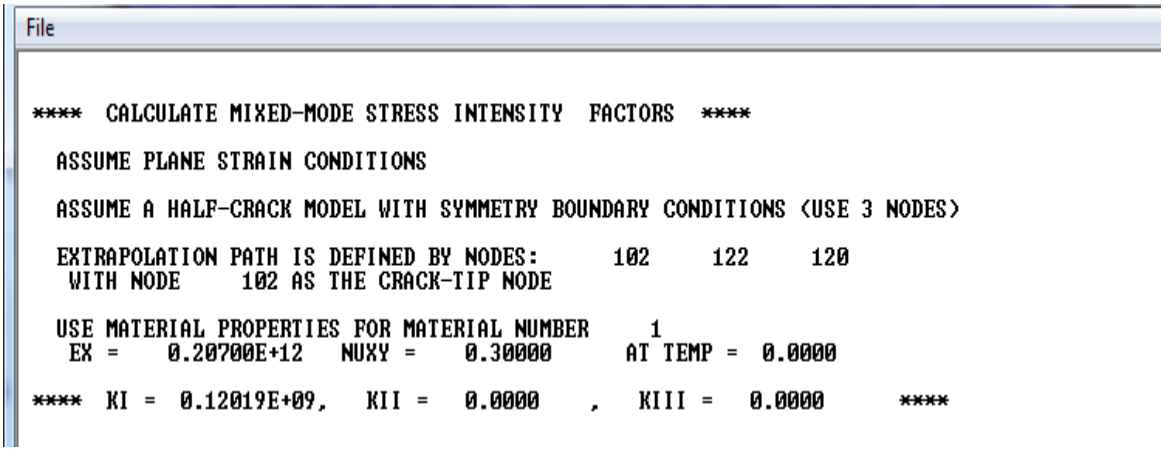

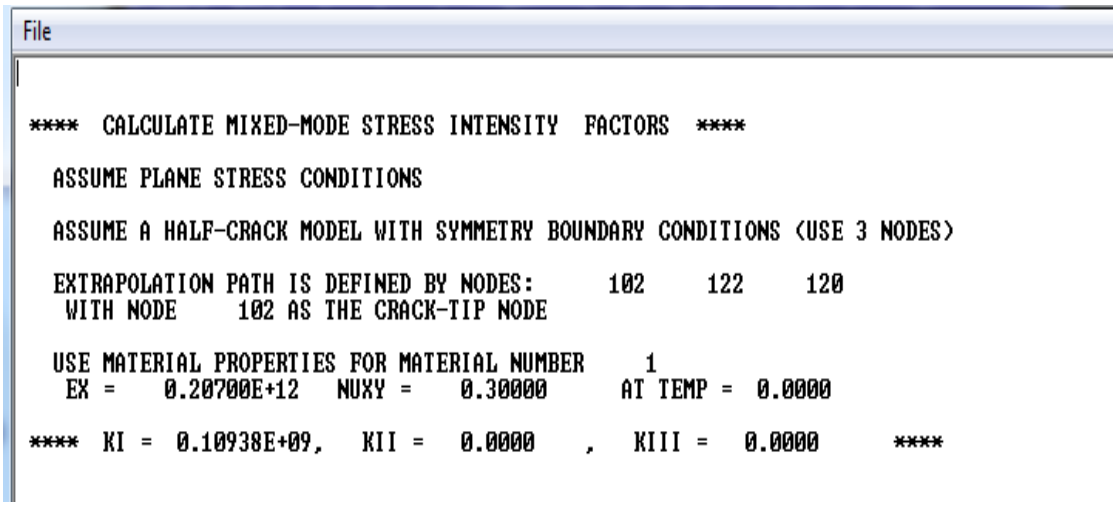

Figure 4.45: stress intensity factor solution for a=16mm and, σ=222.94MPa

Case-5 when a pressure of 122.625MPa is applied on the plate (crack length a=16mm, width, b=40mm, 2h=50mm and thickness=20mm). Wheel vertical load is 98.1KN and speed of train is V=80km/hr. no dynamically magnification factor

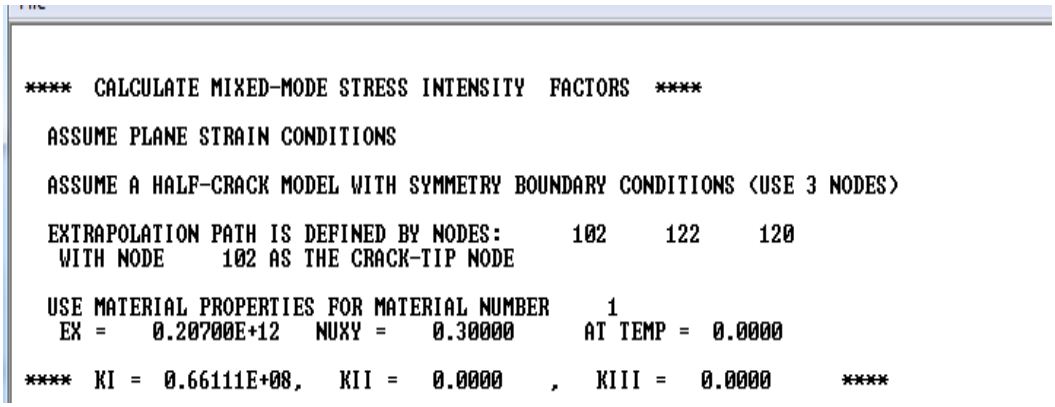

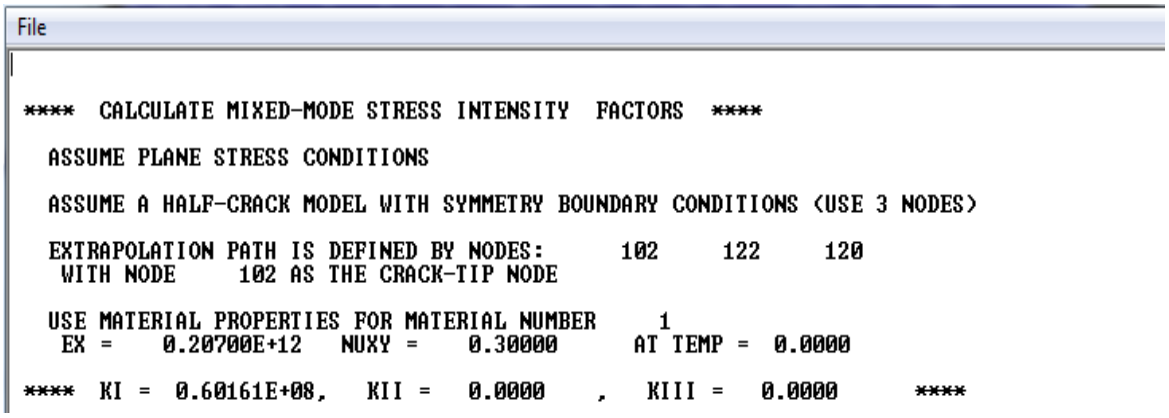

Figure 4.46: stress intensity factor solution for a=16mm and, σ=122.625MPa

Case-6 when a pressure of 200.08MPa is applied on the plate (crack length a=16mm, width, b=40mm, 2h=50mm and thickness=20mm). Wheel vertical load is 160.06KN and speed of train is V=80km/hr. dynamically magnification factor is 1.6316

```
**** CALCULATE MIXED-MODE STRESS INTENSITY FACTORS ****

  ASSUME PLANE STRAIN CONDITIONS

  ASSUME A HALF-CRACK MODEL WITH SYMMETRY BOUNDARY CONDITIONS (USE 3 NODES)

  EXTRAPOLATION PATH IS DEFINED BY NODES:      102     122     120
   WITH NODE     102 AS THE CRACK-TIP NODE

  USE MATERIAL PROPERTIES FOR MATERIAL NUMBER     1
   EX =    0.20700E+12   NUXY =    0.30000      AT TEMP =  0.0000

**** KI =  0.10787E+09,   KII =   0.0000    ,   KIII =   0.0000      ****
```

File

```
**** CALCULATE MIXED-MODE STRESS INTENSITY FACTORS ****

  ASSUME PLANE STRESS CONDITIONS

  ASSUME A HALF-CRACK MODEL WITH SYMMETRY BOUNDARY CONDITIONS (USE 3 NODES)

  EXTRAPOLATION PATH IS DEFINED BY NODES:      102     122     120
   WITH NODE     102 AS THE CRACK-TIP NODE

  USE MATERIAL PROPERTIES FOR MATERIAL NUMBER     1
   EX =    0.20700E+12   NUXY =    0.30000      AT TEMP =  0.0000

**** KI =  0.98161E+08,   KII =   0.0000    ,   KIII =   0.0000      ****
```

Figure 4.47: stress Intensity Factor solution for a=16mm and, σ=200.08MPa

4.3 Discussion

Crack geometry and stresses in the railhead are usually characterized by stress intensity factor, *K*, and resistance to fracture is described by fracture toughness, *KIC* [34]. Fracture resistance in plane strain conditions, *KIC*, is an indication of material resistance to crack propagation in a tensile loading. To obtain *KIC* it is assumed that the crack tip plastic zone is small in comparison with the crack length and the specimen dimensions [34]. To evaluate the possibility for unstable growth of cracks in head of the rail Grade R260- UIC60, a probabilistic approach, based on Linear Elastic Fracture Mechanics Fundamentals can be used. This approach combines the effects of stress, crack length, and material fracture resistance to establish a failure criterion. The criterion for failure embodied in this approach is stress intensity factor, *K*, assumed to be equal to the fracture toughness, *KIC* of the material. The stress intensity factor under mode-I, KI is used

for comparison with fracture toughness, KIC of the material which is assumed constant in this study.

Simulation of side cracks of rail steel plate of 40mm X 50mm X 20mm has been analyzed. For analysis initiated crack lengths of 10mm, 12mm, 14mm and 16mm have been considered and analyzed numerically and by finite element method. For numerical calculation of stress intensity factors KI for these problems are given by a formula used by (Ewalds and Wanhill, 1989) [30]. In Ansys software, the command of KCALC calculation method is used. The KCALC command calculates the mixed-mode stress intensity factors KI, KII and KIII. The stress intensity factor at the crack tip is calculated by fine meshing the nodes around crack tip. The local coordinate system is created at the crack tip point and then the Cartesian coordinate is moved to this specific point, newly created local coordinate system. This command is limited to linear elastic problems with a homogeneous, isotropic material near the crack region. The command is used properly under the consideration of the following two methods.

1. Define a local crack-tip or crack-front coordinate system, with X axis parallel to the crack face and Y axis perpendicular to the crack face,

   Utility Menu>Work Plane>Local Coordinate Systems>Create Local CS>By 3Nodes

   Then, Activate the Local Crack-Tip Coordinate System to the new coordinate system

   Utility Menu>Work Plane>Change Active CS to>Specified Coord Sys...

2. Define a path along the crack face: The first node on the path should be the crack-tip node. Hence a half-crack model is used in this study, two additional nodes are required, both along the crack face. For a full-crack model, where both crack faces are included, four additional nodes are required: two along one crack face and two along the other.

Main Menu>General Postproc>Path Operations>Define Path>By Nodes

Then, activate the crack-tip coordinate system as results coordinate system,

Select **Main Menu>General Postproc>Options for Outp**

Determine the Mode-I Stress Intensity Factor using KCALC

Main Menu>General Postproc>Nodal Calcs>Stress Int Factr

The Ansys results of both stress and strain plane conditions, stress intensity factor, KI are shown under section 4.2. The Nodal and Element Von-Mises Stress Solutions are also shown to reveal that the stresses around crack tips are higher. The results of numerical and that of FE are shown for each crack lengths (table 4.2 below). From the figures given above under section 4.2, it was observed that the stress intensity increases as the applied tensile load increases for each crack lengths. The largest stresses are developed at the tip of the crack for each case. It is more likely that the crack propagates along the crack tip. As the length of the crack increases, the stress intensity factor also increases under the same applied load.

The command of KCALC calculates the stress intensity factors at a crack for linear elastic fracture mechanics analysis. The analysis uses a fit of the nodal displacements in the vicinity of the crack. Both stress plane conditions and strain plane conditions can be used to calculate stress intensity factor, KI for mode-I. To check the failure criterion the results of strain condition can be used because they shows the maximum results of stress intensity factor, KI for mode-I.

Table 4.2: Summary of Results for both Numerical and Analytical (Ansys, assuming stress plane conditions)

case	Remote Pressure (MPa)	KI(stress intensity factor –mode-I) MPa$\sqrt{m}$							
		Crack length							
		a=10mm		a=12mm		a=14mm		a=16 mm	
		Numerical	Ansys	numerical	Ansys	numerical	Ansys	Numerical	ansys
1	153.28	40.78	42.25	49.4	51.44	59.67	62.25	72.29	75.2
2	247.7	65.89	68.27	79.83	83.13	96.43	100.6	116.82	121.52
3	138	36.71	38.03	44.48	46.32	53.72	56.04	65.08	67.7
4	222.94	59.3	61.45	71.85	74.82	86.79	90.54	105.14	109.38
5	122.625	32.62	33.8	39.52	41.16	47.74	49.8	57.83	60.16
6	200.08	53.22	55.15	64.48	67.15	77.89	81.26	94.36	98.16

Graph 4.1: Stress intensity factor as a function of a/b ratio at an applied stress of 247.7MPa

Graph 4.1 shows the stress intensity factor as a function of the ratio between the crack length and the width of the plate for both numerical and FE stress plane condition. As the ratio of crack length to plate length increases, the stress intensity also increases.

Table 4.3: Summary of Results for both Numerical and Analytical (Ansys, assuming plane strain conditions)

Case	Remote Pressure (MPa)	KI(stress intensity factor –mode-I) MPa$\sqrt{m}$ Crack length							
		a=10mm		a=12mm		a=14mm		a=16mm	
		Numerical	Ansys	numerical	Ansys	numerical	Ansys	numerical	ansys
1	153.28	40.78	46.42	49.4	56.53	59.67	68.41	72.29	82.64
2	247.7	65.89	75.02	79.83	91.35	96.43	110.5	116.8	133.5
3	138	36.71	41.8	44.48	50.9	53.72	61.59	65.08	74.4
4	222.94	59.3	67.52	71.85	82.22	86.79	99.49	105.1	120.2
5	122.625	32.62	37.14	39.52	45.23	47.74	54.73	57.83	66.11
6	200.08	53.22	60.6	64.48	73.8	77.89	89.29	94.36	107.8

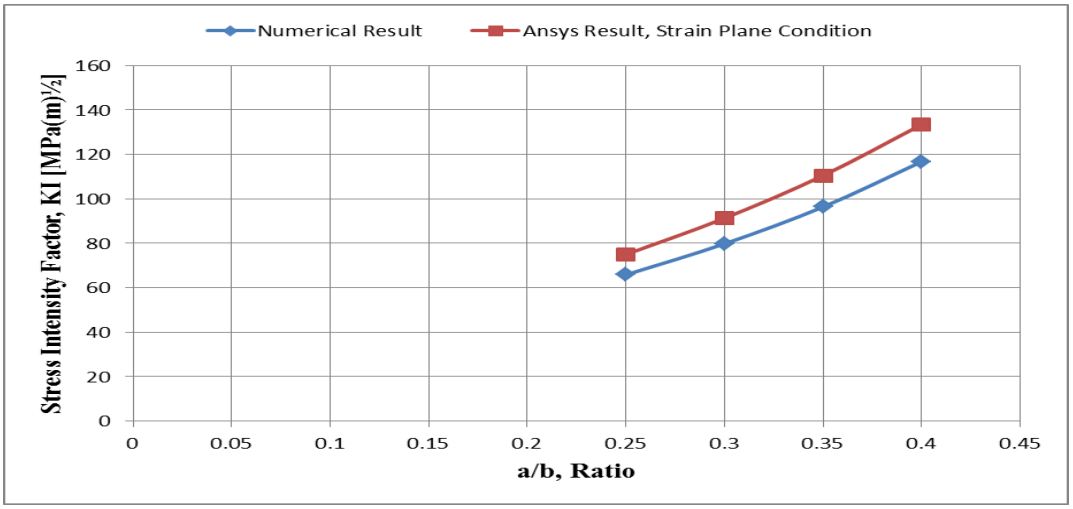

Graph 4.2: Stress intensity factor as a function of a/b ratio at an applied stress of 247.7MPa

The above graph also shows the same result as graph 4.2 using the comparisons between the numerical and FE strain plane conditions.

Graph 4.2 shows the stress intensity factor as a result of the ratio of crack lengths to width. The stress intensity factor at the crack tip increases with the increase in the ratio between the crack length and width of the plate for both the numerical and analytical method.

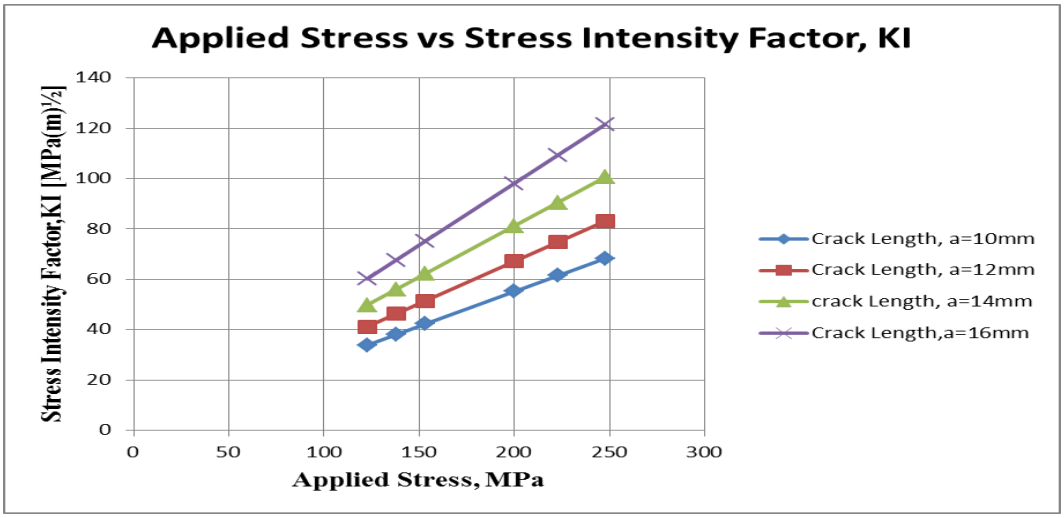

Graph 4.3: stress vs stress intensity factor, KI for different crack lengths

From graph 4.3 we will see that the stress Intensity factor at the crack tip for each crack length increases with the increase in applied tensile stress. Therefore increasing the load on a track with an initiated crack will increase the propagation of the crack.

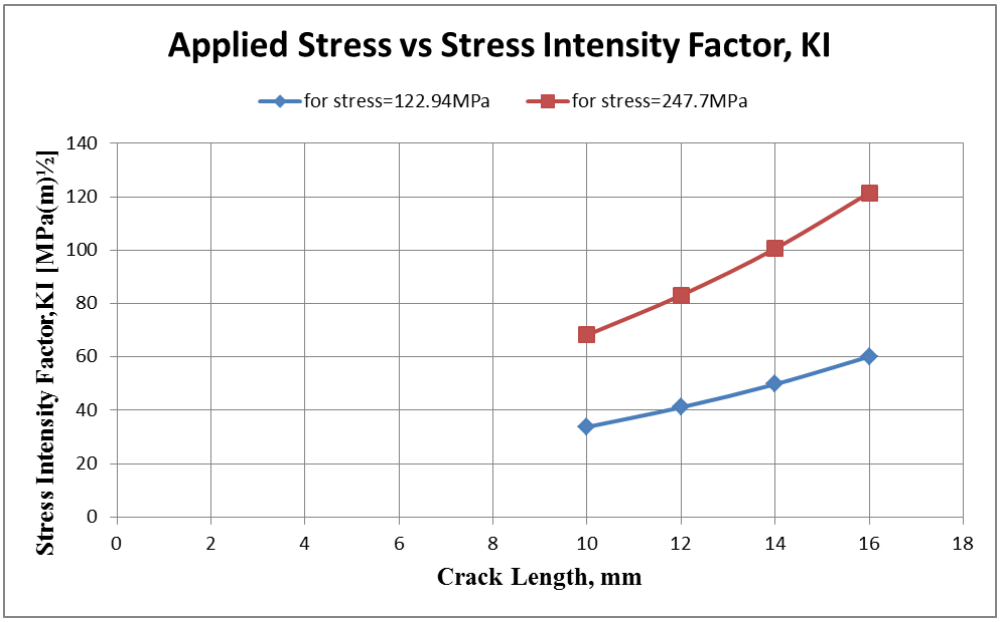

Graph 4.4: Crack length Vs stress intensity Factor for small and large applied stresses

The above graph shows the effect of applied load on different crack lengths. The stress intensity factor for longer crack length is higher than that of smaller crack length under the application of the same load. The stress intensity factor increases with the increase in applied tensile load.

4.3.1 Crack Growth Rate and Life Prediction

To determine the number of loading cycles required to make each crack in the study grow by 1 mm under the application of the given loads. The structure is loaded with stress cycles of constant amplitude. For crack growth calculations we use the un-modified Paris law:

$$\frac{da}{dN} = C(\Delta K)^m$$

Where da/dN is the crack growth per cycle,

ΔK is the stress-intensity range, and C and m are material constants.

In this empirical equation C is the slope of the curve in the linear region and m is the value found by extending the straight line to the stress intensity factor where it is 1 MPa m $^{1/2}$. The constant C in the equation includes effects of material, loading frequencies, mean load and environment. The constant m in the equation is an empirical constant which is in the range of 2 and 7. For ductile materials exponent m is between 2 and 4. The fracture toughness of the chosen material is 41MPa (m)^{½}, Journal of Mechanics of Materials and Structures [33]

The constants C and m values are taken from reference [32], C= 2.8947E-10 and m= 4.3

For the analytical calculation of stress intensity factor, KI from table 4.2, Ansys results of stress plane condition, the rate of crack growth per cycle are also tabulated as follows using the modified version of the Paris law:

$$\frac{da}{dN} = C[(\Delta K)^m - (KIC)^m] = 2.894\text{E-}10[(42.25)^{4.3} - (41)^{4.3}] = \mathbf{0.000343}$$

Where K_{IC} =41MPa (m)^{½} is the fracture toughness of the rail steel material and is taken from reference [33].

Similarly the following values are tabulated for rest of the cases:

Table 4.4: Crack Growth Rate per Cycle based on stress plane condition

Load Case	Remote Pressure [Mpa]	Crack length							
		a=10mm		a=12mm		a=14mm		a=16mm	
		KI [MPa]	da/dN [m/cycles]	KI [MPa]	da/dN [m/cycles]	KI [Mpa]	da/dN [m/cycles]	KI [MPa]	da/dN [m/cycles]
1	153.28	42.25	3.34E-4	51.44	4.12E-3	62.25	1.25E-2	75.2	3.13E-2
2	247.7	68.27	1.98E-2	83.13	4.96E-2	100.6	1.16E-1	121.52	2.64E-1
3	138	38.03	-6.88E-4	46.32	1.72E-3	56.04	7.06E-3	67.7	1.9E-2
4	222.94	61.45	1.17E-2	74.82	3.06E-2	90.54	7.27E-2	109.38	1.67E-1
5	122.625	33.8	-1.41E-3	41.16	4.21E-5	49.8	3.26E-3	60.16	1.05E-2
6	200.08	55.15	6.4E-3	67.15	1.83E-2	81.26	4.47E-2	98.16	1.04E-1

From table 4.4 above, we will see that the crack growth rate increases with the increases in the stress intensity factor. For crack length of 10mm, the stress intensity factor under the application of tensile loads of 138MPa and 122.625MPa is less than the fracture toughness of the material. The crack growth rate under these conditions is negative which means that the life of crack under the application of this loads are infinite or the crack is stable.

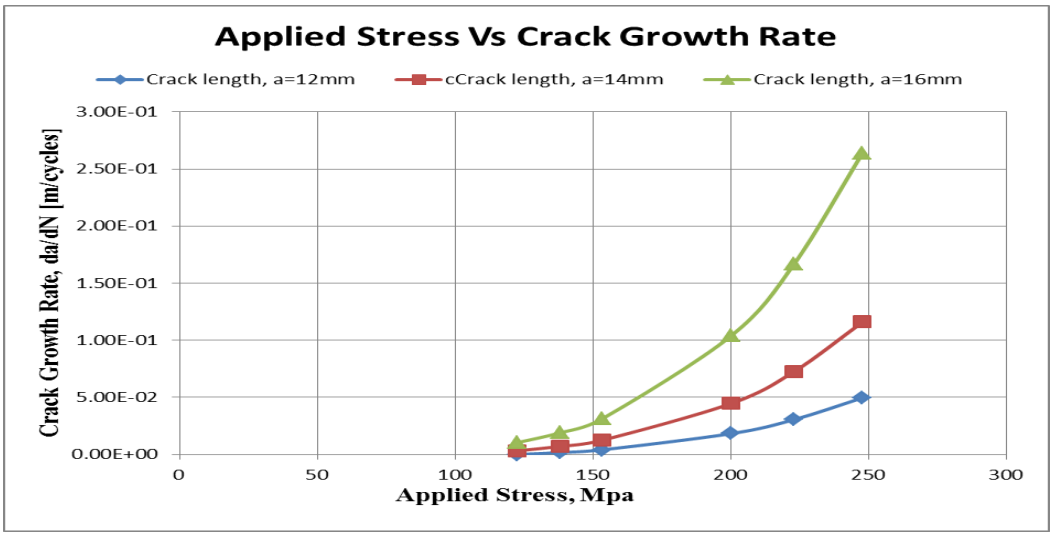

Graph 4.5: Applied Stress vs Crack Growth Rate

As we can see from the graph 4.5, as the applied load increases the crack growth rate also increases.

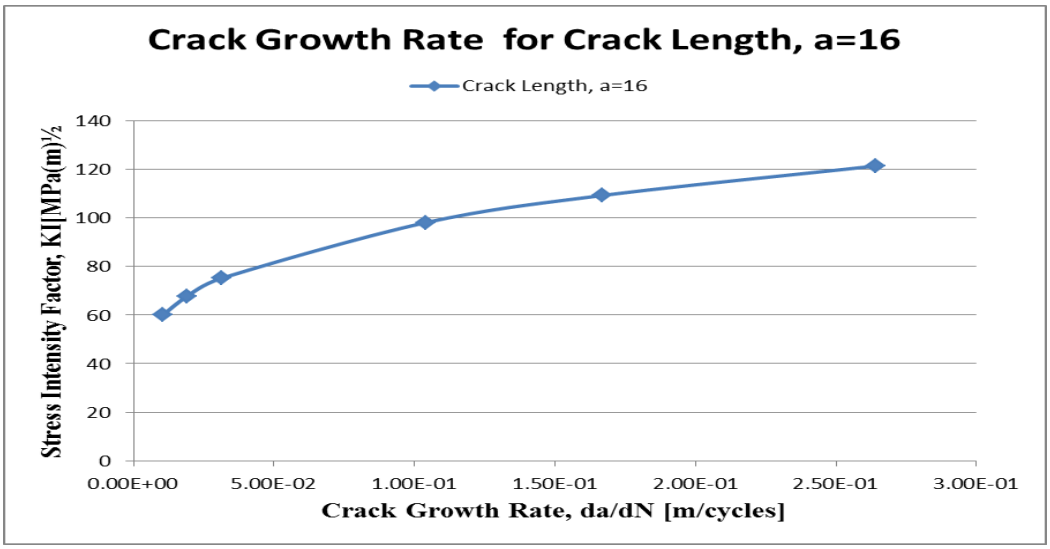

Graph 4.6: Crack Growth Rate Vs Stress Intensity Factor

The crack growth rate increases as the stress intensity factor increases and it is higher for longer crack size (graph 4.6).

Number of cycle of the crack

For the stress Intensity Factors shown in table 4.4 and their crack growth rate, the following Numbers of cycles are shown before their failure:

Table 4.5: Number of cycles of the cracks assuming stress plane conditions

Load Case	**Remote Pressure [Mpa]**	**Crack length**							
		a=10mm		**a=12mm**		**a=14mm**		**a=16mm**	
		KI [MPa]	**N [cycles]**	**KI [MPa]**	**N [cycles]**	**KI [Mpa]**	**N [cycles]**	**KI [MPa]**	**N [cycles]**
1	153.28	42.25	29,940	51.44	2,912.6	62.25	1,120	75.2	511
2	247.7	68.27	505	83.13	241.9	100.6	120.7	121.52	60
3	138	38.03	infinite	46.32	6976.7	56.04	1983	67.7	842
4	222.94	61.45	854.7	74.82	392.16	90.54	192.6	109.38	96
5	122.625	33.8	Infinite	41.16	2,850,356	49.8	4,294.5	60.16	1523.8
6	200.08	55.15	1562.5	67.15	655.7	81.26	313	98.16	153.8

Table 4.6: Number of cycles of the cracks assuming strain plane conditions

Load Case	**Remote Pressure [Mpa]**	**Crack length**							
		a=10mm		**a=12mm**		**a=14mm**		**a=16mm**	
		KI [MPa]	**N [cycles]**	**KI [MPa]**	**N [cycles]**	**KI [Mpa]**	**N [cycles]**	**KI [MPa]**	**N [cycles]**
1	153.28	46.42	2353.26	56.53	1210.3	68.41	621.75	82.64	315.3
2	247.7	75.02	298.7	91.35	153.7	110.54	79	133.5	40
3	138	41.8	3693.55	50.9	1900.2	61.59	976.64	74.4	495.3
4	222.94	67.52	470	82.22	242	99.49	124	120.2	63
5	122.625	37.14	Infinite	45.23	3157.5	54.73	1622.8	66.11	823
6	200.08	60.6	748	73.8	384.63	89.29	198	107.8	100.55

From table 4.5 and 4.6 we will see that the number of cycle of a crack before failure under the applied tensile stress for each crack length decreases with the increases of the applied load. The strain plane conditions shows shorter life of each cracks then the stress plane conditions.

4.4 Summary

In this paper the numerical and analytical (Displacement Extrapolation using stress and strain plane conditions) techniques were used for the calculation of stress Intensity Factor (SIF), KI of plate made of rail steel with edge crack lengths of 10mm, 12mm, 14mm and 16mm. Axle loads of 25tons, 22.5 tons and 20tons are used for the study for mixed use track with the maximum being the design axle load. Speed of the train is considered as: 60km/hr, 70km/hr and 80km/hr. The static vertical wheel load of 122.625KN, 198.16KN, 110.36KN, 178.35KN, 98.1KN and 160.06KN are calculated from each axle loads with the above three train speeds. The wheel loads are dynamically magnified for three cases (case 2, case 4 and case 6). For simulation of the crack a tensile stress loads are calculated based on a formula used by (Ewalds and Wanhill, 1989). Accordingly, the critical stress intensity factors at crack tip are calculated for tensile stress loads of 153.28MPa, 247.7MPa, 138MPa, 222.94MPa, 122.625MPa and 200.08MPa for each crack length.

For these simulations numerical methods based on a formula used by (Ewalds and Wanhill, 1989) is used for the calculation of stress intensity factor, KI. The analytical method uses the Ansys, KCALC command of stress and strain plane conditions. The results are compared for the two cases. From the results it was observed that the stress intensity factor of each initiated crack length increases with the increase of the applied tensile load. The dynamically magnified wheel loads are the higher tensile loads used in cases 2, 4 and 6, which shows the higher stress intensity factors at each crack tips. The life of each crack under the application of these maximum loads is shorter as compared with the wheel loads with no dynamic magnification.

Chapter Five

Conclusion, Recommendation and Future Works

5.1 Conclusions

From this study, it has been observed that the Stress Intensity Factor, SIF value increases with increase in crack length and the crack propagates when the SIF is greater than critical value i.e. fracture toughness of the material. When the stress intensity is less than the fracture toughness of the material the crack is stable and the life of the crack is infinite. Assuming the strain plane condition for estimation of the stress intensity factor, only the life of crack length, a=10mm is infinite when a tensile load of 122.625MPa is applied on it. Because, the SIF based on strain plane condition is 37.14 $MPa(m)^{1/2}$, which is less than $41MPa(m)^{1/2}$, the assumed fracture toughness of the chosen material. For the rest of other cases, the calculated SIF is greater than the fracture toughness of the material and therefore, the cracks are propagating under the application of the above loads. When the stress plane condition is used for the estimation of the stress intensity factor, the life of crack length a= 10mm is infinite under the application of tensile loads of 138MPa and 122.625MPa. The results show that the cracks under dynamically magnified loads with higher speeds are worse (case 2, case 4 and case 6) for each crack length. The stress plane results show that the 2D model results are reasonable to compare with the numerical results. To check the failure criterion the stress plain conditions can be used as these results shows the maximum value for each stress intensity factor, KI for mode –I.

5.2 Recommendation

The results of this study contribute to develop a methodology to predict the need for repair or replacement of rails, and in particular to establish time limits for intervention on rails where one or more defects were detected. Since the results for the dynamically magnified results show the shorter life cycles of the crack, the operation with factors that contribute to the dynamic magnifications has to be minimized. These factors are track irregularity, wheels out of roundness

and rail corrugations. The track with damages like crack initiation has to be dealt with immediately.

5.3 Future works

The following are recommended as an extension of this paper for future work

- The numerically and analytically established closure levels should be confirmed based on experimental data to validate that the obtained values are reasonable.
- The crack lengths should be taken from field observation or from functional railway system
- Different cracks can be analyzed like: cracks at angle, center cracks and elliptical cracks
- Analyzing the cracks for mixed mode cases
- Analyzing the results by different software

6. References

[1]. Mohammad Reza Aalami, A Robust Finite Element Analysis of the Rail-Wheel Rolling Contact, Hindawi Publishing Corporation, Advances in Mechanical Engineering, Volume 2013, Article ID 272350, 9 pages, University of Tabriz, Tabriz 51666-14766, Iran

[2]. Vahid Monfared, Department of Mechanical Engineering, Zanjan Branch, Islamic Azad University, Contact Stress Analysis in Rolling Bodies by Finite Element Method (FEM) Statically, Journal of Mechanical Engineering and Automation 2012, 2(2): 12-16, Zanjan, Iran

[3] V. K. Banthia, "Investigation of Effects of Different Braking Systems on rail wheel Spalling," Department of Automotive Design and Engineering, Railway Wheel Factory, Bangalore 560 064

[4]. _____, (2014). History of Rail Transport, Wikipedia, the Free Encyclopedia http://en.wikipedia.org/wiki/History_of_rail_transport,http://en.wikipedia.org/wiki/Rail_transport_in_Ethiopia. Accessed Date, 20-11-2014

[5]. Jay Prakash Srivastava andP.K. Sarkar," An Approximate Analysis for Hertzian EllipticalWheel-Rail Contact Problem," Department of Mechanical Engineering Indian School of Mines, Dhanbad, India

[6]. Esveld, C. (2001): Modern rail way track. 2nd ed., MTR-Productions, Zaltbommel, The Netherlands.

[7]. Povilaitiene, I. and A. Laurinavičius (2004). Reduction of external rail wearing on road Curves. Journal of Civil Engineering and Management, 10:2, 123-130.

[8].Frich, A. and Dr. Wolfgang, S. (2008). Target Profiles for Grinding A Never Ending

Story. ARM Conference. Swedish Rail Administration.

[9]. Yoshinori OKAGATA (2013). Design Technologies for Railway Wheels and Future Prospects NIPPON STEEL & SUMITOMO METAL TECHNICAL REPORT No. 105

[10]. T.E. Tallian, Failure Atlas for Hertz Contact Machine Elements, ASME press, New York 1992.

[11]. DAVE HANNES (2008), "Master of Science Thesis: Growth of cracks at rolling Contact fatigue, "Royal Institute of Technology, KTH, and Stockholm, Sweden

[12]. P.C. Bastias, G.T. Hahn, C.A. Rubin, V. Gupta, X. Leng, Analysis of rolling contact Spall life in 440C bearing steel, Wear, 1994, 171:169-178.

[13]. J. Dahlberg, B. Alfredsson, Influence of a single axisymmetric asperity on surface Stresses during dry rolling contact, Int J Fatigue, 2007, 29:909-921

[14]. Carter, F.W. (1926), "On the action of a locomotive driving wheel", Proc. R. Soc., London, Series A, 151-157.

[15]. Haines, D.J. and Ollerton, E. (1963), "Contact stress distributions on elliptical contact Surfaces subjected to radial and tangential forces", Proc. Inst. Mech. Eng. 177, 95-104

[16]. Vermeulen, J. and Johnson, K.L. (1964), "Contact of non-spherical elastic bodies Transmitting tangential forces", J. of App. Mech. 31, 338-340

[17]. Kalker, J.J. (1967), "On the rolling contact of two elastic bodies in the presence of dry Friction", Ph.D. Thesis, TU Delft, Delft, The Netherlands.

[18]. Iwnicki, S. (Editor, 2006): Handbook of Railway Vehicle Dynamics. CRC Press, Boca Raton FL (USA), 535 pp.

[19]. Zerbst, U., Lundén, R.b, Edel, K.-O. and Smith, R.A. INTRODUCTION TO THE DAMAGE TOLERANCE BEHAVIOUR OF RAILWAY RAILS, D-21502 Geesthacht, Germany

[20]. Taek-Young Kim, and Ho-Kyung Kim. Three-dimensional elastic-plastic finite element Analysis for wheel-rail rolling contact fatigue, Taek-Young Kim et al. / International Journal of Engineering and Technology (IJET)

[21]. Kalker J. J. (1991): Wheel-rail rolling contact theory. Wear, 144, 243-261.

[22]. Ringsberg, J. W. and Josefson, B. L. (2001): Finite element analyses of rolling contact Fatigue crack initiation in railheads. IMechE: Journal of Rail and Rapid Transit, 215(4),

[23]. Orringer, O., Tang, Y.H., Gordon, J.E-, Jeong, D.Y., Morris, J.M. and Pertman, A.B. (1988): Crack propagation life of detail fractures in rails. U.S. Department of Transportation, FRA, DOT/FRA/ORD-88/13

[24]. Sajjad Zeynali. Checking the Role of Slope in Generated Von Mises Stress of Railroad, Department of Mechanical Engineering, University of Tabriz, Tabriz, Iran, Adv. Environ. Biol., 8(6), 1745- 1751, 2014

[25]. J. SANDSTROM. Evaluation of Dang Van stress in Hertzian rolling contact, Applied Mechanics, Chalmers University of Technology, Sweden,Utvecklingscentrum V¨ast Teknik/Mekanik, Epsilon AB, Sweden

[26]. Venkata Sasidhar Sura. FAILURE MODELING AND LIFE PREDCITION OF RAILROAD WHEELS, Dissertation DOCTOR OF PHILOSOPHY December, 2011 Nashville, Tennessee

[27]. Roya Sadat Ashofteh and Ali Mohammadnia (2014). “Stress Analysis in the Elastic-

Plastic Analysis of Railway Wheels", International Journal of Railway, Volume 7

[28]. Norman E. Dowling, *Mechanical Behavior of Materials,* Pearson Education Inc., 2013.

[29]. G. R. Irwin, "Fracture Dynamics, Fracture of Material", American Society for Metals, Cleveland, 1948, pp. 147 – 166.

[30]. Abdelkader Boulenouar, FE model for linear-elastic mixed mode loading, journal of Theoretical and applied mechanics 52, 2, pp. 373-383, Warsaw 2014,

[31]. Z. Ali, K. Esfahan, S. Meysam, A. Iman, B. Aydin and B. Yashar, "FEM Analysis of Stress Intensity Factor in Different Edge Crack Positions, and Predicting their Correlation using Neural Network Method", Research Journal of Recent Sciences, Vol.3 (2), pp. 69-73, 2014

[32]. Daniel Peixoto, Luís Ferreira, Paulo M.S.T. de Castro, FATIGUE CRACK GROWTH TESTS IN RAILWAY WHEEL AND RAIL STEELS, Department of Mechanical Engineering, University of Porto, Portugal, *15th International Conference on Experimental Mechanics, paper reference number 3838*

[33]. Heshmat A. Aglan and Mahmood Fateh, "Fracture and Fatigue Crack Growth Analysis of Rail Steels", Journal of Mechanics of Materials and Structures, volume 2, No. 2, February 2007

[34]. A. Hassani and R. Ravaee, "Characterization of Transverse Crack and Crack Growth in a Railway Rail", *Iranian Journal of Materials Science and Engineering, Vol. 5, Number 2, May 2008, **Semnan, Iran***

[35]. A. Gopichand, and Y. Srinivas, "COMPUTATION OF STRESS INTENSITY FACTOR OF BRASS PLATE WITH EDGE CRACK USING J-INTEGRAL TECHNIQUE", International Journal of Research in Engineering and Technology, ISSN: 2319-1163

[36]. Upamanyu Banerjee, "Modeling Stress Intensity Factor of Rail Steel under Situation of Growing Fatigue Crack", *Open Journal of Metal*, 2012, 2, 74-78